Nanoliter Sample Preparation for Electron Microscopy and Single-Cell Analysis

Inauguraldissertation

zur
Erlangung der Würde eines Doktors der Philosophie
vorgelegt der
Philosophisch-Naturwissenschaftlichen Fakulät
der Universität Basel

von

Stefan Alexander Arnold

aus Spiringen, Uri, Schweiz

Basel, Schweiz, 2017

Genehmigt von der Philosophisch-Naturwissenschaftlichen Fakultät

auf Antrag von

Prof. Dr. Henning Stahlberg & Prof. Dr. Jan Pieter Abrahams

Basel, den 21. Februar 2017

Prof. Dr. Martin Spiess, Dekan

Summary

Proteins belong to the most fascinating macromolecules found in living systems. These natural nanomachines are involved in virtually all biological processes. Among others, they provide mechanical stability, transport molecules, and catalyze countless chemical reactions. This ubiquity also makes them a major drug target. The function of proteins is directly linked to their three-dimensional structure. Hence, high-resolution protein structures are essential for understanding protein function, and they are a fundamental part of structure based drug design.

Structure determination has long been dominated by X-ray crystallography and nuclear magnetic resonance (NMR) spectroscopy. Until recently, electron microscopy (EM) at cryogenic temperatures (cryo-EM) has played a minor role in high-resolution structure determination due to technical reasons. However, with the advent of direct electron detection cameras, and the ability to record high frame rate movies, instead of single long-exposure images, cryo-EM has quickly caught up and is now recognized as a full-fledged method for structural analysis. In contrast to X-ray crystallography, cryo-EM does not require protein crystals, which are difficult, or sometimes even impossible to grow. On the contrary, cryo-EM allows to image individual protein particles in a nearly physiological, frozen-hydrated environment. And unlike NMR spectroscopy, cryo-EM works well with large protein complexes and requires only a few thousand to million particles to be imaged for structural analysis. This allows, at least theoretically, the structure determination of a protein from extremely low sample volumes. However, EM sample preparation has almost been excluded from the recent advances in the field. It is still dependent on filter paper blotting, a method used to remove excess sample during preparation. This blotting step consumes high amounts of sample, and is often responsible for many problems observed in EM sample preparation, such as reproducibility issues, and loss or degradation of sample. Sample preparation is now widely recognized as the largest remaining bottleneck in the EM structural analysis pipeline.

EM is, in principle, a quantitative and highly sensitive method that can detect single particles and provide structural information in parallel. These qualities can be used for approaches other than structure determination, such as single-cell visual proteomics. Visual proteomics aims at spreading the lysate of a single cell on an electron transparent support and imaging it by EM. Visually distinguishable protein particles are then detected and counted. This, however, requires (i) the lossless preparation of single-cell lysate samples, and (ii) the complete imaging of the prepared sample by EM. Such biological experiments with single-cell resolution have become a major field of research. The main reason for single-cell analysis lies in the heterogeneity of cell populations. Due to the stochastic nature of biological processes, seemingly identical cells can develop different phenotypes. Some of these variations can lead

to serious disorders. Tumor heterogeneity, for example, is limiting the efficiency of medical treatments. And the selective vulnerability of certain neurons could be the basis of many neurodegenerative diseases.

A main goal of this thesis was to extend single-cell analysis to electron microscopy, thus enabling future visual proteomics studies. The major work consisted of developing novel EM sample preparation methods. The focus was laid on minimum sample volume requirements and lossless preparation. Both are a prerequisite for single-cell analysis by electron microscopy.

First, a single-cell lysis instrument was built that allowed live-cell imaging and targeted lysis of individual cells from a mammalian tissue culture through a microcapillary electrode. Subsequently, liquid handling was continually improved, until sample volumes as low as three nanoliters could be controlled by the instrument. Such low volumes demanded new approaches for EM sample preparation. Nanoliter sample conditioning inside a microcapillary tip was developed to transport negative stain in, and salt ions out of the sample plug by diffusion. With this method, nanoliter samples of protein particles, protein nanocrystals, and single-cell lysate were successfully prepared for negative stain EM. To benefit from the most recent developments in cryo-EM, including high-resolution imaging, the instrument was further developed to perform cryogenic sample preparation. Therefore, a dew point stage and plunge-freezing mechanism was invented. The invention allowed to control the temperature of the EM grid, to apply a thin sample film, estimate its thickness through an optical detection, and to quickly plunge-freeze the sample for vitrification. A 5 Å structure of the protein urease was solved by collecting a few thousand imaged particles, prepared from 20 nanoliters of sample.

The ability to lyse and extract single cells from tissue culture, without diluting the sample more than a thousandfold, created alternative opportunities for single-cell analysis. Arrays of single-cell lysate were deposited on nitrocellulose, forming a miniaturized dot-blot, or reverse-phase protein array experiment. This single-cell microarray technology was further investigated and optimized, and different housekeeping proteins were detected at single-cell level. At last, single-cell sampling was interfaced with liquid chromatography-mass spectrometry (LC-MS) to explore the potential for single-cell metabolite analysis. Therefore, arrays of nanoliter-sized sample spots were applied to plastic slides. These slides served as carriers to transfer the samples to the MS facility, where a thin-film chromatography device was used to elute the dried sample spots from the carrier surface and introduce them into the LC-MS instrument. Proof-of-concept experiments compared this new method with conventional sample injection and validated its usability.

Acknowledgments

The work presented here would not have been possible without the help and contribution of many people. First, I would like to thank my advisors Thomas Braun and Henning Stahlberg, who gave me plenty of rope so I could be free in pursuing my research. They were patient and enthusiastic about my work, and always provided valuable ideas and scientific input when required. I also wish to acknowledge Jan Pieter Abrahams for co-refereeing my thesis. Further, I greatly appreciate the work of Shirley Müller, who was always willing to go over my papers and abstracts. She made great efforts in improving the manuscripts by asking critical questions, editing, and correcting, with such a rigor it was demanding at times, but always to the great benefit of the final publication.

I am also grateful to my colleague Stefan Albiez, who started to work under my supervision during a master project, and who continued to support my work during the onset of his own PhD. It was his skills in operating the electron microscopes, that yielded many of the published images and allowed me to focus on the development of the hardware and software needed for our experiments. His valuable feedback helped to further improve our instrument.

I further want to thank all the other colleagues, Andrej Bieri, Benjamin Bircher, Jan Burri, Simon Kemmerling, Nadia Opara, Luca Rima, Nora Sauter, Claudio Schmidli, Anastasia Syntychaki, and Gabriel Zihlmann, who worked with me at some point during my PhD.

I'd also like to thank my colleagues involved in the SNI Argovia project "SCeNA", Gregor Dernick, Christian Berchtold, Götz Schlotterbeck, and Hans-Peter Lang. In particular, I'm grateful to Gregor and his team at Hoffmann-La Roche for their support and contribution with protein microarrays, as well as to Christian and Götz from the Fachhochschule Nordwestschweiz for their involvement and expertise in mass spectrometry. I greatly enjoyed the meetings and creative discussions with Christian and Gregor.

I further want to thank Rosmarie Sütterlin, Andrej Bieri, and Jesil Kasamkattil, who took great care of the cell cultures, as well as Bill Anderson, Ariane Fecteau-LeFebvre, and Kenneth Goldie for maintaining the microscopes.

I greatly appreciate the work of Raymond Strittmatter and his team from the mechanical workshop of the Biozentrum at the University of Basel, and the work of Alexander Stettler from the clean room facility at the Department of Biosystems Science and Engineering, ETH Zurich.

I also want to thank Karen Bergmann, Claudia Wirth and Audrey Fischer, who were dealing with all the administrative work connected with a PhD.

I'm thankful to all my present and former colleagues at C-CINA for their support, the scientific and non-scientific discussions, the coffee and lunch breaks, and the cheerful atmosphere.

I also want to thank Prof. Christian Schönenberger, director of the Swiss Nanoscience Institute

(SNI) and Michel Calame, coordinator of the SNI PhD School and the whole team for their commitment in the SNI and the SNI PhD school and for the many events they initiated and helped to organize.
Last but not least, I want to thank my parents, my brother, and my close friends for accompanying and supporting me during my studies.

Basel, February 2017 Stefan A. Arnold

Contents

Thesis overview

The main goal of this thesis was to develop new methods for EM grid preparation, with a focus on low sample requirement and consumption, and on the ability to handle and prepare single-cell lysate. To evaluate the broader potential for single-cell analysis, the developed instrument was further combined with alternative analysis methods, namely reverse-phase protein arrays (RPPA) and liquid chromatography mass spectrometry (LC-MS).

- **Chapter 1** reviews the current developments in the field of EM sample preparation and outlooks on future possibilities and the potential of improved sample preparation methods.
  A manuscript for publication is in preparation.
- **Chapter 2** describes the implementation of a single-cell lysis and sampling device for analysis by electron microscopy.
  Published in Journal of Structural Biology (2013), 183, 467–473, **DOI:** 10.1016/j.jsb.2013.06.012
- **Chapter 3** reports the development of a sample conditioning method used to prepare nanoliter volumes of protein particles, protein nanocrystals, and single-cell lysate for electron microscopy.
  Published in ACS Nano (2016), 10, 4981–4988, **DOI:** 10.1021/acsnano.6b01328
- **Chapter 4** presents the extension of the previous methods to cryo-EM, allowing nanoliter-volume cryo-EM grid preparation of single-particle solutions and single-cell lysate.
  Published in Journal of Structural Biology (2017), 197, 220–226, **DOI:** 10.1016/j.jsb.2016.11.002
- **Chapter 5** describes the combination of single-cell lysis and reverse-phase protein arrays to detect protein expression at the single-cell level.
- **Chapter 6** presents a novel handover platform that links single-cell sampling with liquid chromatography-mass spectrometry and allows minute amounts of metabolites to be detected from nanoliter sized sample spots.
- **Chapter 7** concludes the thesis and outlooks on possibilities and the future direction of the project.

Chapter 1

Miniaturizing EM sample preparation: Challenges, opportunities and “visual proteomics”

Stefan A. Arnold[a,b], Shirley A. Müller[a], Claudio Schmidli[a,b], Henning Stahlberg[a], Thomas Braun[a,*]

[a] Center for Cellular Imaging and NanoAnalytics (C-CINA), Biozentrum, University of Basel, Switzerland
[b] Swiss Nanoscience Institute (SNI), University of Basel, Switzerland
[*] Corresponding author: thomas.braun@unibas.ch

Abstract

New direct electron detector cameras have paved the way towards high-resolution cryogenic electron microscopy (cryo-EM), as revealed by the dramatic increase in protein structures solved to high resolution by cryo-EM since their introduction. The switch from photographic film to high-end electron detectors has propelled the field into high resolution and opened the door to a digitalized world. Data collection and image processing can now be done in an automated fashion and benefit from the ever-increasing computational power and data storage capacity. In contrast, EM sample preparation has seen very little progress in the last decade and has become one of the main bottlenecks in cryo-EM. The aim of this review is to discuss the challenges in EM sample preparation, highlight current developments, and show the opportunities resulting from advanced sample preparation methods.

1.1 Introduction

The function of proteins is directly linked to their three-dimensional (3D) structure. To be able to study the protein function at atomic level, high-resolution 3D density maps around 3 Å are needed. During the recent decades, X-ray crystallography and NMR spectroscopy were extremely successful in solving protein structures; whereas electron microscopy (EM) only provided a small fraction of atomic models. Now transmission electron microscopy (TEM) of vitrified specimens (cryo-EM) has become a powerful technique for the high-resolution structural analysis of biological matter, and is increasingly recognized as a mainstream tool in biology. This also changed the prerequisite for large protein amounts needed for structural analysis dramatically. In contrast to X-ray crystallography and NMR spectroscopy, only a tiny amount of protein is required to perform structural analysis by cryo-EM: For a single particle project, between 10'000 and a few million individual protein particles must be imaged and analyzed. Therefore, miniaturized techniques can provide enough protein complexes for analysis if combined with microfluidic cryo-EM grid preparation.

The EM pipeline can be roughly divided into four parts: protein sample preparation, EM grid preparation, data collection, and image processing and analysis. Besides the protein production and isolation, the reliable preparation of cryogenic samples is often defined as the largest remaining bottleneck in this workflow (Glaeser, 2016). The trial and error approach of today's cryo-EM grid preparation can consume a significant amount of sample and might rely on additional over-expression and purification of the protein. Reduced sample consumption is, therefore, a main objective of new improved EM grid preparation methods.

Miniaturized EM grid preparation methods do not only minimize sample consumption, but also allow novel strategies for protein isolation, or enable new kind of biological experiments, such as "visual proteomics" analysis of individual cells. In the first case, the miniaturized EM grid preparation can be the last step of a microfluidic protein isolation procedure, only consuming few thousands of cells and purifying proteins in a very short time (<120 min). Finally, the low volume (in the order of nanoliters) of the miniaturized EM grid preparation allows the lysate of individual cells to be prepared for subsequent analysis of the proteome by EM. In this single-cell visual proteomics approach, large protein complexes can be recognized by their shape. To this end, negative stain sample preparation, exhibiting higher signal-to-noise ratio but at lower resolution, might be an alternative to cryo-EM.

In this review, we will first discuss microfluidic EM grid preparation strategies for single particle analysis that have emerged during recent years (section 2). Miniaturization of sample preparation prompts for a higher degree of microscopy automation, which is reviewed in section 3. Finally, we will discuss in section 4 new opportunities opened by these novel sample preparation and microscopy strategies, such as quantitative EM, microfluidic protein isolation techniques and visual proteomics.

1.2 Miniaturized EM grid preparation for single-particle analysis

The ultrahigh vacuum inside an electron microscope generates a very harmful environment for biological specimens, which are generally very sensitive to dehydration. Embedding the biological specimen in a layer of negative stain (heavy metal salts that scatter electrons more strongly than the lighter atoms of biological specimens) prior to inspection is an efficient way to provide both structural support and imaging contrast in the electron microscope. However, keeping a biological sample, such as a protein, in its physiological environment is a key factor for obtaining high-resolution images. Sugar-embedding, *e.g.*, in trehalose, allows certain samples to be imaged at high resolution (Chiu et al., 2011). However, in most cases, cryogenic EM grid preparation is employed, trapping the specimen in a close to physiological environment and helping to conserve its structural composition up to a high-resolution. Imaging at cryogenic conditions further reduces radiation damage on the sample (Baker et al., 2010).

1.2.1 Classical EM grid preparation

The above-mentioned methods were implemented many decades ago and are still in use today. The sample is introduced into the electron microscope on an EM grid, a thin, 3 mm diameter mesh, commonly made from copper, nickel, or gold. A thin electron transparent film is deposited on top of the mesh for the sample to rest on. Depending on the application, different support films are used (Thompson et al., 2016). For negative stain EM, a two-layer film is often applied; first, a nanometer-thin polymer film, such as Parlodion or Formvar is deposited on the raw grid, followed by the evaporation of a thin amorphous carbon film on top (Figure 1.1a). In cryo-EM, beam intensity is generally weaker, and thick support films lower image contrast and resolution. Hence, the application of a perforated (holey) film, commonly made from carbon or gold (Russo et al., 2014), has become state-of-the-art in cryo-EM (Figure 1.1b). With such a film, the sample is suspended freely inside the tiny holes (only a few micrometers in diameter) of the holey film. If still required, an additional, continuous film of carbon, or graphene can be added on top. The main principles of conventional negative stain and cryo-EM sample preparation are depicted in Figure 1.1c and d, respectively. Most protocols for classic negative stain sample preparation (Harris et al., 2014) start by applying 3–5 µl of a 0.005 to 3 mg/ml protein solution, depending on the size of the protein, to an EM grid. The same volume is also applied to grids for cryo-EM, however, higher sample concentration is usually required, since a continuous film that further concentrates particles is often lacking. The excess sample is then blotted away with filter paper. Thereby, most of the sample is absorbed by the filter paper and lost. Furthermore, selective adsorption to the EM grid, or the blotting-paper, can disturb the relative frequency between objects of interest observed, making a quantitative EM analysis difficult. Negative stain is then introduced by incubating a drop of heavy metal salt solution (uranyl acetate, phosphotungstic acid, *etc.*) for a few seconds on the grid. After which, the grid is blotted again and let to dry. Between sample deposition and negative stain application, additional grid washing/blotting steps

can be required to remove excess salts from the sample (not shown in figure). For cryo-EM, plunge-freezing is initiated directly after the sample is blotted away (see section 2.4 for further details).

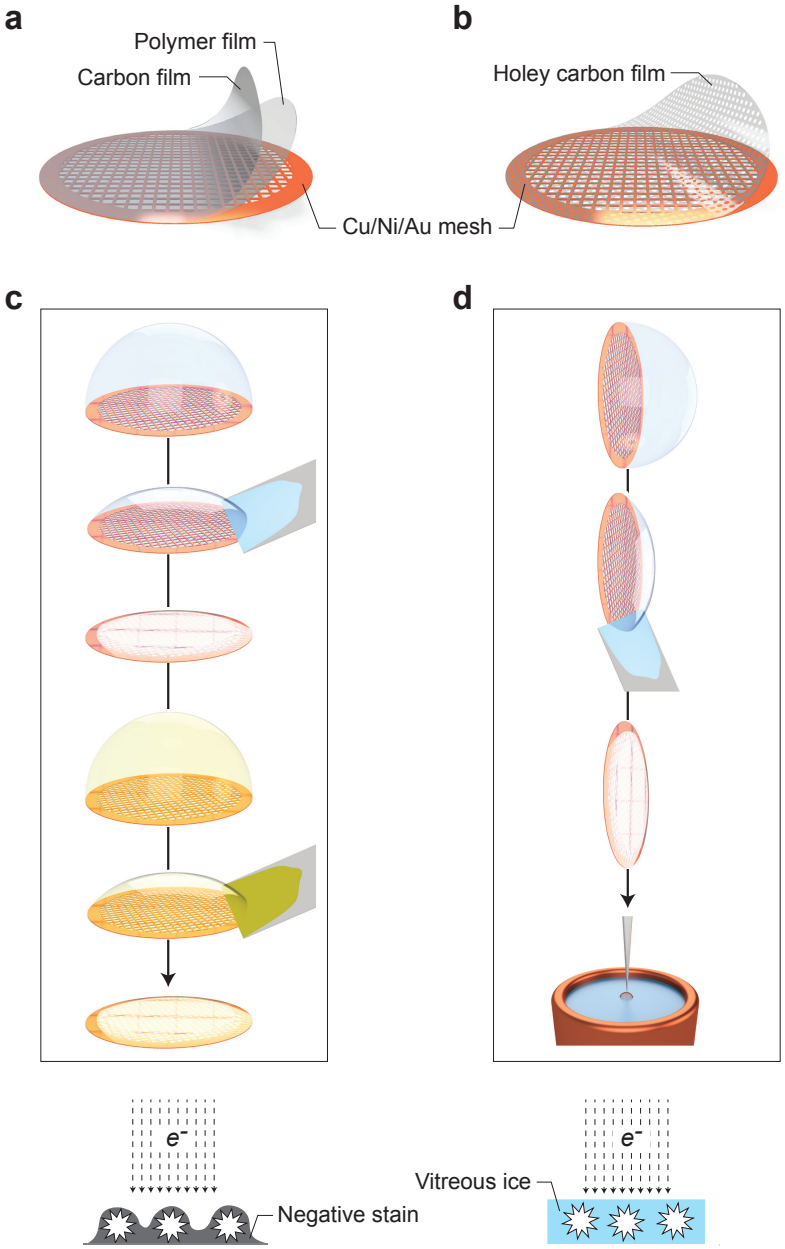

Figure 1.1: *Typical structure of EM grids and most common sample preparation for negative stain and cryo-EM. (a) A typical EM grid used for negative stain EM, showing a copper structure coated with an amorphous carbon layer on polymer support film. (b) EM grid with holey carbon film, which is mostly used for cryo-EM. Note alternative supports are used in some cases for high-resolution imaging, such as gold films (Russo et al., 2014). (c) Basic negative stain EM grid preparation with sample deposition and negative staining, and respective paper-blotting steps in between. (d) Standard cryo-EM grid preparation with paper-blotting and rapid plunge-freezing.*

1.2.2 Microfluidic sample conditioning

Biological samples are purified and stored in carefully chosen buffers containing various salts and additives, such as detergents or glycerol, that enhance the solubility and stability of the proteins (Structural Genomics Consortium et al., 2008). Such buffer components, however, are often unfavorable for EM grid preparation or imaging (Thompson et al., 2016). Hence, tools for rapid removal of buffer constituents or exchange of buffers on a small scale shortly before EM grid preparation can be important for EM grid preparation and sample stability in the electron beam. Such sample conditioning is commonly done in negative stain EM, where the sample is washed on the grid to remove excess salts, and where it is stained with heavy metals (Figure 1.1c). Also in cryo-EM, the sample buffer is often modified prior to plunge-freezing, *e.g.*, to remove glycerol from a sample, which produces bubbles in the electron beam.
During classical preparation methods, the biological sample is often adsorbed on a carbon film as first step. This allows sample conditioning in an elegant way, by exchanging the small droplet on the grid with alternating paper-blotting and incubation steps (Figure 1.1a and c). However, these methods for washing, staining, or sample conditioning require at least microliter volumes and cannot be used for cryo-EM grid preparation, where holey carbon films are employed (Figure 1.1b and d). Biochemists developed many methods to modify buffer conditions in batch prior to EM grid preparation. This includes microdialysis, spin columns, affinity columns or electrophoretic methods. All these methods are (i) time consuming (hours to days) and need (ii) large sample volumes of at least few tens of microliters. If very small liquid volumes need to be handled and manipulated, microfluidic principles and technology are appropriate (Brody et al., 1996) and open new opportunities. A microfluidic device, the H-filter, makes use of different diffusion coefficients to filter out molecules by their size between two parallel laminar flows (Brody et al., 1997). Microdialysis fibers with a diameter of 200 μm are used to exchange small molecules, such as salt ions, across the fiber wall, while maintaining the larger particles inside the fiber (Kemmerling et al., 2012). A stationary nanoliter plug inside a microcapillary can be conditioned with its neighboring liquid volume by diffusive-exchange, whereas small molecules diffuse faster in and out of the sample plug (Arnold et al., 2017). This allows sample conditioning of a 5 nl plug within few minutes. Some of these principles can and have been used to condition samples for EM, as discussed in the next section.

1.2.3 Negative stain EM grid preparation

The negative stain preparation method (Figure 1.1c) embeds the biological sample in a thin layer of amorphous heavy metal salts. Biological matter scatters electrons much less than heavy metals and the structures of interest appear on a dark background, hence called "negative stain". The advantage of this method is (i) the high signal-to-noise ratio (SNR), (ii) the simple transport and storage of prepared grids and, (iii) the relative high electron dose, which can be used for image recording. However, the resolution is seriously limited (to

maximally 16 Å) and the harsh environment of heavy metal salts can harm protein structures, although surprisingly few cases of structure alterations were reported (Ohi et al., 2004). Sample consumption can be reduced by decreasing the amount initially applied to the EM grid. For example, ink-jet spotters can be used to deposit pico- or nanoliter volumes on an EM grid (Castro-Hartmann et al., 2013; Jain et al., 2012; Mulligan et al., 2014), although at least one microliter of sample needs to be aspirated first into the reservoir of the ink-jet spotter (Razinkov et al., 2016). Alternatively, a microcapillary can be employed to aspirate only nanoliter volumes of sample and deposit it on an EM grid (Arnold et al., 2017; Kemmerling et al., 2013).
So far, three devices have been built to stain protein samples with heavy metal salts and to prepare EM grids (Figure 1.2). These are based on (a) staining within a microfluidic chip (Mukhitov et al., 2016), (b) staining by diffusion in a microdialysis fiber (Kemmerling et al., 2012), and (c) staining by diffusion in a microcapillary tip immersed in negative stain solution (Arnold et al., 2016). Although all three approaches are suitable for negative stain EM grid preparation, only the latter method using a diffusion-driven exchange in a microcapillary tip fulfills the low sample consumption criteria. The microdialysis fiber approach needs

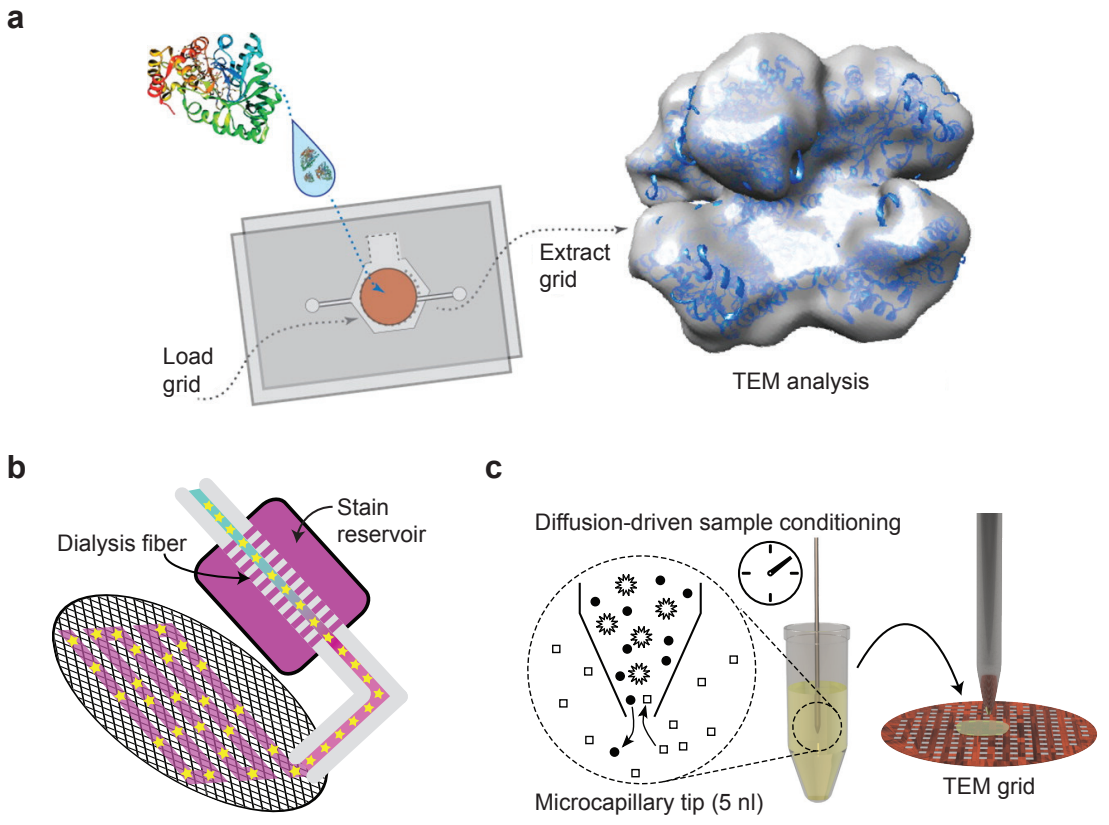

Figure 1.2: *Three microfluidic approaches to negative staining of biological samples. (a) On chip sample loading and staining, adapted with permission from Mukhitov et al., Anal. Chem., 2016, 88 (1), 629–634. Copyright (2016) American Chemical Society; (b) inline staining in a microdialysis fiber spanning a reservoir of negative stain; (c) diffusion-driven staining at the tip of a microcapillary.*

a volume of several hundred nanoliter to a few microliters of sample and a considerable amount of sample is lost by unspecific adsorption to the walls of the dialysis fiber and its connecting tubing. Even larger sample volumes (20 µl) are needed to run the microfluidic chip shown in Figure 1.2a, proposed to perform stopped-flow experiments, though it might be possible to further reduce the required volume by optimizing the chip design. All other methods, including ink-jet based sample preparation, still require manual washing, staining and blotting of the EM grid.

1.2.4 Cryo-EM grid preparation

Grids for single-particle cryo-EM are generally prepared by applying a few microliters of purified protein particles at concentrations higher than those required for negative stain EM on the holey carbon film of an EM grid (Figure 1.1b and d). In conventional cryo-EM grid preparation, filter paper (*e.g.* Whatman #1) is used to blot away excess sample from the grid surface. This has also been implemented in the commercial vitrification robots, where one (Leica Grid Plunger) or two (FEI Vitrobot) filter paper pads from one, or either side are pressed against an EM grid prior to plunge-freezing. On a microscopic level, the surface texture of filter paper is quite rough, and so it is not surprising that the outcome of a paper blotting step can result in areas of various ice thickness across the grid. The filter paper itself consists of cellulose and contains various amounts of trace elements, such as calcium or magnesium. Contact with filter paper might influence pH and other properties of the sample. Blotting action also generates strong forces that are known to deform large filamentous structures (J. Lee et al., 2012). Thus, it is not surprising that various cryo-EM projects struggle, or even fail, at the level of cryogenic grid preparation, and that the paper blotting step is often held responsible.
After blotting away excess sample with filter paper, the remaining sample film is vitrified. This process of sample vitrification, or plunge-freezing, is performed by rapidly plunging the EM grid into a cup filled with a cryogen, *e.g.*, liquefied ethane, cooled to temperatures below -150 °C with the help of liquid nitrogen (Dobro et al., 2010; Dubochet et al., 1988; Dubochet et al., 1981; Thompson et al., 2016). Such cryogenic grid preparation embeds the sample in a frozen-hydrated, close to physiological environment that is, ideally, only slightly thicker than the particles under investigation. If the sample film is too thick, image contrast and resolution will be too low, or it might even be impossible to record any images. A too thin film, on the other, hand will quickly melt under electron exposure. The formation of a perfectly thin vitreous ice film is, therefore, a crucial point in cryogenic grid preparation. The problem can be analyzed in two steps. First, a thin liquid film must be formed on the grid surface, and second, the established thin film needs to stay stable until it is vitrified.
Thin film formation was described very comprehensively by Robert M. Glaeser and colleagues (Glaeser et al., 2016). One conclusion was that blotting with filter paper from the edge of an EM grid does not remove enough liquid to form a thin layer suitable for cryo-EM. Hence, paper blotting is always performed by blotting against the face of the EM grid. The same principles can be applied to very small sample volumes in the nano- or picoliter range. Even

Method	Advantages and drawbacks	References
Microcapillary deposition/aspiration	Nanoliter working volumes. Sample conditioning by diffusion inside the microcapillary. Applicable to fragile supports, that would get damaged by filter paper. Only small area of grid covered with sample.	Arnold et al., 2017; J. Lee et al., 2012
Ink-jet spotters	Fast, deposition of pico- to nanoliter volumes. System must be primed with approx. 1 µl of sample. Surface tension prevents thin ice, specially prepared "self-blotting" grids required.	Jain et al., 2012; Razinkov et al., 2016
Electrospraying	Fastest method, used for time-resolved studies. High impact power of electrospray droplets can damage carbon film. High sample consumption.	Feng et al., 2017; Lu et al., 2014, 2009; White et al., 2003
Reservoir grids	Ice thickness defined by geometry, on chip mixing of samples. Most expensive grids, too thick for vitrification so far.	Patents WO2015134575 A1 and EP2626884 A1
Engineered "coverslips"	Surfactants lower the surface tension and allow sample thinning. Formation of a phospholipid monolayer at the air-water interface can act as a coverslip, stabilizing the resulting, thin aqueous film.	Glaeser et al., 2016
	Two laminated graphene layers can form a liquid cell encapsulating the protein of interest.	Yuk et al., 2012
Evaporation	Often present, but difficult to quantify or control. Optical thin film measurement and temperature control of the grid surface can help to control evaporation.	Arnold et al., 2017

Table 1.1: *Different sample deposition and liquid film thinning approaches used, or envisioned, for cryo-EM grid preparation (also illustrated in Figure 1.3).*

though such small volumes are not limited from spreading by the boundaries of the EM grid, they do not form a continuously thin film. This is due to surface tension, which energetically favors the shape of a spherical cap. Treating the grid surface with a mild plasma (air, H2, O2, Ar or a mixture of these gases) is a standard method to activate the surface and to reduce the contact angles (Aebi et al., 1987). Nevertheless, such a treatment generally doesn't lower the contact angle for the applied sample below 15°. Therefore, even very small sample volumes in the nano- or picoliter range will form droplets that are still too thick for cryo-EM (Jain et al., 2012). The main conclusion is that no liquid film thin enough for cryo-EM will form itself spontaneously, and mechanical means for wicking or sucking away excess liquid are required. However, even by doing so, it was shown that such a thinned sample film, if thinner than 100 nm, is inherently unstable. Dewetting then usually occurs at the thinnest points of the film, and to minimize its surface to volume ratio, the liquid film contracts into thicker

puddles, forming a complex pattern of wet and dry areas (Glaeser et al., 2016).
Table 1.1 and Figure 1.3 summarize different miniaturized methods for sample deposition or liquid film thinning that do not require a filter paper blotting step.

Blotting with microcapillaries

Microcapillary aspiration was first presented as an alternative to paper blotting and it was shown that microcapillary blotting is generating less shear-forces than conventional paper blotting (J. Lee et al., 2012). Microcapillary-based devices also allow a very controlled uptake and deposition of sample in the low nanoliter range (Arnold et al., 2017; Arnold et al., 2016). A microcapillary mounted on a micromanipulator or high-precision motorized stage can be positioned with sub-micrometer precision on a grid surface. The microcapillary can then also be used to deposit and spread the sample on the grid (Figure 1.3a), before aspirating excess sample from the grid surface (Arnold et al., 2017). This method can also be used to exchange buffer components immediately before grid preparation by a diffusive exchange taking place at the tip of the microcapillary (Arnold et al., 2016).

Ink-jet spotting of small volumes

Ink-jet spotters have become a standard in liquid handling applications. Not surprisingly, they also found use in the EM field (Figure 1.3b). As mentioned earlier, even pico- or nanoliter drops are restricted by surface tension from spreading wide enough to form suitable thin films for cryo-EM. This problem was also observed for ink-jet spotters (Jain et al., 2012). It is thus not surprising, that the latest breakthrough was only possible in combination with a new type of self-blotting EM grids (Razinkov et al., 2016). These grids are specially treated to grow nanowires on their copper surface (F. Zhang et al., 2013). The nanowires form a porous mesh that effectively acts as blotting paper to whisk the sample from the window area into the surrounding copper grid bars. Although ink-jet spotters have to be prefilled with at least one microliter of sample (Razinkov et al., 2016), they hold great potential for cryo-EM applications, as the time spent between sample application and vitrification can be very short.

Electrospraying

Electrospraying (Jaworek et al., 2008) is probably the fastest available method for cryo-EM grid preparation and, therefore, has been used for time-resolved cryo-EM experiments (Lu et al., 2014, 2009; White et al., 2003). The grid passes a spray of sample as it is being plunged into the cryogen (Figure 1.3c). The micron sized droplets spread on the carbon coated surface, forming sufficient areas with thin ice for data collection. Nevertheless, creating such small droplets might imply spray conditions that not every sample can meet. In addition, microdroplet impact was shown to damage conventional holey carbon grids and an

additional carbon coating (20–30 nm) was required for reinforcement before applying a (5 nm) continuous carbon support film (Lu et al., 2014). Recently, a 3 Å resolution structure of apoferritin was determined using a sample grid prepared by electrospray deposition. A major drawback, however, is the 10-fold or higher sample consumption compared to conventional preparation, that is currently required for each burst of spray (Feng et al., 2017).

Reservoir grids

A completely different approach was proposed by L. Wang who developed the idea of a sandwich structure with electron transparent silicon nitride windows. Well defined spacer layers would form chambers to accommodate the sample while providing a high degree of control of the ice thickness (Figure 1.3d). In addition, the often-detrimental air-water interface would be prevented by such a device. A similar approach was developed by K. Molhave et al. who designed a microfluidic chip to be loaded with sample and imaged in the electron microscope. Although patent applications were filed on both subjects (WO2015134575 A1 and EP2626884 A1), it remains unclear whether such chips have been successfully fabricated and tested for cryo-EM. At least no scientific results related to cryo-EM have been published up to now. It is questionable, if such larger assemblies would be freezing efficiently to form vitreous ice, and whether the background signal would allow high resolution data to be acquired. However, such devices also hold great potential, *e.g.*, for mixing minute amounts of sample *in situ*, just milliseconds before plunge-freezing.

Engineered "coverslips"

In light microscopy, glass coverslips are commonly used to confine liquid samples in a flat layer of even thickness. An electron-transparent kind of coverslip could be engineered for cryo-EM. Surfactants like phospholipids can reduce the surface tension, spread across a sample film, and form a potentially stabilizing monolayer at the air-water interface, as illustrated in Figure 1.3e (Glaeser et al., 2016). The choice of the ideal surfactant might be difficult, and it is very likely to vary from sample to sample. However, researchers are often trying new surfactants when preparing protein samples, either to stabilize the proteins during purification, to prevent aggregation, or to reduce the adsorption of proteins to the air-water interface. It could help to build some sort of database, where all the positive and negative results obtained with surfactants and detergents in combination with different samples are gathered. Such a database might in the future allow a faster selection of the optimal surfactant for a given project.
An alternative type of "coverslip" can be engineered with graphene. Therefore, two graphene coated EM grids are superimposed face-to-face, and excess sample is removed. After drying and removal of the top grid, small liquid volumes remain entrapped between the two layers of graphene (Figure 1.3f). Such a liquid cell made from two laminated sheets of graphene has been used to study colloidal nanocrystal growth (Yuk et al., 2012).

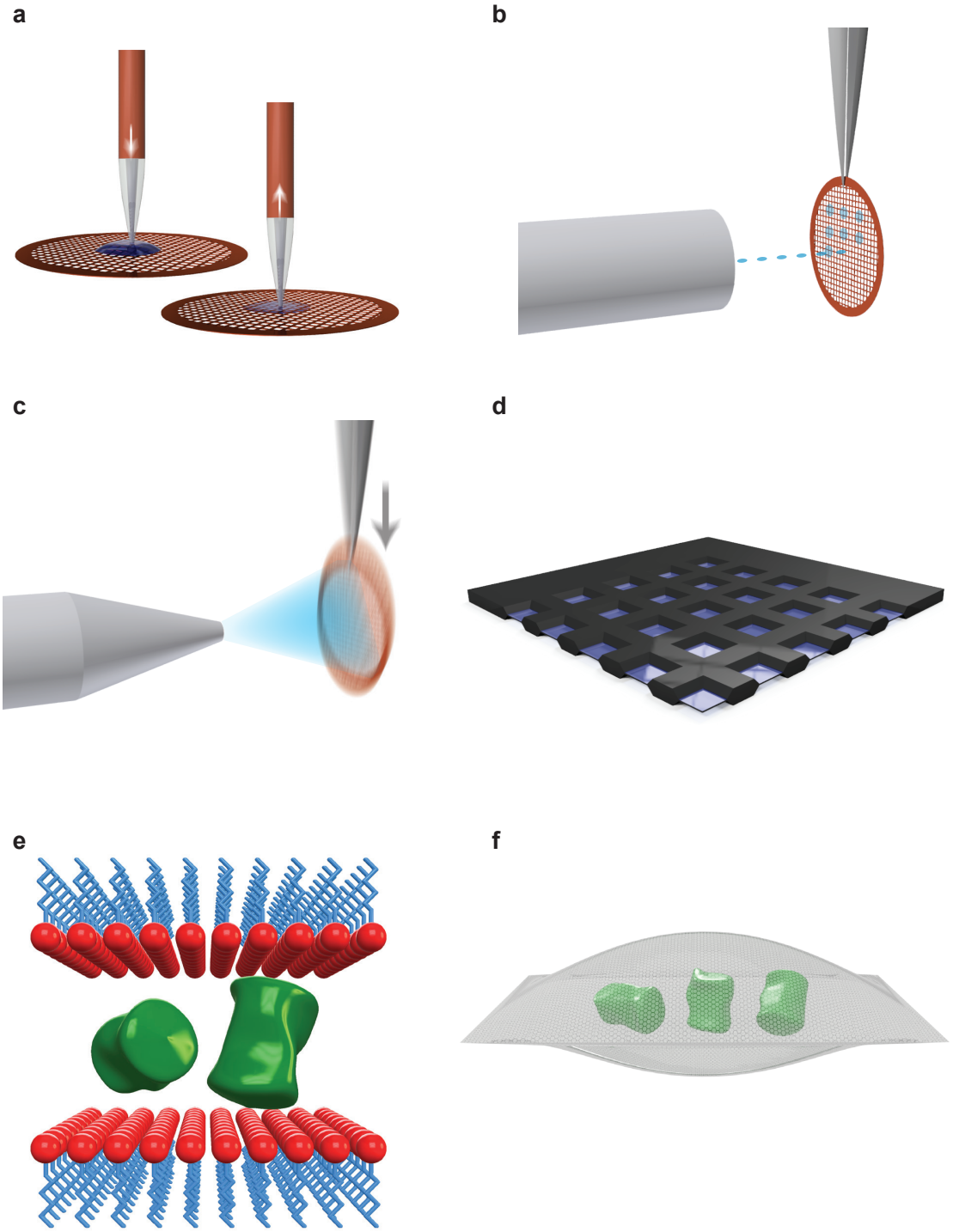

Figure 1.3: *Miniaturized sample deposition and film thinning methods for cryo-EM. (a) Microcapillary dispensing and re-aspiration of excess sample. (b) Ink-jet spotting of pico- or nanoliter sized droplets on self-blotting grids. (c) Electrospraying of sample onto a grid during plunge-freezing. (d) Microfabricated silicon/silicon nitride sandwich array with defined sample wells. (e) Surfactant "coverslip", stabilizing a thin sample film. (f) Graphene liquid cell with encapsulated proteins.*

Evaporation

At last, evaporation is also involved in cryo-EM sample preparation. Evaporation is commonly considered damaging to the sample and unwanted for imaging, since salts and other sample constituents can concentrate and create a grainy image background. Hence, vitrification robots are enclosed in humidity-controlled chambers with relative humidity of 80 to 100%. Note that 100% relative humidity is hardly ever reached, the local humidity near the grid is an unknown and so is the evaporation that occurs on its surface. It is commonly observed that vitrification robots operated at nearly 100% relative humidity, and with very short breaks between blotting and plunge-freezing, produce grids with thick ice, unsuitable for imaging. This might give hints to some uncontrolled evaporation that occurs with conventional grid preparation.
The only method relying to some extend on evaporation was developed by Arnold et al. (Arnold et al., 2017). Around 3 nl of sample are spread on a grid with a microcapillary and the evaporation of the deposited thin film is observed with an optical system. The optical system consists of a laser diode with its laser beam incident perpendicular on the grid, and a detector placed underneath the grid. The light passing through the sample film and the windows of the grid is measured on the photodetector and compared to a reference value of the dry grid itself. Interference peaks corresponding to constructive and destructive interferences at the fixed wavelength of 780 nm give further indication about the film thickness. To slow down the process of evaporation, the grid is cooled close to the dew point. Thus, evaporation can be followed in real-time and plunge-freezing is initiated once a specific signal amplitude is reached. However, the sample is exposed to an air-water interface for a few seconds, and concentration of buffer ingredients might harm the sample or influence image quality. Hence, a preconditioning of sample, *e.g.*, to reduce salt concentration, might be required in certain cases.

1.3 Automation and high-throughput application

A major drawback of all novel devices, especially those built for negative stain EM, is the added complexity compared to the classic grid preparation, where only a pipette and a filter paper is required. It therefore remains questionable if these technologies will find broad application soon. Nevertheless, the use of computer controllable pipetting tools (spotters, syringe pumps, motorized stages, *etc.*) can make grid preparation more reproducible, and in combination with inline sample conditioning and negative staining, presents a first step towards fully integrated and automated EM sample preparation. The diagnostic use of electron microscopes, *e.g.*, for the detection of viruses or specific, disease-related protein assemblies, would benefit from such a development (see section on "visual proteomics"). Most EM labs with focus on structural biology, however, will continue to use negative stain EM as a screening and quality control tool without the requirement for more sophisticated preparation methods, if they are not limited in one way or another by the classic preparation steps.

Nevertheless, instruments were also developed specifically for EM screening applications. A TEM equipped with a 96-grid carousel was developed for 2D crystallography (Coudray et al., 2011) and up to 96 grids can be prepared automatically with samples from 2D crystallization screens. Therefore, 4 µl of sample are automatically deposited on every grid using an eight channel pipettor, followed by washing and negative staining with the same device. However, the instrument has not been widely used in the field. This might be because common low-range electron microscopes employed for negative stain screening applications usually lack multiple grid handling capabilities, such as autoloader grid boxes; it is not very attractive to produce many grids that need to be tediously analyzed one after the other. A similar device, also built for 2D crystallization screening, consists of a robot responsible for loading individual EM grids from a 96-well grid tray into an EM sample holder. A second robot then transfers and inserts the sample holder into an electron microscope (Hu et al., 2010). An alternative screening approach was demonstrated by the deposition of 96 different samples of inorganic nanoparticles onto a single EM grid (Mulligan et al., 2014). Similarly, different samples, including biological material, were spotted onto a single grid (Castro-Hartmann et al., 2013). Deposition of multiple samples on a single grid significantly reduces both sample consumption and the microscopy time required to analyze the samples. However, the same washing and staining procedure might not be ideal for every sample present on the grid, and cross-contamination during washing and staining must be controlled.
As discussed above, the complexity of novel negative stain grid preparation methods could prevent their widespread application. This argument however, does not hold true for cryo-EM, since most labs working in this field are already using sophisticated and semi-automated plunge-freezing robots, such as the Leica Grid Plunger or FEI's Vitrobot. Increasing automation and throughput can thus be expected from next generation vitrification robots. With the new, paper-blotting free preparation methods, sample will be applied directly to grids already equipped with autoloader rings. Such grids can then be inserted into an autoloader grid box right after plunge-freezing, and within minutes, a full autoloader box will be ready for installation in the microscope. In addition, without the large paper blotting pads around the EM grid, space becomes available for new analytical tools, *e.g.*, to monitor thin film formation. First steps in this direction were already performed with a simple laser and photodetector (Arnold et al., 2017).

1.4 New opportunities and outlook

With all these methods and recent developments at hand, new opportunities arise in the field of electron microscopy. Three ideas that benefit from the aforementioned developments are discussed in the remaining part of this paper, *i.e.* a fully integrated and miniaturized EM pipeline, quantitative EM and visual proteomics.

1.4.1 Fully integrated and miniaturized EM pipeline

Once sample loading, deposition, and vitrification will eventually be automated, the EM bottleneck might shift further back towards sample purification. If in the future, only a few nanoliter of sample will be required to generate high-resolution 3D electron density maps of protein particles, there might be no need to express and purify large quantities of material anymore. It might suffice to lyse a couple of cells, extract the target (endogenous) protein in a microfluidic device, and deposit the extracted particles on an EM grid for analysis.
One way of collecting endogenous target proteins out of cell lysate was demonstrated by Giss et al. for the 26S proteasome of HEK 293 cells (Giss et al., 2014). The cell lysate was incubated with polyclonal anti-20S proteasome antibodies crosslinked with a photo-cleavable NHS-biotin cross-linker (Figure 1.4a). After incubation, a few microliters of the suspension corresponding to about 40'000 lysed cells were passed over streptavidin coated magnetic

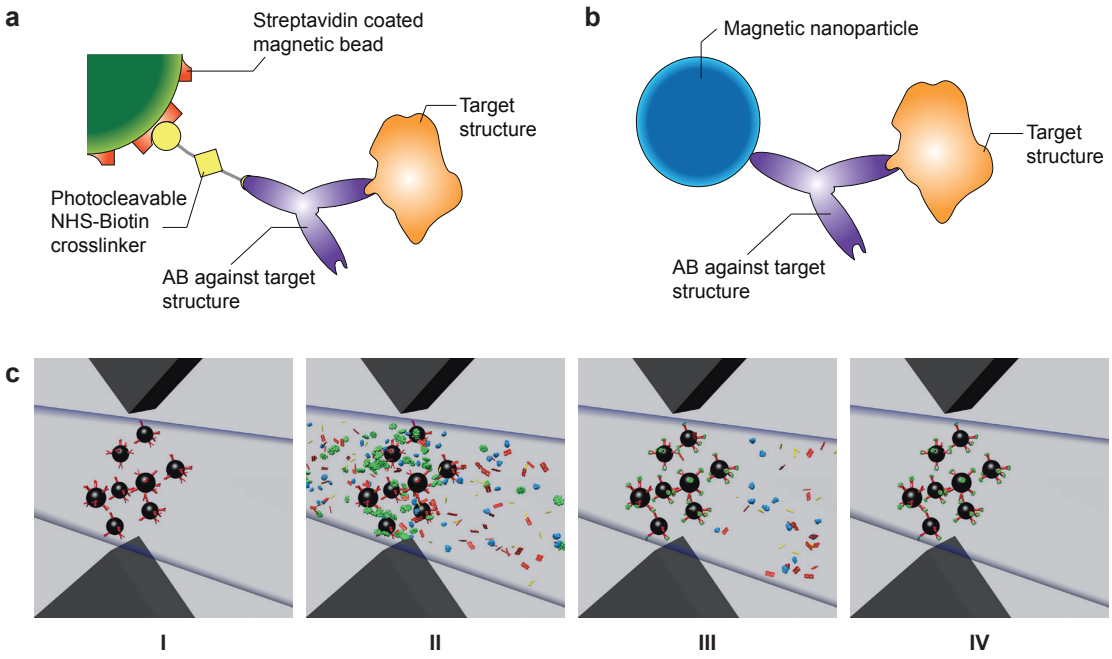

Figure 1.4: *Protein isolation from cell lysate. (a) Magnetic bead bound to a capturing antibody via a photo-cleavable crosslinker. (b) The large magnetic bead is replaced by a magnetic nanoparticle. The capturing antibody is linked directly to the nanoparticle. (c) Workflow: (I) Magnetic beads or nanoparticles are trapped in a microcapillary by a magnetic field gradient, created by external magnets. (II) Cell lysate is flushed across the trapped particles, and the target protein binds to the capturing antibodies. (III) Non-bound lysate components are flushed away. (IV) Only the captured target protein bound to magnetic beads or nanoparticles remains inside the magnetic trap. Illumination with UV light breaks the photo-cleavable crosslinker, and the isolated and purified target protein can be removed from the microcapillary and deposited on an EM grid. Alternatively, the target protein coupled to magnetic nanoparticles can be applied on an EM grid together. The magnetic nanoparticles thus serve as electron dense labels. Panels (a) and (b) adapted with permission from Giss et al., Anal. Chem., 2014, 86 (10), 4680–4687. Copyright (2014) American Chemical Society. Panel (c) courtesy of Claudio Schmidli, C-CINA, University of Basel.*

beads immobilized in a microcapillary by external magnets (Figure 1.4c). Subsequent flushing steps removed any non-bound cell lysate while the bound target proteins remained attached to the magnetic beads. Illumination with UV light cleaved the biotinylated cross-linker and allowed to flush the extracted target proteins onto a grid for EM analysis. Alternatively, smaller magnetic nanoparticles could be functionalized in a similar way, but without a photo-cleavable linker (Figure 1.4b). Such a construct would function as an electron dense label on the EM grid. Further optimization and integration of such or a similar protocol with the recently developed EM grid preparation tools will allow extremely fast and cost-effective protein structure determination in the future.

1.4.2 Quantitative EM

In principle, EM is a very sensitive technique that can detect particles down to the single molecule. Three methods that were discussed above, if combined, allow a quantitative analysis: (i) inline negative staining of sample, (ii) lossless, blotting-free deposition of pico- or nanoliter volumes, and (iii) automated data collection.
A defined nanoliter volume of sample can be stained inside a microcapillary tip via diffusion, and can be deposited on an EM grid as a small spot with an area of roughly 0.5 mm^2 (Arnold et al., 2016). If the sample is deposited on a substrate without grid bars, *e.g.*, a slot grid or a large Si_3N_4 window, the complete sample is available for imaging by automated data collection software. With the volume known, and with an estimate of losses by diffusion, a very accurate and absolute quantitative analysis can be performed from a volume so small it is impossible to pipette it by hand. Negative stain EM is favored over cryo-EM for several reasons: Images can be acquired at a lower magnification with negative stain EM thanks to the higher contrast. The low contrast of cryo-EM data further hinders particle picking compared to negative stain data. Holey or lacey carbon grids needed for cryo-EM limit the imaging area dramatically, as well as thick ice that might occur on some areas. The major problem of quantitative negative stain EM is caused by the so-called coffee ring effect. The name arises from the characteristic pattern created when a drop of coffee dries on the table or a piece of paper. Fluid dynamics inside the drying droplet create a flow of particles towards the edge of the droplet, where they are deposited during the drying (Bhardwaj et al., 2009; Deegan, 2000). This effect causes a strong aggregation of particles at the edge of the dried spot, which can be so severe that it becomes impossible to count all the particles aggregated in this area. The coffee ring effect is particle-shape dependent and especially pronounced for round particles (Yunker et al., 2011). By keeping the grid at a temperature close to the dew point, the evaporation of the sample can be slowed down effectively. This greatly reduces the formation of a coffee ring, as it slows down the convective currents that draw particles to the edge of the drying droplet, and gives more time to the particles to adhere to the surface during drying.

1.4.3 Visual proteomics

Proteomics is the study of all proteins in a biological system, including their abundances, their interaction networks, and their post-translational modifications. The proteome of an organism is very complex. It can vary from cell to cell and change over time, as different proteins are expressed in response to environmental or genetic changes. The term visual proteomics is commonly linked to electron tomography (ET) of single cells and sub-cellular compartments. In this context, visual proteomics aims at identifying the proteins and interaction networks in the recorded tomogram. Since ET is limited to very thin (1 µm or below) cells or sections of cells, and the process of data acquisition and analysis is very time-consuming and cumbersome, an alternative method for visual proteomics was developed (Kemmerling et al., 2013, 2012). The lyse-and-spread visual proteomics approach is illustrated in Figure 1.5. It uses single-cell lysis and sampling devices to collect the lysate of a single cell and spread it over a grid for negative stain EM. The goal is to collect images of the entire cell lysate, and use software to identify major classes of particles. A comparison of these classes between control cells and cells treated with drugs, might give valuable information about the proteins involved in a disease. Eventually, visual proteomics could also be applied to diagnostics, *e.g.*, to detect filamentous protein assemblies, that are commonly observed in neurodegenerative disorders (Ciryam et al., 2013; Ross et al., 2004).

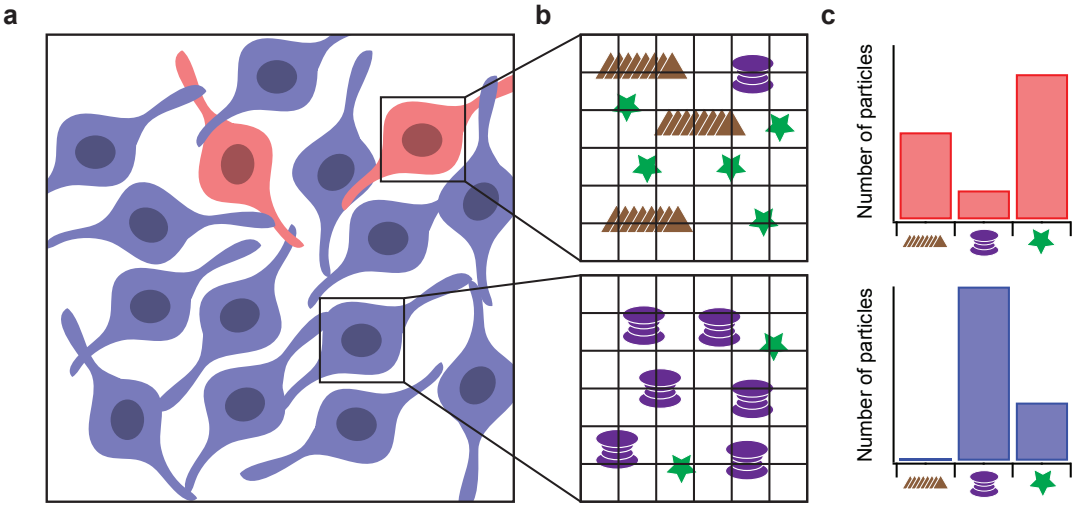

Figure 1.5: *Visual proteomics on single-cell lysate. (a) Individual cells are selected, e.g., based on their phenotype or fluorescence signal, lysed and spread on an EM grid for analysis in the EM. (b) Larger protein complexes can be recognized by particle detection algorithms. (c) The particle population of the different phenotypes can be compared.*

CHAPTER 2

Single-cell lysis for visual analysis by electron microscopy

Simon Kemmerling[a,1], Stefan A. Arnold[a,1], Benjamin A. Bircher[a], Nora Sauter[a], Carlos Escobedo[b], Gregor Dernick[c], Andreas Hierlemann[b], Henning Stahlberg[a], Thomas Braun[a,*]

[a] Center for Cellular Imaging and NanoAnalytics (C-CINA), Biozentrum, University of Basel, Switzerland
[b] Department of Biosystems Science and Engineering (D-BSSE), ETH Zurich, Basel, Switzerland
[c] Discovery Technologies, Pharma Research and Early Development (pRED), F. Hoffmann-La Roche AG, Basel, Switzerland
[1] Authors contributed equally
[*] Corresponding author: thomas.braun@unibas.ch

Published in Journal of Structural Biology, 183 (3), 467–473, (2013); **DOI:** 10.1016/j.jsb.2013.06.012

Abstract

The stochastic nature of biological systems makes the study of individual cells a necessity in systems biology. Yet, handling and disruption of single cells and the analysis of the relatively low concentrations of their protein components still challenges available techniques. Transmission electron microscopy (TEM) allows for the analysis of proteins at the single-molecule level. Here, we present a system for single-cell lysis under light microscopy observation, followed by rapid uptake of the cell lysate. Eukaryotic cells were grown on conductively coated glass slides and observed by light microscopy. A custom-designed microcapillary electrode was used to target and lyse individual cells with electrical pulses. Nanoliter volumes were subsequently aspirated into the microcapillary and dispensed onto an electron microscopy grid for TEM inspection. We show, that the cell lysis and preparation method conserves protein structures well and is suitable for visual analysis by TEM.

2.1 Introduction

The aim of systems biology is to understand the emergence of biological functions from interaction networks (Westerhoff, 2011). This requires knowledge of the intracellular players and their interconnections, for which an inventory of the individual components of the system, i.e. the transcriptome, the proteome, the metabolome and, finally, the interactome, has to be assembled. Such an inventory will strongly vary from cell to cell, as the stochastic nature of biological processes leads to "biological noise" (Eldar et al., 2010; Raj et al., 2008). This makes the study of individual systems, e.g., single cells, a necessity (D. Wang et al., 2010). Genome sequencing (Zong et al., 2012) and expression profiling (Flatz et al., 2011) are far advanced, and amplification techniques are ready to be applied to single cells (Kalisky et al., 2011). The analysis of the metabolism of a biological system profits from the experience and advances of analytical chemistry (Fiehn, 2001); for example, mass spectrometry (MS) can be used to identify metabolites with single-cell sensitivity (Amantonico et al., 2008). Moreover, excellent imaging techniques, such as light- and electron microscopy (EM) or X-ray diffraction imaging, are available for structural analyses.
However, proteomic studies at the single-cell level are hampered by the low expression level of many proteins and the lack of amplification techniques. Although powerful and valuable techniques, such as MS (Picotti et al., 2009) and cryo-electron tomography (cryo-ET) (G. P. Henderson et al., 2007; Medalia et al., 2002; Nickell et al., 2006), are applied for single-cell proteomic studies, such studies still remain a challenging task, especially for eukaryotic cells (Bantscheff et al., 2007; Diebolder et al., 2012; Mader et al., 2010). Thus, adjuvant techniques utilizing novel or hybrid approaches are beneficial to further untangle the complexity of single-cell protein networks.
A combination of microfluidics and TEM was suggested as an alternative and complementary approach to investigate the protein content of single eukaryotic cells (Engel, 2010; Engel, 2009). The idea is to physically lyse single cells and spread the entire sample onto EM grids for structural analysis by transmission electron microscopy (TEM), or mass measurements by scanning TEM (STEM). This "lyse and spread" approach provides access to EM imaging at a higher signal-to-noise ratio (SNR) than when in the cellular background, and enables a more straightforward correlation of structural information with mass data. A prerequisite of this envisaged approach is a targeted lysis of individual cells and an efficient preparation of their lysate for TEM analysis.
A variety of different techniques for single-cell lysis exists today, and most of them have been implemented in microfluidic systems (Brown et al., 2008). Many of these systems utilize the principle of electroporation (Fox et al., 2006; Movahed et al., 2011) to lyse detached or suspended cells in flow-through configurations, whereas only a few report on electrical lysis of "standard" adherent eukaryotic cells in cultures (Han et al., 2003; Nashimoto et al., 2007). However, despite their popularity none of these systems has been utilized to prepare samples of a single-cell lysate for electron microscopy.
Here, we present a system for the electrical lysis of individual adherent eukaryotic cells and subsequent preparation of minute sample volumes for negative-stain TEM. The setup includes

a custom-designed microcapillary electrode (Figure 2.1), which targets and lyses individual cells observed in a light microscope. Immediately after lysis, the cell-fragments are aspirated into the microcapillary, deposited on an EM grid and negatively stained. This method offers the potential for an alternative approach to analyze proteins and protein complexes from individual eukaryotic cells.

2.2 Materials and methods

2.2.1 Instrument Setup

The principle and basic design of the system developed for the electrical lysis of single cells is shown in Figure 2.1A. The system is designed for use with an inverted optical microscope (OM; Zeiss Axiovert 40C). The microscope is equipped with a custom-built stage that has a customized mounting frame on the objective guide. The latter accommodates an indium tin oxide (ITO)-coated glass slide (ground electrode and sample platform) and can be moved manually in the xy-plane. Miniaturized Petri dishes on the surface of the glass slide (see below) allow cell cultures to be grown. A tapered gold-coated microcapillary that serves as second electrode can be positioned in close proximity above the glass slide. The upper

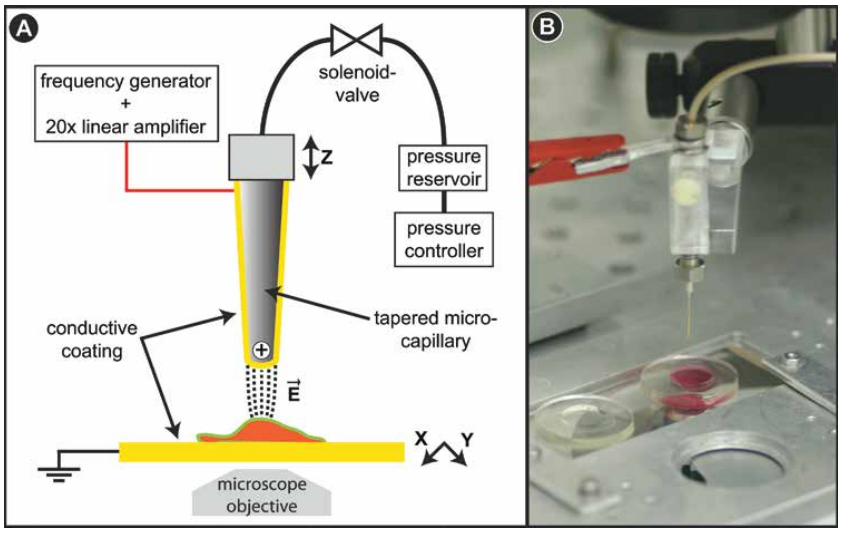

Figure 2.1: *Single-cell lysis instrumentation. (A) Schematic representation of the single-cell lysis setup, which is mounted on an inverted optical microscope. A camera allows for live-cell imaging. The stepper motor approaches the gold-coated microcapillary to the ITO-coated glass slide, where individual cells can be targeted. The function generator sends a voltage pulse to the capillary tip to lyse the cell. Meanwhile, the pressure controller builds up a negative pressure on the closed solenoid valve. Upon cell lysis, the valve is opened for a defined period of time, and the cell lysate is aspirated into the capillary. (B) Lysis microcapillary and cell culture slide. The upper end of the gold-coated microcapillary is inserted into a steel adapter and electrically connected with silver paste. The other end of the steel adapter is attached to a piece of PEEK tubing that connects the microcapillary to the pressure controller via a pressure reservoir. The microcapillary is positioned above a grounded, ITO-coated, glass slide with a PDMS ring on its surface. Slide and ring form a mini Petri dish that can be filled with cell culture medium (red).*

un-tapered end of the microcapillary is inserted in a steel adapter and electrically connected with silver paint (Figure 2.1B). The insulating holder of the adapter is attached to a stepper motor (PI M-126.PD2, Physik Instrumente, Germany) mounted on top of an xy-platform on the microscope stage. This platform allows the microcapillary tip to be centered above the objective lens of the OM. The stepper motor moves the capillary in the z-direction. The other end of the steel adapter holding the capillary is connected via a PEEK (poly(ether-ether-ketone)) tube (inner diameter (ID) 250 μm) to a pressure reservoir (Figure 2.1). The tube is intercepted by a solenoid valve (LVFA0550310H, The Lee Company, USA) that is controlled by the computer through an NI USB-6009 module. A pressure controller (PCNC-0001-00, Seyonic, Switzerland) is used to apply positive or negative pressure to the system via the pressure reservoir. A function generator (33220A, Agilent, Switzerland) delivers a voltage signal, which is amplified 20 times by a linear voltage amplifier (F20A, FLC Electronic AB, Sweden). The output of the linear amplifier is electrically connected to the capillary, and the conductive glass slide is grounded. All electronic components of the system are controlled by a LabVIEW-based, custom-made software (Supporting Figure A.1). A camera (GC750 GigE, Prosilica, USA), mounted on the microscope, enables live-cell imaging and video recording. The next version of the control software will be available as an open-source plug-in for the openBEB (open biological experiment browser) system (www.openBEB.org).

2.2.2 Microcapillaries

Fused-silica (FS) microcapillaries (outer diameter (OD) 350 μm, ID 250 μm, Polymicro) were cut to a length of 10-15 cm. The polymer coating in the middle was removed over a length of 1 -2 cm, using hot chromic-sulfuric acid (102499, Merck, Switzerland). Afterwards, the microcapillaries were rinsed thoroughly with double distilled H_2O (ddH_2O), followed by isopropanol and subsequently pulled with a laser-based micropipette puller (Sutter Instruments, P2000) to obtain a taper with a 30–50 μm ID at the tip. The tapered microcapillaries were plasma-cleaned before the sputter-deposition of a 2 nm Ti adhesive layer, followed by a 50-100 nm Au layer on their outer surface to increase conductivity. Coating was successively performed from two opposite sides at an angle of 45 degrees to obtain a closed conductive layer around the microcapillaries.

2.2.3 Miniaturized petri dishes on conductive glass slides

Commercially available ITO-coated glass slides (Diamond Coatings UK, 8-12 Ω/square) were used as a conductive substrate for cell culturing. These slides have a silver electrode at each end for electrical connections. They were washed and sonicated in detergent solution (1% Alconox, Alconox Inc., USA), rinsed with ddH_2O and stored in ethanol until use.
PDMS (poly(dimethylsiloxane), Dow Corning SYLGARD 184) rings with an ID of 1 cm and a height of 2-3 mm, were fabricated and reversibly bonded onto glass slides to form sample wells with a volume of about 250 μl. These miniaturized Petri dishes allowed cells to be

grown and kept in a physiological buffer solution during the experiment. An ITO glass slide with a PDMS ring filled with cell culture medium is shown in Figure 2.1B.

2.2.4 Cell culture

Adherent baby hamster kidney fibroblasts (BHK21; ECACC 85011433) were cultured in polystyrene T75-flasks containing 30 ml DHI-5 medium (see below) at 37 °C and 5% carbon dioxide. To split the cells, the medium was removed, and the flask was washed with 10 ml of 37 °C warm PBS w/o calcium and magnesium (Dulbecco's Phosphate Buffered Saline, D8537, Sigma, Switzerland). To detach the cells, 3 ml of trypsin-EDTA solution (0.05% Trypsin, 0.53 mM EDTA; 25300-054, Invitrogen, Switzerland) were added, and the cells were incubated at 37 °C for 5 min. The detached cells were diluted with 7 ml of 37 °C warm DHI-5 medium and homogenized using a pipette. 0.5 ml of the homogenized cell suspension and 30 ml of fresh media were returned to the flask for further cultivation. The rest of the cell suspension was used for experiments or disposed. A miniaturized Petri dish was filled with approximately 250 µl of medium, and 1-2 µl of cell suspension were added. The cells were incubated on the glass slide base of this dish for 1-2 days at 37 °C and 5% CO_2.
DHI-5 medium is a 1:1:2 mixture of DME (Dulbecco's Modified Eagles Medium; D6171, Sigma, Switzerland), HamF12 (Nutrient Mixture F-12Ham; N8641, Sigma, Switzerland), and IMDM (Iscove's Modified Dulbecco's Medium; I3390, Sigma, Switzerland) media, supplemented with 5% FCS (Fetal Bovine Serum; E7524, Sigma, Switzerland) and complemented with non-essential amino acids (MEM non-essential amino acid solution; M7145, Sigma, Switzerland), L -glutamine (L -glutamine solution; G7513, Sigma, Switzerland), and vitamins (RPMI1640 vitamins solution; R7256, Sigma, Switzerland).
For the single-cell lysis experiments, the medium was removed from the sample well, and the cells were washed twice with 37 °C warm PBS (Dulbecco's Phosphate Buffered Saline; D8662, Sigma, Switzerland), ISB (isotonic sucrose buffer: 0.25 M sucrose, Bio-Rad, 161-0720; 5 mM HEPES pH 7.4, AppliChem A3724) or HEPES buffer (0.15 M NaCl; 20 mM HEPES pH 7.4; 5.5 mM KCl; 2 mM $CaCl_2$; 1 mM $MgCl_2$). The cells remained in the wash buffer solution during the experiment.

2.2.5 Cell lysis

Live BHK21 cells were lysed in situ in PBS, HEPES or ISB buffer. During the experiments, the conductive glass slide hosting the cell culture was electrically grounded, and the microcapillary was connected to a function generator. The miniaturized Petri dish, formed by a PDMS ring and the glass slide, was positioned on the OM stage. An individual cell was then selected and centered in the field of view with the help of the microscope. Next, the tip of the gold-coated microcapillary was immersed in the buffer solution, brought in close proximity to the conductive surface of the glass slide (distance $\approx$ 20 µm) using the stepper motor and aligned directly above the targeted cell by moving the microscope stage. A camera mounted on the

microscope allowed for live-imaging of the individual cells and their surroundings during the following lysis procedure. After aligning the microcapillary tip above a targeted cell, a burst of five to ten DC square pulses with amplitudes of 6-10 V and a frequency of 10 kHz (pulse duration: 50 µs) was applied to the gold-coated microcapillary using the function generator. This generated a strong electric field (3-5 kV/cm) across the selected cell and resulted in cell lysis. Note, for the compensation of electrode aging, higher voltages were applied in rare cases (maximally 20 V). Right after the burst, the solenoid valve was opened towards the partially evacuated pressure reservoir (Figure 2.1A) and remained open for a defined period of time, aspirating sub-microliter volumes (200–400 nl) of lysate and buffer into the microcapillary. The amount of sample aspirated was controlled by the pressure difference (-50 to -600 mbar) and the opening time of the solenoid valve (50-400 ms). To transfer the sample, an EM grid was clamped by tweezers and centered under the microcapillary. The tip of the microcapillary was approached close to the surface of the grid by the stepper motor. The aspirated sample was then dispensed directly onto the carbon film of the grid by applying a positive pressure to the microcapillary.
Single-cell lysis and aspiration experiments were also performed with fluorescently stained HEK 293 cells (see Supporting material and Supporting movies 1 and 2).

2.2.6 Electron microscopy

Loaded sample grids were incubated for 60 sec - 20 min in a humidity chamber to prevent desiccation. Grids with adsorption times of longer than 3 min were washed on four drops of ddH_2O and blotted once at the end and air-dried. All samples were negatively stained with two 5 µl drops of 2% uranyl acetate (UA) or 2% ammonium molybdate (AM) and imaged in a Phillips CM10 electron microscope operated at 80 kV. The images were recorded on a 2k x 2k CCD camera (Olympus SIS, Münster, Germany).

2.2.7 Enzyme activity assay

Horseradish peroxidase (HRP) conjugated goat anti-mouse IgG (8.5 mg/ml, A2554, Sigma, Switzerland) was diluted to a concentration of 4.25 µg/ml in PBS. 3 µl of the sample was placed onto an ITO coated glass slide, and the microcapillary electrode was placed in the drop, about 20 µm above the glass slide. Different voltages (0 V, 4-18 V in 2 V steps and 22 V), each with a burst count of 5 and a single pulse length of 50 µs were applied. 2 µl were removed from the treated sample droplet, diluted to 8.5 ng/ml in PBS, and the enzymatic activity of HRP was analyzed by enhanced chemiluminescence (ECL) on a dot plot (Amersham ECL Prime Western Blotting Detection Reagent; RPN2232, GE Healthcare, UK).

2.3 Results

The single-cell lysis setup (Figure 2.1) allows for live-cell imaging, lysis of single adherent eukaryotic cells, rapid aspiration of the lysate, and transfer of the sample onto EM grids. This is demonstrated using adherent BHK21 cells. The adherent cells were individually lysed in situ in buffer solution, while the process was monitored by means of optical microscopy. To achieve lysis, a gold-coated microcapillary tip was positioned in close proximity to and directly above the selected BHK21 cell growing on the ITO coated glass slide inside of a miniaturized Petri dish (Figure 2.1B). The distance between the capillary tip and the conductive surface of the glass slide was approximately 20 μm; there was no direct cell contact. As documented by light microscopy, the electric field, generated across the cell by a burst of five to ten 50 μs DC square pulses with amplitudes of 6-10 V applied to the microcapillary electrode, was sufficient to reproducibly and efficiently lyse the BHK21 cells in PBS or HEPES buffer (Figure 2.2A-C). Electrical pulses alone were sufficient to achieve lysis as indicated by a necrotic morphology of the targeted cells, nevertheless, cells were not completely disrupted, and cell fragments stayed in place if not aspirated (Figure 2.2A and supp. Figure A.2A). Moreover, aspiration alone was not sufficient to lyse, disrupt or detach cells.
As demonstrated, only the targeted cell is lysed and neighboring cells remain unaffected, due to the small electrode dimensions and when conductive buffers are used (Figure 2.2A-C and Supporting Figure A.2A-D). This findings are supported by finite-element analysis (FEA) results, which show that a high electric field is only generated in very close proximity to the cell, between the microcapillary tip and the ITO support (Figure 2.3A). Further, adaptation of the electrical parameters to obtain a higher peak-voltage and longer pulse duration allowed the cells to be lysed in low-conductivity, isotonic sucrose buffers, but in this case neighboring cells were also affected (Supporting Figure A.2E and F).
FEA was also used to estimate the maximal temperature increase by Joule heating due to five 50 μs DC square pulses with amplitudes of 10 V. This estimation predicts a maximal local temperature of 34 °C for a time span of less than 1 ms (Figure 2.3B and Supporting Figure A.3 and A.4). The average cell temperature stays below 30 °C throughout the overall time span used for simulation. To experimentally study the effects of the short temperature increase, the enzymatic activity of horseradish peroxidase (HRP) after applying electrical pulses was quantified. HRP is known to be irreversibly impaired by exposition to increased temperatures (Chattopadhyay et al., 2000 and Supporting Figure A.5). Figure 2.3C shows the normalized activity of HRP after exposing 3 μl droplets to electrical pulses of different voltages. The effect was measured by quantification of the chemoluminescent reaction catalyzed by HRP. Our results show, that the activity is not significantly decreased below 10 V, but effects are clearly seen around 14 V and higher. Similar experiments performed with synthetic filamentous actin did not reveal signs of protein aggregation or structural damage of the filaments below 10 V (Supporting Figure A.6). Immediately after the applied burst, lysate and surrounding buffer were aspirated into the microcapillary to prevent diffusion of the cellular content. Subsequent to cell lysis and aspiration, the sub-microliter volumes (200-400 nl) were loaded onto EM grids, negatively stained and inspected by TEM.

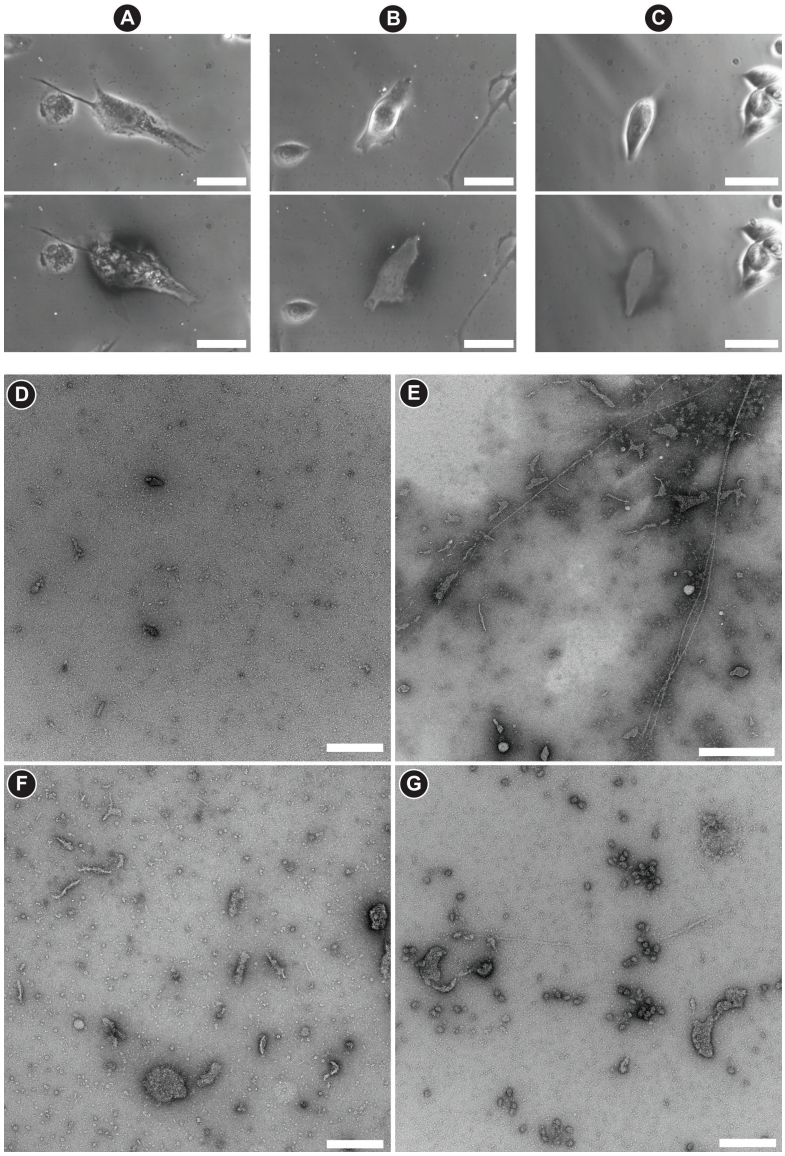

Figure 2.2: *Single-cell lysis and lysate analysis. (A-C) Phase contrast light microscopy images of individual adherent BHK21 cells in PBS (A,B) and HEPES (C) before (top row) and after (bottom row) different procedures. Scale bars: 50 µm. (A) After applying electrical pulses (5 x 50 µs, 10 V DC), the targeted cell is not completely disintegrated but shows necrotic morphology. (B,C) After applying electrical pulses (B: 10 x 50 µs, 6 V DC; C: 5 x 50 µs, 10 V DC) with aspiration, only a ghost imprint of the targeted cell remains; the surrounding cells are not affected (bottom row). (D) Overview TEM image of PBS aspirated from the cell culture well after the washing steps but before a cell lysis event. Such control experiments showed predominantly small particles, but distinctive particles and structures were not detected. Negative stain: 2% UA, Scale bar: 200 nm. (E) TEM image of the aspirated lysate of a single cell showing some µm-long filament and membrane patches. Negative stain: 2% AM. Scale bar: 500 nm. (F) TEM image of the aspirated lysate of a single cell showing some membrane structures, helical filaments and particles resembling the shape and dimensions of Hsp60 and the 20s proteasome. Negative stain: 2% UA. Scale bar: 200 nm. (G) TEM image of the aspirated lysate of a single cell showing membrane structures. Negative stain: 2% UA. Scale bar: 200 nm*

TEM images of buffer solution, aspirated from the miniaturized Petri dish in the proximity of a cell after the washing steps, but before a cell lysis event, showed a background of predominantly small particles as expected (Figure 2.2D); these are most likely residues from the growth medium that were not removed by the buffer washes (see Materials and Methods). TEM images of the sample aspirated from the immediate proximity of an individual adherent BHK cell directly after lysis, reveal cellular content (Figure 2.2E-G, Figure 2.4). Membrane patches, filaments and other structures with distinctive shapes can be recognized and correlated to the specific cell using the light microscopy information. Further examples of prominent structures observed in the lysate of single cells are shown in Figure 2.4. Although the control experiments documented the presence of some (predominantly small) particles in the bare buffer solution (Figure 2.2D), distinctive structures similar to those found in the lysate (Figure 2.2E-G and Figure 2.4) were not detected.

2.4 Discussion

We present a setup for the controlled lysis of single, adherent eukaryotic cells and a subsequent visual inspection of cellular components by negative-stain TEM. The developed instrument enables (i) live-cell monitoring before and during cell lysis by optical microscopy, (ii) precise selection of individual cells, (iii) fast lysis ($<$500 ms) without prior disturbance of the cell and (iv) immediate aspiration of the cellular components into a microcapillary for further treatment.

The ITO coating on the glass slide that forms the base of these dishes, features the required electrical and optical properties and serves as ground electrode. In contrast to gold, ITO is suitable for fluorescence microscopy, allows live-cell imaging, and can be combined with various functionalization options to support cell growth if needed (Luo et al., 2008; Shah et al., 2009). The ability to carry out live-cell imaging prior to cell lysis, not only allows studying biological processes, but also enables lysis to be initiated at a defined time-point by means of an optical feedback; for example, a target cell in a specific state can be identified and selected by fluorescence signals of genetically labeled proteins.

Microfluidic chips with fixed electrodes often suffer from bubble formation due to electrolysis. In the flexible-electrode setup described here, sample aspiration and downstream processing were not affected by electrolysis, and there were no signs of bubbles inside the capillary. Furthermore, microfluidic chips with embedded electrodes depend on cells being in suspension and are not well suited to study adherent eukaryotic cells, which must be detached before lysis.

Biological processes involving proteins elapse within time frames of milliseconds to days (Souchelnytskyi, 2005). This makes the total lysis time an important parameter for cellular dynamics studies. As the method presented here combines fast electrical lysis ($\leq$1 ms) with rapid sample loading ($\leq$400 ms), the described technique offers a temporal resolution that is suitable to study dynamic processes in protein networks of single cells.

The complete detachment and disruption of the cells, observed after sample aspiration (Figure 2.2B-C and Supporting Figure A.2B-F), was most likely due to the additional shear forces

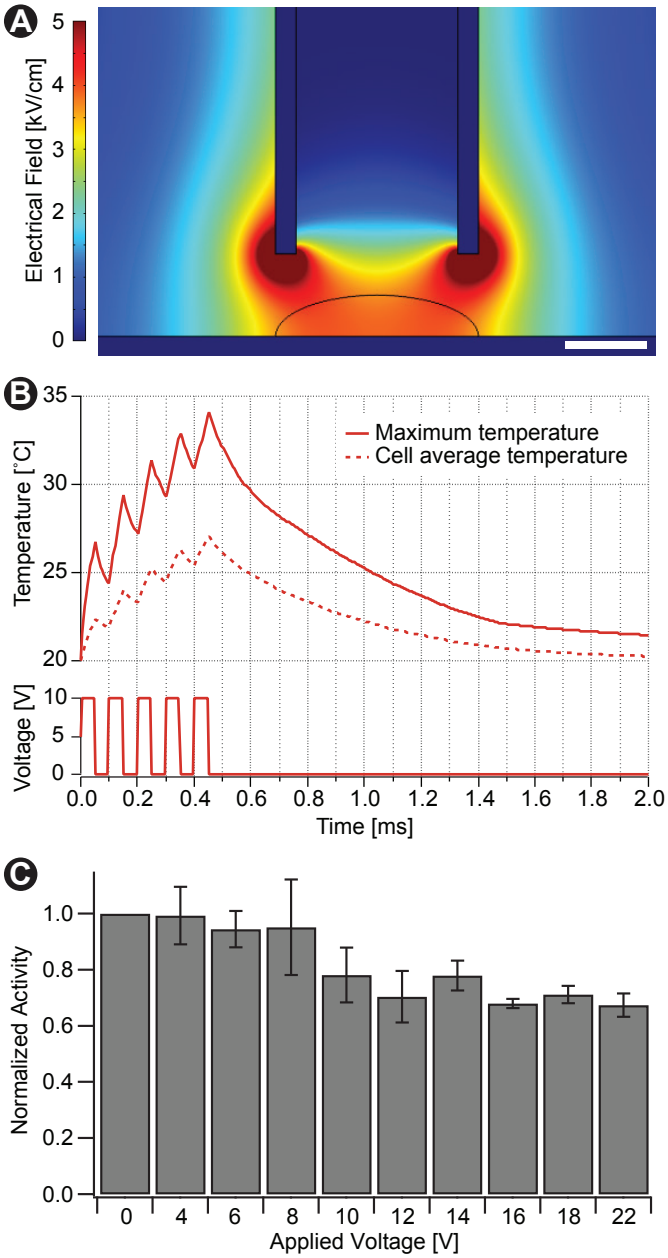

Figure 2.3: *Finite element analysis (FEA) of electroporation characteristics and data on horseradish peroxidase (HRP) stability. (A) FEA simulation to estimate the electric field strength (kV/cm); Scale bar: 20 µm. A potential of 10 V was applied to the microcapillary electrode immersed in PBS buffer; the inter-electrode distance was 20 µm. The profile of a cell (curved black line) placed on the bottom electrode (ITO) was added to the model for illustration. (B) Estimated temperature changes predicted by FEA. The solid line (top panel) shows the variation of the maximum temperature in the solution over time as result of electric pulses (10 V) applied via the gold-coated microcapillary. The dotted line shows the average temperature within the cell region, depicted as curved black line in panel A. (C) Voltage dependence of HRP activity after applying electric pulses. The activity was normalized to that of the control experiments (0 V).*

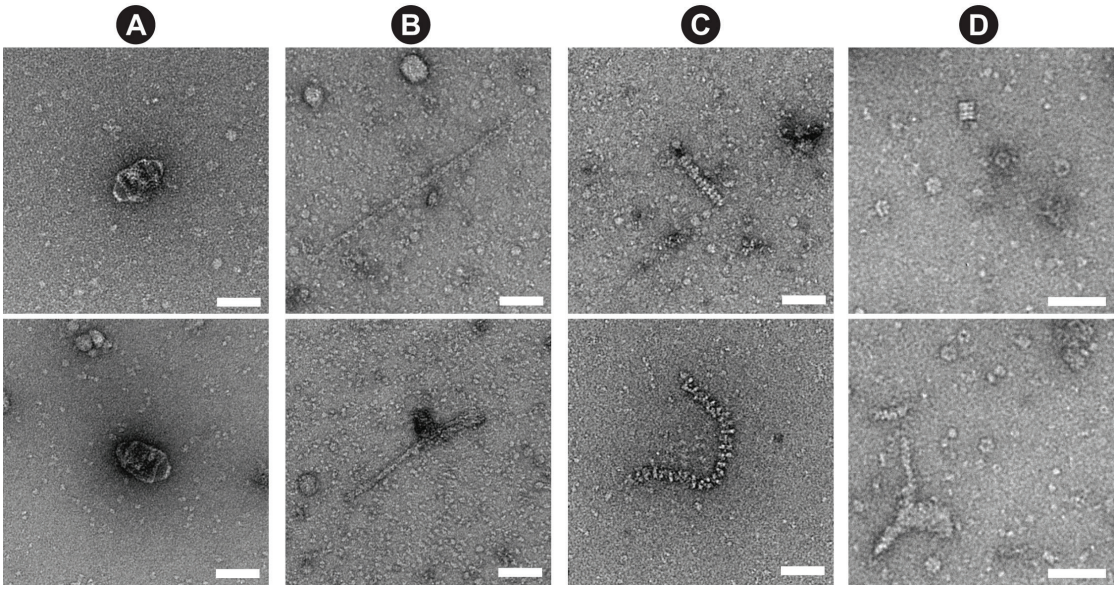

Figure 2.4: *Examples of distinctive structures observed in negatively stained cell lysates of individual cells. Negative stain: 2% UA. Scale bars 50 nm. (A) Structures that resemble vault organelles, which are large ribonucleoprotein particles found predominantly in the eukaryotic cytoplasm (Kedersha et al., 1990). (B) Helical structures that have the shape and dimensions of actin filaments (Aebi et al., 1986). (C) Examples of other less abundant structures observed in the lysate of individual cells. These resemble (top) the CplXAP complex (Ortega et al., 2004) and (bottom) nucleoprotein filaments (Sehorn et al., 2004). (D) More detailed view of the frequently observed ring-like structures shown in Figure 2.2F. These have variable dimensions and resemble top views of Hsp60 (De Carlo et al., 2008) and the 20s proteasome (Cascio et al., 2002); the rectangular structure in the top image resembles a side view of one of the latter complexes.*

occurring during the aspiration process. The combination of electrical pulses and mechanical forces, allows applying relatively mild conditions for electrical lysis (low pulse amplitudes and short pulses) in comparison to those reported previously (Han et al., 2003; Nashimoto et al., 2007).

The preservation of the native protein structure and supramolecular assemblies is crucial for the subsequent visual analysis in EM. FEA predicts elevated temperatures on time scales $\leq$1 ms (Figure 2.3B and Supporting Figure A.4) and indicates that thermal protein denaturation is unlikely to occur. All our experimental data corroborate these findings: Quantitative assays using HRP did not show a significant degradation of enzyme activity at the conditions used to lyse individual cells (Figure 2.3C). Furthermore, experiments with synthetic actin filaments only showed structural effects at voltages exceeding the ones used for lysis (Supporting Figure A.6).

Negative-stain TEM revealed a variety of cellular components, such as membrane patches, filaments and other particles (Figure 2.2 and 2.4), and indicates the structural preservation of the observed cellular components. No signs of protein aggregation were observed (compare to Supporting Figure A.6D). Due to the unique and distinct shape of several particles, assumptions about their identity can be made directly from the raw images, e.g., for the

vault organelles (Kedersha et al., 1990). Future template matching algorithms must include scoring algorithms for quantitative analysis, (Beck et al., 2009, 2011; Best et al., 2007) or complementary, labeling procedures (Giss et al., manuscript in preparation) can be employed. Although the aspects of protein structure and protein complex preservation have to be further consolidated and the recovery of sample constituents has to be improved in the future, the TEM images clearly demonstrate the potential of this method to prepare the lysate of a single cell for a visual analysis in negative-stain TEM. Furthermore, single cell lysis of adherent eukaryotic cells is also of great interest for other analysis methods, such as mass spectrometry (Aebersold et al., 2003) or reverse-phase protein arrays (RPPA, Dernick et al., 2011). The application of our lysis method for the detection of actin by RPPA is shown in Supporting Figure A.7.

The "lyse and spread" approach for visual analysis of eukaryotic cells presented here is envisaged to complement classical methods, such as cryo-ET or mass spectroscopy. In comparison to cryo-ET of whole vitrified cells or cellular sections, the here presented approach does not provide information about the 3D arrangement of the proteome. In addition, the excellent preservation capabilities of vitrification have to be replaced by mild and physiological conditions during sample preparation and eventually supported by crosslinking procedures. On the other hand, the "lyse and spread" method, focusing particularly on the cytosolic fraction, has several advantages: (i) Adherent eukaryotic cells can be studied; (ii) the proteins can be prepared by negative staining what provides higher SNR; and (iii) the physical segmentation renders the cell components directly accessible for separation and labeling experiments (Giss et al., in preparation). In contrast to mass spectroscopy, mass determination by STEM is less accurate and the visual analysis by TEM is less high-throughput amenable. However, the single molecule detection limit of the EM allows low-abundance proteins and protein complexes to be studied. Moreover, EM provides additional structural information and facilitates the study of large protein assemblies.

The presented single cell lysis method is only a first step towards the global approach described above as "lyse and spread visual proteomics". Currently, a limiting step is the low transfer efficiency of the cell lysate onto the EM grid, involving several blotting and washing steps. Therefore, the combination with methods exhibiting higher transfer efficiency will be beneficial in order to obtain a more complete access to the proteome. For example, the use of a microfluidic sample-conditioning device, combined with lossless micropatterning of the sample onto an EM grid, could be a suitable solution as shown by Kemmerling et al. (Kemmerling et al., 2012).

2.5 Conclusion and outlook

The system presented here allows single-cell lysis to be performed in less than a millisecond and to aspirate the cellular components into a microcapillary within a few hundred milliseconds for further preparation and subsequent analysis. The combination of this setup with an optical system facilitates live imaging and the evaluation of lysis and sample loading. The system is compatible with standard adherent-cell culturing methods and tools, and can

potentially also be applied to biological tissues. Moreover, the system can be easily adapted to different sample carriers, which facilitates the use with additional or alternative analysis techniques such as reverse phase protein arrays (Supporting Figure A.7).
In combination with a lossless sample deposition onto the EM grids and optional procedures for crosslinking, protein separation and labeling this method for single cell lysis offers the potential for targeted and quantitative visual proteomics studies on eukaryotic single cells.

Acknowledgments

We thank Andreas Engel for his inspiring ideas and support, the workshop of the Biozentrum of the University Basel for their aid and Shirley Müller for carefully reading the manuscript and expert discussions. The project was financially supported by the SNF (NSX1003, granted to T.B.), SystemsX.ch (CINA, granted to H.S., co-PI is A.H.) and the NCCR Nanoscience.

Supporting information

The supporting information associated with this article can be found in Appendix A.

Chapter 3

Total sample conditioning and preparation of nanoliter volumes for electron microscopy

Stefan A. Arnold[a,b], Stefan Albiez[a], Nadia Opara[a,b,c], Mohamed Chami[a], Claudio Schmidli[a,b], Andrej Bieri[a], Celestino Padeste[c], Henning Stahlberg[a] Thomas Braun[a,*]

[a] Center for Cellular Imaging and NanoAnalytics (C-CINA), Biozentrum, University of Basel, Switzerland
[b] Swiss Nanoscience Institute (SNI), University of Basel, Switzerland
[c] Paul Scherrer Insitute (PSI), Villigen, Switzerland
[*] Corresponding author: thomas.braun@unibas.ch

Published in ACS Nano, 10 (5), 4981–4988, (2016); **DOI:** 10.1021/acsnano.6b01328

Abstract

Electron microscopy (EM) entered a new era with the emergence of direct electron detectors and new nanocrystal electron diffraction methods. However, sample preparation techniques have not progressed, and still suffer from extensive blotting steps leading to a massive loss of sample. Here, we present a simple but versatile method for the almost lossless sample conditioning and preparation of nanoliter volumes of biological samples for EM, keeping the sample under close to physiological condition. A microcapillary is used to aspirate 3 to 5 nl of sample. The microcapillary tip is immersed into a reservoir of negative stain or trehalose, where the sample becomes conditioned by diffusive exchange of salt and heavy metal ions or sugar molecules, respectively, before it is deposited as a small spot onto an EM grid. We demonstrate the use of the method to prepare protein particles for imaging by transmission EM and nanocrystals for analysis by electron diffraction. Furthermore, the minute sample volume required for this method enables alternative strategies for biological experiments, such as the analysis of the content of a single cell by visual proteomics, fully exploiting the single molecule detection limit of EM.

3.1 Introduction

In recent years, electron microscopy (EM) has experienced a renaissance in the field of biological research. This is based on improved instrumentation, through direct electron detection cameras (Kühlbrandt, 2014; Li et al., 2013; Subramaniam et al., 2016), and advances in image processing software systems (Grigorieff, 2007; Scheres, 2012). Related fields such as electron diffraction of 3D nanocrystals has equally progressed significantly (Nederlof et al., 2013; Rodriguez et al., 2015). While cryo-EM of two-dimensional crystals (Goldie et al., 2014) or single protein 'particles' (Cheng et al., 2015) allows the structural investigation of biological samples under physiological conditions at high resolution, the enhanced signal-to-noise ratio (SNR) makes negative stain EM (De Carlo et al., 2011) especially suited to the analysis of complex samples, *e.g.*, dynamic protein assemblies.
Unfortunately, standard methods used to prepare samples for EM suffer from two major drawbacks: Typically, a large sample volume (around 3 µl) containing the biological species at high concentration (0.1 mg/ml to 3 mg/ml protein) is adsorbed to a carbon-film coated EM grid, blotted with filter paper, stained, and blotted again, before being air-dried for inspection in a transmission electron microscope (TEM). These blotting steps remove more than 99% of the sample volume. In addition, since adsorption to the carbon film depends on the specific sample-carbon interaction, blotting can promote the uncontrolled and preferential removal of sample subclasses, leading to a nonrepresentative sample population on the EM grid, which can interfere with the analysis of (large) biomolecule assemblies, such as proteoliposomes, dynamic protein complexes, or other (synthetic) particles. The effect is even more pronounced when protocols include washing procedures.
Advanced methods for the preparation of EM samples are needed. Recent efforts have mainly addressed three aspects: (i) the reduction of sample loss, (ii) the increase of throughput and (iii) the reduction of sample consumption. Wash- and blotting-free negative staining procedures were recently developed to reduce sample loss, *i.e.*, biological samples can now be stained in microdialysis fibers and directly deposited onto an EM grid in a controlled manner (Kemmerling et al., 2012). However, as some sample is still lost along the microcapillary and dialysis fiber of the inline staining system, that method does not allow the analysis of nanoliter sample volumes or solutions with low protein concentrations. To increase throughput, multiple grids can be prepared in parallel (Coudray et al., 2011), or printing (Castro-Hartmann et al., 2013) and inkjet picoliter dispensing tools such as the Spotiton system (Mulligan et al., 2014) can be used to deposit an array of samples on a single EM grid. Although, these are exciting developments and represent an excellent method to prepare minimal volumes of sample per grid in a fast and efficient manner, these approaches rely on a larger sample stock, and for preparing negative staining TEM grids, they would require additional washing and/or blotting steps.
Here, we present a method for negative stain sample preparation or trehalose embedding (Chiu et al., 2011) that only consumes 5 nl or less of biological material. For sample conditioning and EM grid preparation, a microcapillary with sample loaded in its tip, is immersed into a reservoir of conditioning solution; the conditioning is driven by diffusion,

utilizing the different diffusion constants of salt molecules and proteins (Figure 3.1). We show that this method has manifold applications, *e.g.*, to prepare single particles for cryo- or negative stain imaging, single cells for visual proteomics (Kemmerling et al., 2013, 2012) or nanocrystals for electron diffraction studies.

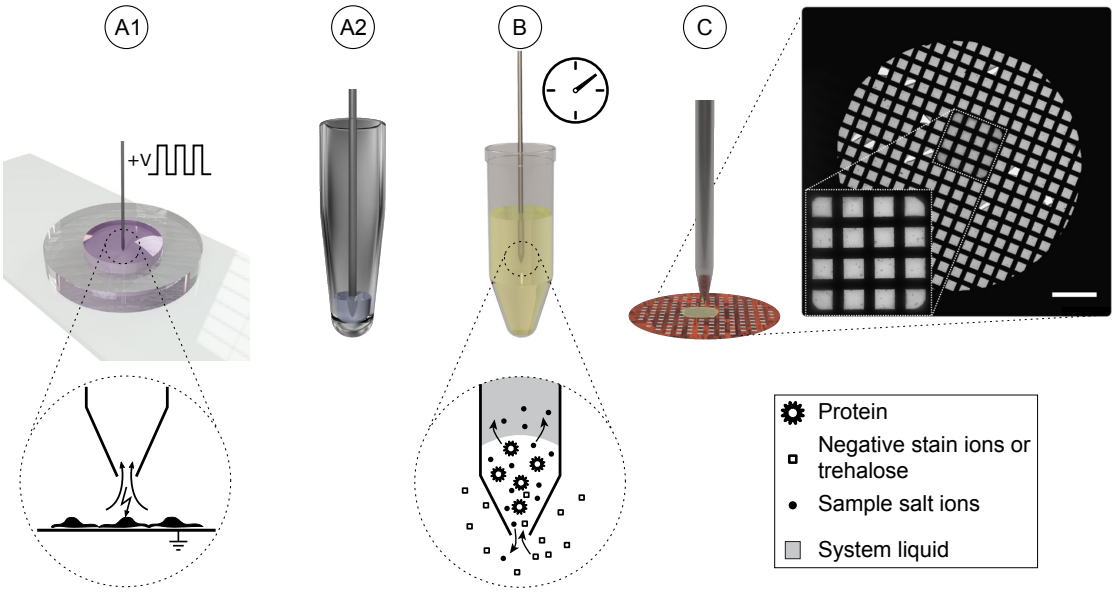

Figure 3.1: *Sample preparation process. (A1) Electroporation and aspiration (lysis) of a single cell from cell culture; or (A2) aspiration of 5 nl of sample from sample stock. (B) Immersion of loaded microcapillary tip into the conditioning liquid, here negative stain, for diffusion-driven desalting and staining of the sample. (C) Deposition of 5 nl of sample on a glow-discharged EM grid and analysis by EM. Scale bar 500 µm.*

3.2 Results and discussion

We implemented the sample preparation method (Figure 3.1) in an instrument initially developed for single-cell lysis (Kemmerling et al., 2013). The setup (Figure 3.2) is built on an inverted microscope and allows the precise positioning of a microcapillary, which is connected to a high-precision pump capable of aspirating and dispensing liquid in the subnanoliter range. The microcapillary is used to aspirate sample from a stock solution, to lyse individual eukaryotic cells and to dispense conditioned sample onto the EM grid *i.e.*, all processing is performed in the same capillary without significant sample transport.

3.2.1 Theoretical background and experimental considerations

Sample conditioning must ensure three crucial issues: First, sample salts must be removed; second, heavy metal salts (in the case of negative staining) must be introduced; and, third, the formation of insoluble precipitates between sample salts and the heavy metal ions must be prevented.

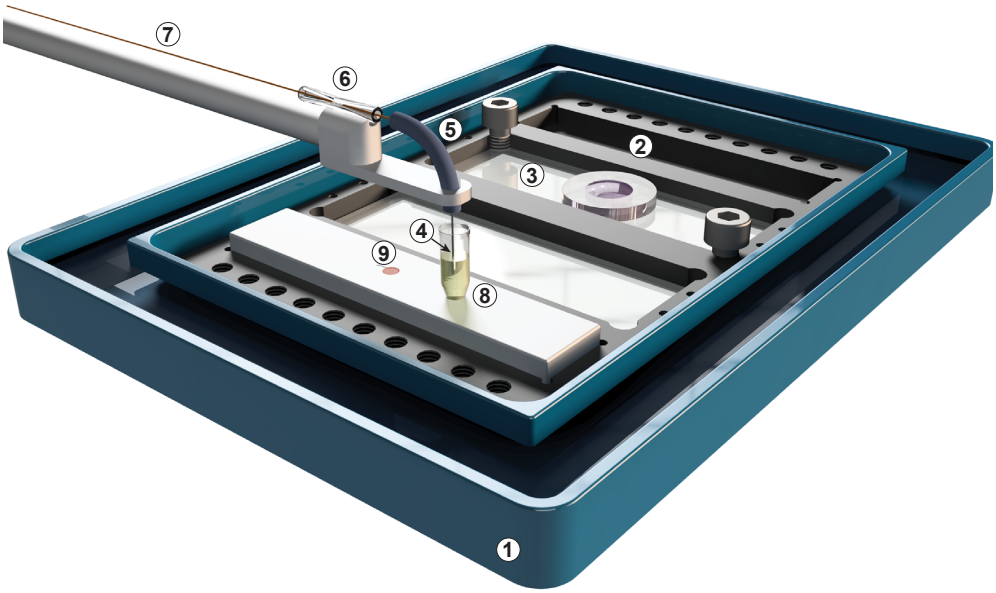

Figure 3.2: *Single-cell lysis and sample conditioning setup. The essential components are placed on a work-platform mounted in a live-cell incubator stage (1). For single-cell experiments, miniaturized Petri dishes are used to culture the cells (2). These poly(dimethylsiloxane) (PDMS)-based wells are reversibly bonded to an indium tin oxide (ITO)-coated microscopy slide (3). Cells are lysed by electroporation and the lysate is immediately aspirated (3–5 nl) by a microcapillary (4).13 Alternatively, samples can be loaded into the capillary from a sample well (not shown). The microcapillary is guided by a conductive sleeve (5) and connected by a press-fit mechanism (6) and a microcapillary (7) to a high-precision pump system (not shown). All capillaries are filled with system liquid (water), which is in direct contact with the aspirated sample (see Figure 3.1). For sample conditioning, the microcapillary tip is immersed in negative stain or trehalose solution contained in a 200 µl tube (8). Subsequently, the sample is deposited on a carbon-coated EM grid held in place by a groove (9) or a pair of tweezers (not shown).*

The conditioning process depends on the diffusion constants of the molecules and particles present, the viscosity of the liquids, and, last but not least, the geometry of the microcapillary tip. Finite element method (FEM) simulations were used to model the diffusive exchange of salt and negative stain ions between the sample plug and its environment (Figure 3.3A, B). Note that the diffusion process occurs at two interfaces: (i) at the capillary tip toward the conditioning reservoir and (ii) between the sample-plug and the system liquid (ddH_2O or negative stain) above it in the microcapillary (Figure 3.3C). Because the area of the latter interface is larger, the diffusion process toward the system liquid is faster. The use of capillaries with larger inner diameters not only accelerates the conditioning process but also minimizes the glass surface the sample is exposed to (assuming that the volume is the same) and, therefore, avoids excessive sample loss by unspecific binding to the capillary walls.
Besides microcapillary geometry, the conditioning time also depends on sufficient desalting of the sample volume as well as on reaching a good negative stain or trehalose concentration inside the sample plug. Samples with a higher salt concentration need to be immersed for a longer period of time, because if the residual concentration of salt molecules is too high, salt crystals will form on the EM grid upon drying, as shown in Supporting Information S1.

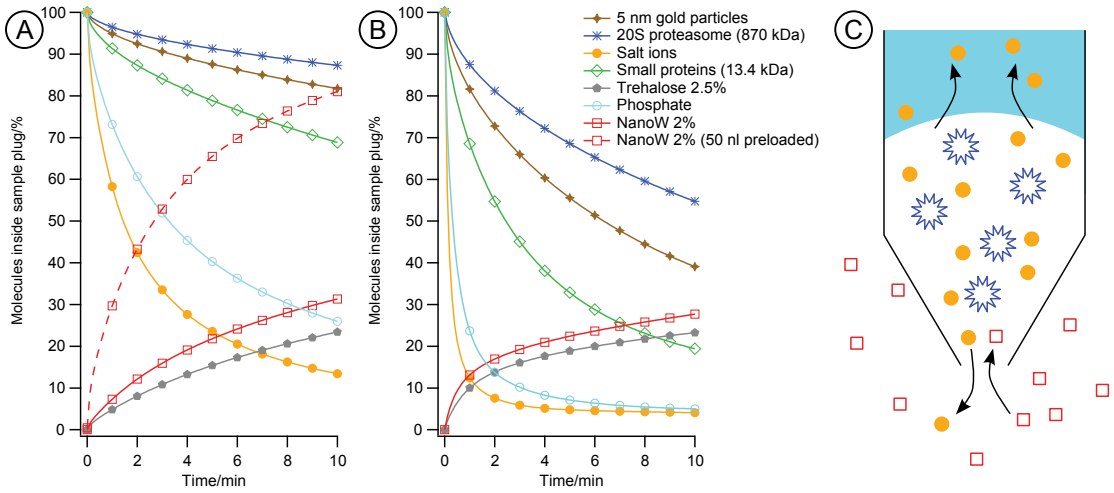

Figure 3.3: *FEM simulation of the 3D diffusion process in the microcapillary and at its tip for two different geometries: (A) 100 µm inner diameter (ID) and 30 µm tip orifice, and (B) 250 µm ID and 40 µm tip orifice. For each species, the number of molecules was integrated over the initial sample plug volume of 4.5 nl and normalized by its initial number of molecules. Diffusion was allowed to occur between the sample tip and the stain (NanoW or trehalose) reservoir, as well as between the sample plug and the system liquid (ddH_2O) above it in the microcapillary. The dashed line represents the case for shorter conditioning times, where system liquid also contains negative stain (2% NanoW), which is suited for certain low-salt-containing buffers. Diffusion coefficients can be extracted from Table 3.2. (C) Illustration of the diffusion process at the two interfaces.*

Fine-tuning is also required when the sample buffer, *e.g.*, phosphate-buffered saline (PBS), forms insoluble precipitates with the heavy metal ions of the stain. Thus, the conditioning time is highly buffer dependent. The conditioning time can be significantly reduced by the use of buffers that, unlike PBS, do not form insoluble precipitates with the heavy metal salts of the negative stain. In this case, the system liquid can also contain negative stain solution for a faster increase of negative stain concentration inside the sample volume. Furthermore, conditioning time can be further reduced by using a low-salt buffer (see application note 1). In order to validate the FEM simulations, we prepared EM grids with solutions of 5 nm nanogold beads (supplied by Cell Microscopy Center, Department of Cell Biology, University Medical Center Utrecht, The Netherlands), with and without conditioning. The nanogold particles were diluted in 50 mM ammonium bicarbonate buffer. The same buffer was used for conditioning and as system liquid. The results shown in the Supporting Information S2 demonstrate that the relative loss of particles is in good agreement with our simulations presented in Figure 3.3. The graph in Figure 3.3 also reveals the effect of different diffusion coefficients on the amount of diffusive exchange. Due to the large difference (several orders of magnitude) between the diffusion coefficients of salt ions and larger proteins with masses ranging from few tens to thousands of kDa, sample loss via diffusion can be neglected. Nevertheless, small protein molecules ($<$ 10 kDa molecular weight or $<$ 5 nm in diameter) will be lost with time (Figure 3.3). Although these molecules are below the size usually analyzed by EM, they might be potential binding partners of large protein complexes. If this is the case,

we propose the use of one or both of the following measures: (i) Chemical fixation of protein complexes before sample preparation (X. Tang et al., 2009), or (ii) reduction of the conditioning time by the use of lower ionic strength buffer systems and/or buffers that do not form insoluble precipitates with heavy metals, such as Tris (Tris(hydroxymethyl)-aminomethane) buffers; conditioning times and protein-loss due to diffusion can thus be kept at a minimum (see Figure 3.5). As the physics of the exchange process taking place by diffusion is well understood, use of the immersion-diffusion method does not preclude quantitative evaluation of subsequent TEM measurements. Calibration factors can be estimated, allowing the relative occurrence of particles to be corrected.
So far, sample conditioning was a poorly addressed problem by microfluidic technologies. Mainly classical H-filters (Yager et al., 2006) were used, less frequently microdialysis technology was employed (Kemmerling et al., 2012). Both approaches are technologically more challenging to implement than the immersion and diffusion method proposed here. Furthermore, the sample is exposed to larger surface areas than in the presented method, leading to significant loss by unspecific adsorption of proteins to the wall. In the proposed method the sample does not need to be transported during conditioning, which makes it also suitable for complex and more viscous samples.

3.2.2 Application note 1: Negatively stained single particles

Single particle preparations of tobacco mosaic virus (TMV) or 20S proteasome (20SP) samples were suspended in a standard PBS buffer (2.7 mM KCl, 1.5 mM KH_2PO_4, 136.9 mM NaCl, 8.9 mM $Na_2HPO_4 \bullet 7H_2O$, pH 7.4), which represented a worst-case buffer for sample preparation by negative stain. Volumes of 5 nl of sample were loaded into the tip of a microcapillary and dipped into a reservoir of negative stain solution for several minutes, to allow diffusive exchange of negative stain and salt ions. To sufficiently remove the phosphate salts from the sample, immersion times of 6-7 min were required. After staining, the total 5 nl sample volume was deposited onto a glow-discharged EM grid. Three different negative stains (2% NanoW, 2% NanoVan, and 0.5% ammonium molybdate) were tested and good staining quality was achieved (Figure 3.4). Compared to the commonly used uranyl acetate stain, which has a pH around 4.3, these stains have a more physiological pH, ranging from pH 6.8 to pH 8. They were also advantageous because uranyl-based negative stains tend to cross-link biological samples in solution.11 The known characteristics of the different negative stains were reflected by the results obtained using our method, *e.g.*, very light staining was achieved using NanoVan as expected.
The conditioning time was significantly reduced by the use of a low-salt Tris-buffer. Figure 3.5 shows the staining achieved when single particle preparations (mix of TMV and Escherichia coli phages) in a low-salt Tris-buffer (20 mM Tris-HCl pH 7.4 with 50 mM NaCl) were conditioned for 3 min in a 2% NanoW solution with additional 10 nl of 2% NanoW loaded in the system liquid. This shorter incubation time not only allows higher throughput for automated sample preparation, but also ensures that any loss of small proteins is considerably reduced (see discussion above).

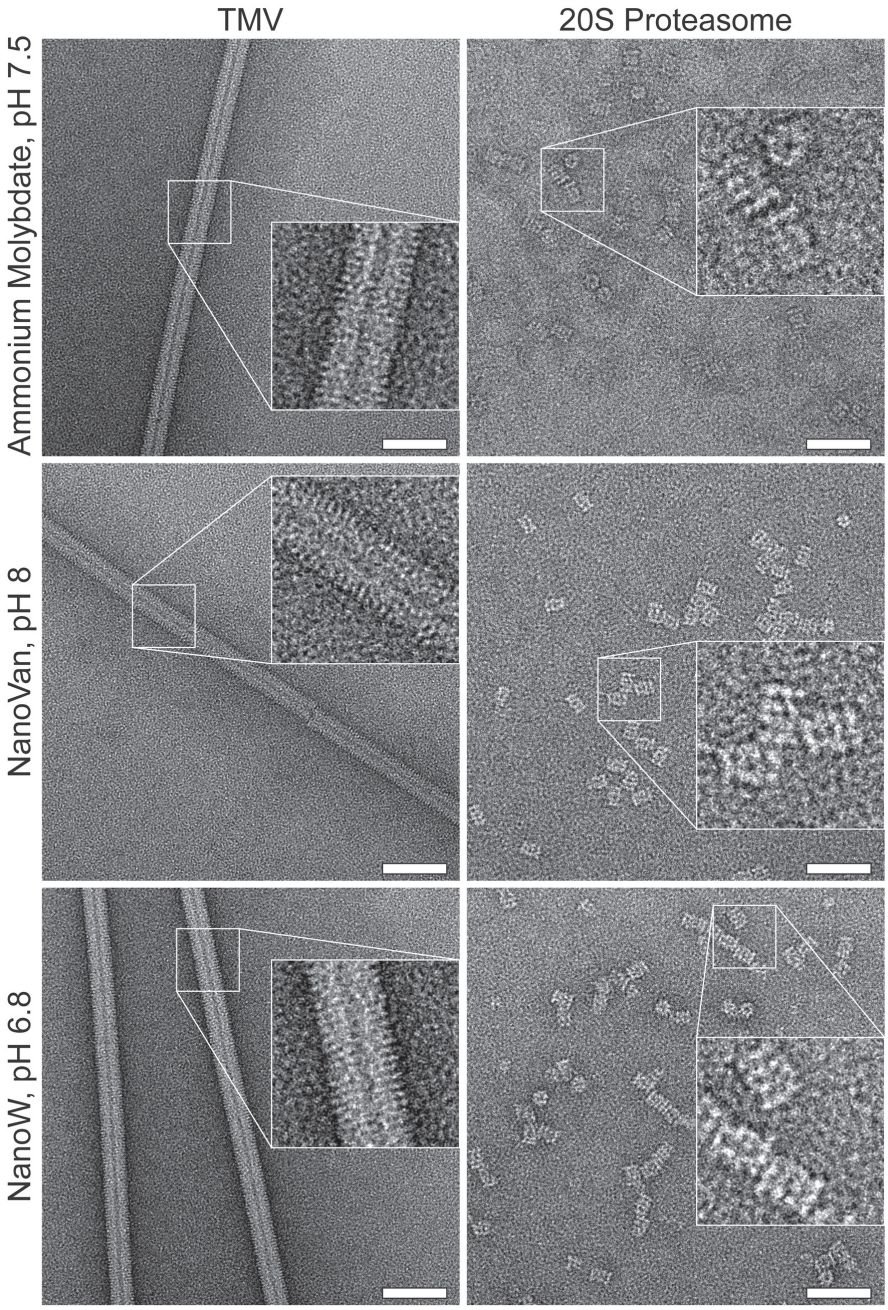

Figure 3.4: *Single particles negatively stained by immersion-diffusion sample conditioning of samples solved in PBS buffer. Note that PBS buffer forms insoluble aggregates with heavy metal salts; therefore, longer conditioning times are needed (compare with Figure 3.5). Test samples of TMV (left column) and 20S proteasome (right column), both in PBS buffer, were prepared using the indicated negative stain solutions by condition for 7 min in 2% solution (NanoW or NanoVan) or 0.5% (ammonium molybdate). These stains differed in pH and staining characteristics. Note the lighter staining obtained with NanoVan at pH 8. Scale bars represent 50 nm.*

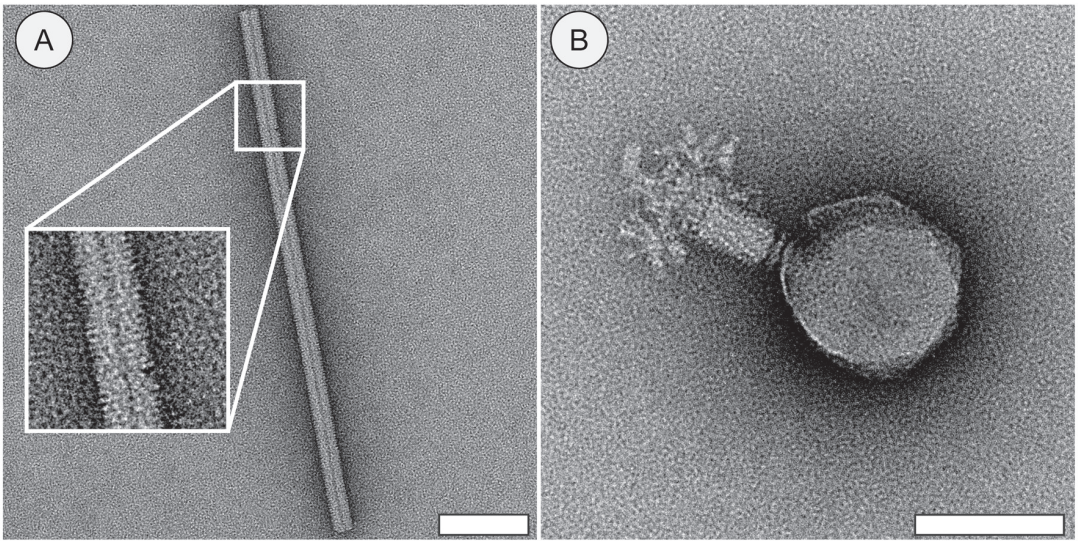

Figure 3.5: *Single particles negatively stained by immersion-diffusion sample conditioning of samples solved in 20 mM Tris-buffer. Scale bars represent 80 nm. The inset in (A) is magnified three times.*

3.2.3 Application note 2: Single-cell visual proteomics

An individual adherent mammalian HEK 293 cell was lysed using three voltage pulses (3 x 250 µs, 20 V) applied by a microcapillary electrode (MCE) positioned in PBS buffer 20 µm above the cell. Its lysate was immediately aspirated into the MCE tip in a 3 nl liquid volume of PBS. After immersion of the MCE tip into a reservoir of 2% NanoW, pH 6.8 for 10 min, a total of 5 nl liquid was deposited from it onto a glow-discharged EM grid. The larger volume was required to dilute the highly concentrated lysate sample for EM. The high quality of the staining is documented by Figure 3.6. A filamentous structure resembling actin is evident in Figure 3.6A, and membranes decorated with distinctive protein heads are visible in Figure 3.6B. These membrane structures look like mitochondrial membranes with ATP-synthases (Walker et al., 2006).

Figure 3.7A shows a representative image of the negatively stained single-cell lysate from a heat-shocked cell, and panel B shows the corresponding negative control. For the heat-shock, the HEK 293 cell culture was exposed to the elevated temperature of 40 °C for 1 h, whereas the negative control lysate was from a cell cultured in parallel and treated identically except that it was always at the physiological temperature of 37 °C. The frequency of ring-shaped structures was significantly increased in the single-cell lysate of the heat-shocked cell. Visually, these structures resemble negatively stained heat-shock proteins, *e.g.*, the ring-like shape and the 13±0.7 nm diameter of the large rings (Figure 3.7A, arrows) are in good agreement with the reported structure of the Tric/CCT complex (Booth et al., 2008; Leitner et al., 2012; Schirmer et al., 1996).

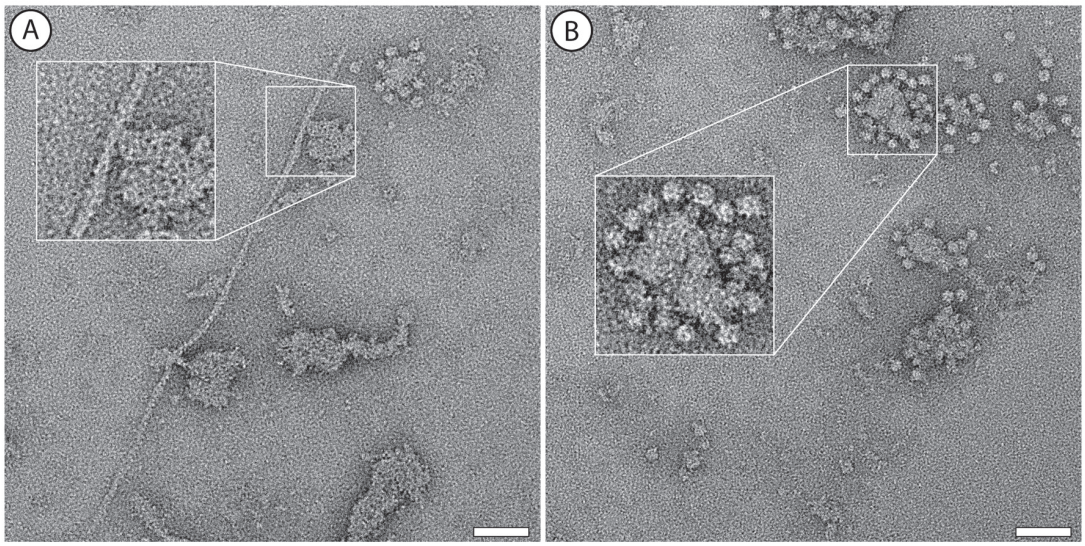

Figure 3.6: *TEM image of negatively stained single-cell lysate from a HEK 293 cell. Prior to the cell lysis, the cell-culturing medium was exchanged with PBS buffer. (A) Filamentous structures resembling F-actin. (B) Membranes decorated with distinctive heads, resembling mitochondrial membranes with ATP-synthases. Negative stain: 2% NanoW, pH 6.8. Scale bars represent 50 nm.*

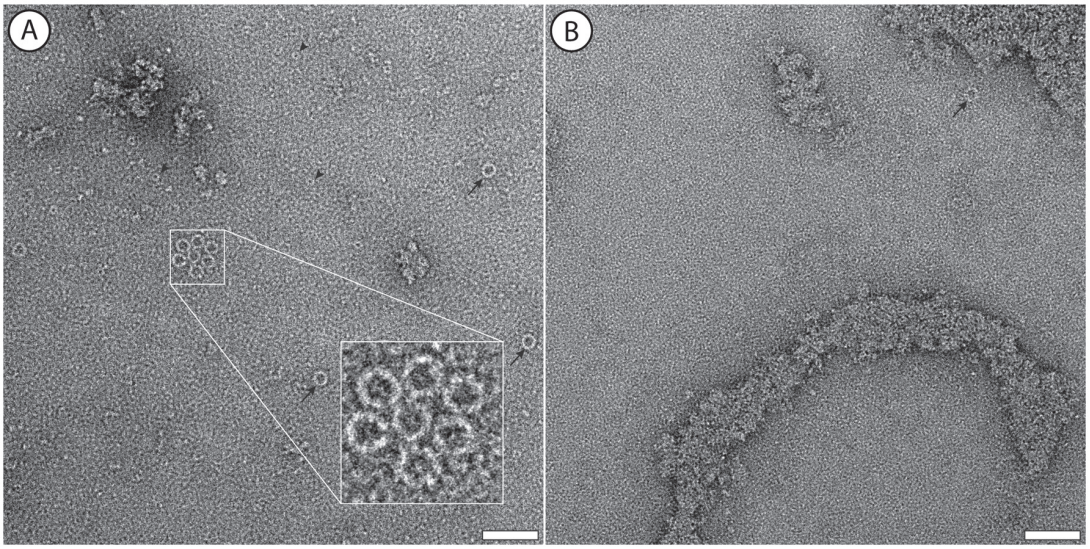

Figure 3.7: *The effect of heat-shock on HEK 293 cells visualized by negative stain TEM of single-cell lysate in PBS buffer. (A) Cell lysate from a single HEK 293 cell after exposure to a 1 h heat-shock at 40 °C. Multiple ring-shaped structures were found, and were related to heat-shock proteins, such as Tric/CCT. Some of them are marked by arrows (large complex) and arrowheads (small complex). (B) Representative negative-control image of single-cell lysate from a cell without prior heat-shock. Only occasionally ring-like structures resembling heat-shock proteins are visible (arrow). Negative stain: 2% NanoW. Scale bars represent 50 nm.*

3.2.4 Application note 3: Embedding protein nanocrystals in trehalose for cryo-EM

Figure 3.8 shows an overview TEM image and the diffraction pattern of a lysozyme nanocrystal. Lysozyme nanocrystals were grown by the sitting drop method in a 96-well crystallization plate (McPherson, 2004). 5 nl of a suspension containing nanocrystals not recognizable in a light microscope were aspirated from a crystallization well and conditioned in a 2.5% (w/v) trehalose solution for 6 min as described above, dispensed onto the EM grid, and air dried. The grid was subsequently frozen by manual plunging into liquid nitrogen, mounted into a cryo-EM sample holder, and inspected at liquid nitrogen temperature in a TEM by electron imaging and electron diffraction studies. Diffraction patterns with discernible spots at resolutions beyond 1 Å were recorded (Figure 3.8). In contrast, when the trehalose conditioning step was omitted, the grid was covered by large clumps of electron dense material (Supporting Information Figure B.3). The examination of pure water samples conditioned and deposited on the EM grid in the same way as the nanocrystals showed that trehalose was indeed present, forming a thin layer on the carbon/parlodion film covering the EM grid. Conditioning of the nanocrystals with pure water instead of trehalose, resulted in electron dense structures, however no diffraction was observed, suggesting that trehalose embedding and partial drying before freezing is a suitable method to preserve the structure of protein nanocrystals for EM investigations.
These results show that the conditioning method can be used for the preparation of 3D nanocrystals. This is not only of interest for investigations by electron diffraction and EM imaging but also for other analysis methods, such as serial crystallography achieved using synchrotron radiation or femtosecond exposures by X-ray free electron laser sources (Hunter et al., 2014).

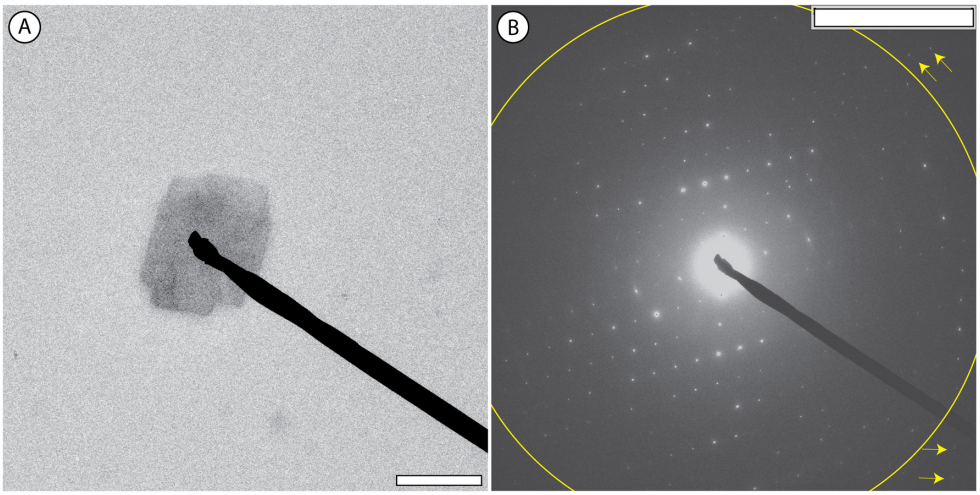

Figure 3.8: *Nanocrystals conditioned in 2.5% (w/v) trehalose for embedding. (A) Overview image showing a lysozyme protein crystal. (B) Electron diffraction of the nanocrystal depicted in (A). The yellow circle marks the resolution of 1/1 Å. Higher resolution diffraction spots are visible (yellow arrows). The scale bar represents 1 µm in (A) and 1/1.7 Å in (B).*

3.3 Conclusion

We present a method for the conditioning and preparation of nanoliter sample volumes for subsequent analysis by EM. We show that the method can be used to prepare protein samples for single particle negative stain TEM (Figure 3.4) and to embed nanocrystals in trehalose for high-resolution analysis by electron diffraction Figure 3.8). The minute amount and volume of material needed for sample preparation and the almost lossless procedure make it possible to study protein complexes of individual cells by a single-cell visual proteomics approach, as demonstrated by the heat-shock experiments (Figure 3.7).

3.4 Materials and methods

3.4.1 Instrument setup

The instrument setup (Figure 3.2) is a further development of the setup described by Kemmerling and Arnold et al. (Kemmerling et al., 2013), which was initially built for single-cell lysis. It is mounted on an optical table (TMC Ametek, USA) and built around an inverted microscope (Zeiss Axiovert 200, Germany) with a motorized stage (Prior Scientific, UK) and a live-cell incubator (Tokai Hit, Japan). A microcapillary or, for single-cell lysis, a microcapillary electrode (MCE), is fixed to a z-axis stage (M-404.2PD, Physik Instrumente, Germany). The microcapillary tip is centered over the microscope objective. For single-cell lysis, the MCE surface is electrically connected to a 20 x linear voltage amplifier (F20A, FLC Electronic AB, Sweden) and a function generator (33220A, Agilent, Switzerland) via a conductive sleeve. Cells are grown on a functionalized indium tin oxide (ITO) surface, which is grounded. The distal end of the microcapillary is connected to a high-precision syringe pump (Cetoni GmbH, Germany) and is filled with water (system liquid). Two surveillance cameras help to observe the experiments. All instruments are controlled via LabVIEW software. The openBEB software framework (www.openbeb.org, Ramakrishnan et al., 2014), developed in house, is used to load each instrument program as an independent plug-in. Many experimental steps, *e.g.*, cell lysis, sample loading, and sample deposition are now automatized using the macro language of openBEB.

3.4.2 Microcapillaries and microcapillary electrodes (MCE)

Three types of fused silica microcapillaries (New Objective Inc., Woburn, MA, USA) were used. These had the same outer diameter (OD), but different inner diameters (ID) and tapered tips (Table 3.1). The outer surfaces of the glass tips were made hydrophobic by quickly flaming the tip, followed by immersion in a solution of sulfuric acid and polydimethylsiloxane (Regenabweiser, WSM Penzing). For electrical cell lysis, the outer surface of the microcapillaries was coated in house with 2 nm of Ti/W and 200 nm of Pt by sputter deposition, and subsequently functionalized by immersion into a 1 M ethanolic solution of 1-dodecanethiol for 24 h to increase the hydrophobicity.

Type, OD-ID-TipD (μm)	Outer surface	Use
FS360-250-40	Fused silica glass	Test sample / Nanocrystals/ Au beads
FS360-250-40	Pt	Single-cell analysis
FS360-100-30	Fused silica glass	Low salt test samples / Nanocrystals / Au beads
FS360-100-30	Pt	Single-cell heat shock

Table 3.1: *Microcapillary specifications and application. FS: Fused Silica; Pt: additional in house coating with a Ti/W sticky layer and 200 nm Pt; OD: outer diameter; ID: inner diameter; TipD: inner diameter at the tip; Type: manufacturer's reference number.*

3.4.3 Sample conditioning by immersion-diffusion

The process of sample conditioning by immersion and diffusion is depicted in Figure 3.1. A few nanoliters of sample are aspirated from a lysed cell (Figure 3.1, A1) or from a sample stock delivered in a PCR tube (Figure 3.1, A2). Note that all capillaries are filled with system liquid (usually ddH_2O, in some cases also a 2% solution of negative stain ions in ddH_2O), which is in direct contact with the sample. The loaded microcapillary tip is immersed in a conditioning reservoir (100 μl) of negative stain (NanoW 2%, pH 6.8, or NanoVan 2%, pH 8, both from Nanoprobes, USA, or ammonium molybdate 0.5%, pH 7, #277908 from Sigma, Switzerland) or in a 2.5% (w/v) trehalose solution (TC-177, HiMedia Laboratories Pvt. Ltd., India) in H_2O for 6 to 12 min, mainly depending on the geometry of the microcapillary and the salt concentration in the sample. The transfer from the point of sample aspiration to the conditioning reservoir is automatized and only takes a few seconds. After conditioning via diffusive exchange of salt and negative stain ions or trehalose molecules (Figure 3.1B), the microcapillary is positioned above and close to a previously glow-discharged EM grid (200 mesh Cu grid, covered by a carbon-coated parlodion film). The sample is then dispensed onto the carbon surface and left to dry. A small spot that covers a few squares of the EM grid is formed (Figure 3.1C).

3.4.4 Diffusive exchange simulation

Diffusive exchange between the negative stain ions or trehalose, respectively, in the reservoir and the sample present in the microcapillary tip, as well as diffusive exchange between the sample and system liquid above it in the microcapillary, was simulated by the FEM in COMSOL Multiphysics 4.4. A 3D diffusion model was used with the transport of diluted species physics package. A simplified tapered microcapillary tip geometry with the tip centered inside a cube of 8 μl of negative stain or trehalose, was modeled. The negative stain or trehalose in the conditioning reservoir and the salt and protein in the sample plug were assigned typical concentrations and diffusion coefficients. The system liquid (double distilled water, ddH_2O, or negative stain) had a total volume of 50 nl. The concentration was integrated over the volume of the sample plug (4.5 nl) on a time scale from 0 to 10 min. The parameters used in the simulation are summarized in Table 3.2.

Solute	Conc. (mM)	Diff. coeff. (m^2/s)	Reference
Salt	130	2e-9	Bruus, 2008
Phosphate	10	8.8e-10	Stewart, 2003
NanoW 2%	80	8.8e-10	Approx. from Stewart, 2003
Trehalose 2.5%	66.1	5e-10	Stewart, 2003
Small proteins (13.4 kDa)	0.0746	1.14e-10	Young et al., 1980
Gold particles (5 nm)	0.00132	4.39e-11	Einstein, 1906
20S proteasome (870 kDa)	0.00115	2.28e-11	Tanaka et al., 1988

Table 3.2: *Simulation parameters. Typical concentrations were assigned to each solute. Diffusion coefficients were either obtained from literature, estimated by the Einstein-Stokes equation (gold particles), or approximated from known diffusion constants (tungstate and phosphate having similar hydration shells).*

3.4.5 Single particle test samples

20S proteasome (0.5 mg/ml, 20SP, human, purified, BML-PW8720-0050, Enzo Life Sciences) and TMV (kindly supplied by Ruben Diaz-Avalos, New York Structural Biology Center, USA) were aspirated from 0.2 ml PCR tubes containing a few microliters of sample prepared in PBS buffer (pH 7.4). A sample mixture containing TMV and Escherichia coli phages (vB_EcoM_CBA120 from Petr Leiman, Laboratory of Structural Biology and Biophysics, EPFL) in 20 mM Tris-HCl buffer (pH 7.4) with 50 mM NaCl served as the low-salt-containing sample.

3.4.6 Cell culture on conducting glass slides

Adherent mammalian cells (HEK 293, Sigma, Switzerland) were cultured in polystyrene T25 flasks at 37 °C and 5% carbon dioxide with eagle's minimal essential medium (E-MEM, M2279, Sigma-Aldrich) supplemented with 2 mM Glutamax (35050-038, Gibco), 1% MEM nonessential amino acids (M7145, Sigma, Switzerland), and 10% fetal bovine serum (10270-098, Gibco). To split the cells, the medium was removed, and the flask was washed with 5 ml of 37 °C warm PBS (Dulbecco's phosphate buffered saline; D8537, Sigma, Switzerland, 2.7 mM KCl, 1.5 mM KH_2PO_4, 136.9 mM NaCl, 8.9 mM $Na2HPO_4 \bullet 7H_2O$, pH 7.4). To detach the cells, 1 ml of trypsin-EDTA solution (0.05% trypsin, 0.53 mM EDTA; 25300-054, Invitrogen, Switzerland) was added, and the cells were incubated at 37 °C for 3 min. The detached cells were diluted with 5 ml of 37 °C warm E-MEM and homogenized using a pipet. After centrifugation, the cells were resuspended in 5 ml of fresh, 37 °C warm E-MEM for seeding. For single-cell experiments, an aliquot of the cell suspension was seeded onto miniaturized Petri dishes on ITO-coated glass slides (Diamond Coatings UK, 8-12 Ω/square). The Petri dishes were produced as follows: ITO-coated glass slides were sonicated in detergent solution (1% Alconox, Alconox Inc., USA) and ethanol for 10 min each, rinsed with ddH_2O, and dried in N2. Shortly before the cells were seeded onto the ITO slides, the slides were glow discharged and incubated with a 1:10 solution of poly-L-lysine in H_2O (P8920, Sigma, Switzerland) for 5 min. After a short wash with ddH_2O, the slides were dried at 60 °C for 1 h.

Poly(dimethylsiloxane) (PDMS, Dow Corning SYLGARD 184) rings were then pressed onto the ITO surface to form sample wells, *i.e.*, miniature Petri dishes, with a volume of about 300 µl. The PDMS wells were filled with cell culture medium (300 µl), and around 50 µl of HEK 293 cell suspension (10^4 cells) were added. The cultures were incubated for 1-2 days at 37 °C and 5% CO_2. Prior to the single-cell lysis experiments, the cell culture medium was removed, and the cells were washed twice with 37 °C warm PBS. The cells remained in PBS during the subsequent experiments.

3.4.7 Single-cell lysis

The ITO glass slide containing a sample well with live HEK 293 cells in PBS was placed in the slide holder on the inverted microscope of the cell lysis setup and put to electrical ground (Figure 3.2 A1). An individual cell was selected under the microscope, and the MCE tip was immersed into the buffer and placed 20 µm above it. Three short voltage pulses (3 x 250 µs at 16–20 V) were delivered via the MCE to the targeted cell. The cell lysed within milliseconds, and its content was directly aspirated into the MCE tip in 3 nl of liquid by the syringe pump. For more details, see our previous work (Kemmerling et al., 2013).

3.4.8 Heat-shock experiments

An ITO-coated glass slide with HEK 293 cells in cell culture medium was inserted into the live-cell incubator stage (Figure 3.2). A temperature sensor was used to measure the temperature of the cell culture medium and to give feedback to the temperature controller. The cells were held at 40 °C for 1 h under a 5 % CO_2 atmosphere. The culture medium was then replaced by 37 °C warm PBS buffer, and cell lysis was performed as described in the previous section. As a negative control, samples were prepared as described above from single cells from the same passage that were cultured in parallel without heat-shock, but otherwise under identical conditions.

3.4.9 Protein nanocrystallization and trehalose embedding

A lysozyme crystallization trial was set up in a 96-well plate with sitting drop geometry (McPherson, 2004). Wells were filled with 150 µl of reservoir solution containing 0.6 M NaCl and 0.1 M sodium acetate at three different pHs. Lysozyme (A 3711.0010, BioChemica, Germany) was dissolved in ddH_2O at a concentration of 50 mg/ml. Sitting drops were composed of 2 µl of lysozyme solution mixed with 2 µl of reservoir solution. After 7 days, 5 nl of crystallization solution were collected from a well (pH 4.5) that showed no visible crystals under the light microscope. The microcapillary tip containing this solution was then immersed in a reservoir of 2.5% (w/v) trehalose for sugar embedding. After 6 min, the microcapillary was raised, and the sample was directly deposited from its tip onto a glow discharged EM grid.

3.4.10 Electron microscopy

Low-magnification overview images were acquired with a Philips CM10 (LaB6) TEM operated at 80 kV and equipped with a 2k CCD camera (Olympus SIS, Münster, Germany). Higher magnification images were taken on a Philips CM200 (FEG) TEM operated at 200 kV and equipped with a TVIPS F416 4k CMOS camera (TVIPS, Germany). Electron diffraction was performed on the Philips CM200 TEM. The grid was cooled to liquid nitrogen temperature, placed in a Gatan-626 cryo-holder, inserted into the microscope, and imaged at cryo temperatures at around -180 °C. The camera length was 1 m. The exposure time was 200 ms, and the electron dose per recording was approximately 5 e-/Å^2.

Acknowledgments

We thank the workshop of the Biozentrum of the University Basel for their support and S. Müller (C-CINA, Biozentrum, University of Basel) for carefully reading the manuscript. The project was supported by the Swiss Nanoscience Institute (SNI, projects P1201, P1305 and Nano Argovia SCeNA) and the Swiss National Foundation (SNF, project 200021_162521).

Competing financial interests

The authors declare the following competing financial interest: The conditioning concept is part of the patent application PCT/EP2015/065398.

Supporting information

The Supporting Information is available free of charge on the ACS Publications website at DOI: 10.1021/acsnano.6b01328. S1 shows the desalting progress of single-cell lysate sample during conditioning. S2 shows experimental verification of the FEM simulations. S3 demonstrates the need for conditioning of 3D crystals prior to EM grid preparation
Supporting information associated with this article can also be found in Appendix B.

Chapter 4

Blotting-free and lossless cryo-electron microscopy grid preparation from nanoliter-sized protein samples and single-cell extracts

Stefan A. Arnold[a,b], Stefan Albiez[a], Andrej Bieri[a], Anastasia Syntychaki[a], Ricardo Adaixo[a], Robert A. McLeod[a], Kenneth N. Goldie[a], Henning Stahlberg[a] Thomas Braun[a,*]

[a] Center for Cellular Imaging and NanoAnalytics (C-CINA), Biozentrum, University of Basel, Switzerland
[b] Swiss Nanoscience Institute (SNI), University of Basel, Switzerland
[*] Corresponding author: thomas.braun@unibas.ch

Published in Journal of Structural Biology, 197 (3), 220–226, (2017); **DOI:** 10.1016/j.jsb.2016.11.002

Abstract

We present a sample preparation method for cryo-electron microscopy (cryo-EM) that requires only 3 to 20 nanoliters of sample to prepare a cryo-EM grid, depending on the protocol used. The sample is applied and spread on the grid by a microcapillary. The procedure does not involve any blotting steps, and real-time monitoring allows the water film thickness to be assessed and decreased to an optimum value prior to vitrification. We demonstrate that the method is suitable for high-resolution cryo-EM and will enable alternative electron microscopy approaches, such as single-cell visual proteomics.

4.1 Introduction

In recent years, transmission electron microscopy (TEM) of vitrified specimens (cryo-EM; Dubochet et al., 1988) has become a powerful technique for the high-resolution structural analysis of biological matter (Liao et al., 2013), and is now increasingly recognized as a mainstream tool in biology (Callaway, 2015; Kühlbrandt, 2014; Nogales, 2015). Several technical achievements have made this development possible, the most prominent being the recent introduction of direct electron detection (DED) cameras (Milazzo et al., 2011; Ruskin et al., 2013; Veesler et al., 2013), and the availability of improved data processing algorithms (Grigorieff, 2007; Lyumkis et al., 2013; Scheres, 2012).
Cryogenic sample-grid (cryo-EM grid) preparation and imaging methods ensure that biological specimens withstand the ultra-high vacuum inside electron microscopes, allow their investigation while trapped at physiological conditions that conserve the structural arrangement of the biomolecules and reduce the effect of radiation damage (Baker et al., 2010; Dubochet et al., 1988; Lepault et al., 1983). However, these preparation methods have not improved significantly over the last 20 years and have some major drawbacks: A 2-4 µl sample volume is required, and 99.9% of the sample volume is lost during grid preparation, due to an extensive blotting step made with filter paper (Kemmerling et al., 2012). Furthermore, blotting with filter paper can lead to protein aggregation or denaturation. The current state of the art sample preparation methods are recognized as one of the most significant limitations in cryo-EM (Glaeser, 2016).
Improved cryo-EM grid preparation strategies that reduce sample consumption are now an essential requirement. A device that combines ink-jet picoliter dispensing with a plunge-freezing apparatus was presented in 2012 (Jain et al., 2012), and was recently refined by the use of self-blotting grids to allow cryo-grid preparation in combination with ink-jet spotting (Razinkov et al., 2016). Here, we present a paper blotting- and spotting-free method that requires total sample volumes of just a few nanoliters (*e.g.*, 3-20 nl). It uses a microcapillary to directly 'write' the sample on holey carbon EM grids and subsequently vitrifies the deposited liquid, producing thin layers of vitrified specimen in the holes of the carbon film.

4.2 Materials and methods

The instrument presented here is described in the results section. Additional aspects were published previously, such as the conditioning and preparation of nanoliter volumes for negative stain EM, or the single-cell lysis and aspiration device using a microcapillary electrode (Arnold et al., 2016; Kemmerling et al., 2013). Supporting Information C.1 provides a detailed description of the setup, including a parts lists and details of the method. Supporting Information C.2 describes the control software.

4.2.1 Chemicals and buffers

All chemicals were ordered from Sigma-Aldrich, Switzerland if not otherwise indicated. The following buffers were used: PBS, Dulbecco's Phosphate Buffered Saline, 2.7 mM KCl, 1.5 mM KH_2PO_4, 136.9 mM NaCl, 8.9 mM $Na_2HPO_4 \bullet 7H_2O$, pH 7.4; Tris-HCl buffer, 20 mM Tris-HCl, 50 mM NaCl (pH 7.4); HEPES buffer, 10mM HEPES pH 8.0, 50 mM KCl.

4.2.2 Test samples

The test samples were (i) tobacco mosaic virus (TMV) in PBS containing 0.1% decyl-β-D-maltopyranoside (DM, Anatrace), (ii) a mixture containing apoferritin and phages against *Escherichia coli* (vB_EcoM_CBA120) in Tris-HCl buffer, and (iii) a purified 200 kDa membrane protein (name not disclosed) reconstituted in amphipols. In this case, the bulk membrane protein sample was applied to a S200 10/300GL size exclusion chromatography column equilibrated with HEPES buffer complemented with 5 µM sodium azide. A single 300 µl fraction corresponding to the center of the major A280 peak was used to prepare cryo-EM grids (a) by using the cryoWriter and (b) by using a Vitrobot IV plunge-freezer (FEI, USA). The protein concentration of this fraction was 0.35 mg/ml as determined by absorbance measurement using an UV-Vis spectrophotometer (Nanodrop 2000, Thermo Fisher Scientific Inc.) and assuming Abs(0.1%)=1. (iv) Urease from *Yersinia enterocolitica* bacteria at a concentration of 0.35 mg/ml in PBS buffer.

4.2.3 EM grids

Various EM grids were used with the cryoWriter, such as 200-mesh copper grids with holey carbon film (R2/2, R2/1, and R1.2/1.3, Quantifoil, Germany), as well as holey carbon grids with an additional layer of continuous carbon, and lacey carbon grids. EM grids were glow discharged for 30 s in air plasma immediately before use. Note that the flatness of the grid is an important aspect, both for the mechanical writing step and for efficient heat-transfer when the grid is on the temperature controlled dew point stage (DP-stage) of the cryoWriter.

4.2.4 Cryo-grid preparation

The two deposition protocols used with the cryoWriter setup are detailed in the sections below and in Supporting Information C.1.

4.2.5 Electron microscopy and single particle analysis

Unless otherwise specified, the EM grids with test samples were placed in a Gatan-626 cryo-holder and imaged in a Philips CM200 (FEG) TEM operated at 200 kV and equipped with a TVIPS F416 4k CMOS camera (TVIPS, Germany).

Images of urease for single particle analysis were acquired using a FEI Titan Krios, operated at 300 kV and equipped with Gatan Quantum-LS (zero-loss slit width of 20 eV) and Gatan K2 Summit DED camera. Low dose conditions were applied with a total electron dose of 50 e-/Å^2 at a dose rate of 5-6 e-/physical-pixel/sec for a stack of 40 images obtained in movie mode. Drift- and contrast transfer function (CTF) correction was applied to the urease data with the Zorro software (McLeod et al., 2017) using CTFFIND4 (Rohou et al., 2015). Approximately 10'000 particles were manually selected from the 51 micrographs recorded using EMAN2 (G. Tang et al., 2007) and subsequently processed in RELION-1.4 (Scheres, 2012). After particle alignment, around 8'700 particles yielded good 2D class averages that were subsequently used for the 3D classification. The two best 3D classes were selected (containing 7'800 particles) and iteratively refined. A final sharpening of the map was then performed, yielding the final 3D reconstruction of the urease complex. The atomic model (PDB: 10.2210/pdb4z42/pdb) was fitted into the 3D map using the UCSF chimera software (Pettersen et al., 2004).

4.3 Results

4.3.1 Principles and setup

The cryoWriter setup and the principles of the method are depicted in Figure 4.1; further details can be found in Supporting Information C.1 and C.2. The cryoWriter is integrated into a liquid handling and transfer system developed previously for nanoliter-volume sample conditioning and EM grid preparation for negative stain and trehalose embedding (Arnold et al., 2016) and is not enclosed in a humidity-controlled environment. The method uses a high-precision pipetting system to control liquid uptake and dispensing by a microcapillary, a temperature-controlled DP-stage to control the environment of the EM grid, a real-time monitoring system to control the thickness of the sample layer, and a pick-and-plunge-mechanism for sample vitrification. The entire process is controlled by an openBEB (Ramakrishnan et al., 2014) plug-in developed in LabVIEW (Elliott et al., 2007) and can be automated using macros (see Supporting Information C.2).
The setup for cryo-grid preparation and the basic procedure (Figure 4.1) are as follows:
(i) Grid cooling: a glow-discharged standard holey carbon film EM grid held by tweezers is positioned on the cold DP-stage. (ii) Sample up-take; a microcapillary and high-precision pump system are used to aspirate a liquid plug from a sample stock or the lysate of a single cell immediately after electrolysis, as described previously (Arnold et al., 2016; Kemmerling et al., 2013). (iii) Sample deposition (Figure 4.1a), the microcapillary tip is brought into close proximity of the grid surface. The sample is then dispensed from the microcapillary to form a small liquid droplet that spans the gap between the microcapillary tip and the hydrophilic (glow-discharged) holey-carbon surface of the EM grid. Simultaneously, the grid is moved relative to the nozzle in a sinusoidal or circular pattern; the liquid sample is spread-out over the surface filling the holes of the carbon film. (iv) Sample stabilization and thinning by controlled water evaporation (Figure 4.1b and dedicated section below); the temperature

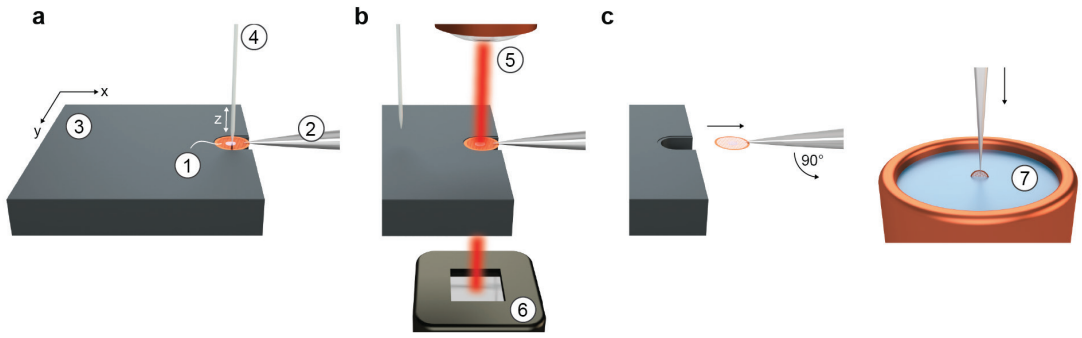

Figure 4.1: *Working principle of the cryoWriter device. For further details, see Supporting Information C.1–C.2. (a) A standard holey carbon film EM grid (1) is mounted between the tips of tweezers (2) and positioned flat (horizontal) in a slot in a temperature-controlled dew point stage (DP-stage) (3). The DP-stage temperature is set close to the dew point temperature and can be regulated using a PID Peltier controller. The EM grid is in good thermal contact with the stage. The DP-stage (3) is mounted on a motorized xy axis to move the grid relative to a microcapillary (4), which can be lowered to a few micrometers above the grid. This microcapillary deposits a few nanoliters of sample while the stage is moving in a sinuous pattern, covering an area of about 0.5 mm^2. (b) After sample deposition, the microcapillary is withdrawn and the stage (3) moves to position the grid (1) between an IR laser (λ = 780 nm; 5) and a photodiode (6). Light scattering and interference effects from the thin aqueous sample film on the grid change as water evaporates (see Fig. 4.2 and Supporting Information C.3). (c) A trigger automatically initiates plunge-freezing when the photodiode signal reaches a defined threshold level. The tweezers and grid are rapidly withdrawn from the stage, flipped by 90 degrees into the vertical position and plunged into a cryogen (7). This whole pick-and-plunge process takes a few hundred milliseconds. See Supporting Movie 1 (online).*

of the DP-stage is set to keep both the EM grid and the suspended sample at a specified temperature close to the dew-point temperature of the room, throughout. Note that the grid is not immediately vitrified, but can be kept on the stage for a short time (between <1 and 10 s, depending on the chosen offset temperature), so that a certain amount of sample water can evaporate. Interference/scattering effects from interaction of the grid and applied aqueous sample with a 780 nm laser beam can be used to monitor the evaporation (Figure 4.2). The controlled loss of some water is important to ensure that a thin water film spans the holes of the carbon layer. (v) Cryo-grid pick-and-plunge freezing (Figure 4.1c); the mechanism is triggered by the monitoring system or after a pre-set time, rapidly plunging the grid (and tweezer tips) into a liquid ethane/propane (40:60) bath (Tivol et al., 2008) for vitrification (see also Supporting Information C.1 and Supplementary Movie 1).

Two deposition protocols can be used with this basic procedure, depending on the experiment and sample. In Protocol 1, a relatively large volume (20 nl) is deposited on the grid, excess sample is removed and recovered by re-aspiration with the dispensing microcapillary; this protocol is ideal for the preparation of large EM imaging areas of purified protein complexes for single-particle analysis and high-resolution structure determination. In Protocol 2, a ~3 nl sample volume is directly deposited on the grid, avoiding the need for a re-aspiration step. This protocol is better suited for applications that are restricted to minute volumes, *e.g.*,

single-cell visual proteomics (Arnold et al., 2016; Engel, 2010; Kemmerling et al., 2012). These protocols are described in detail below:

Protocol 1: Deposition with recovery of excess sample

The microcapillary and the high-precision pump system are used to aspirate a few tens of nanoliters from a sample stock. The microcapillary tip is then lowered to the glow-discharged grid surface (separation 10 μm) and a 20 nl drop of sample is dispensed from it. The drop spans the gap between the microcapillary tip and the EM grid and can be spread further to cover an area of ∼0.5 mm^2 by moving the grid relative to the microcapillary (Figure 4.1a). Subsequently, the microcapillary tip is lowered to touch the grid surface within this area and re-aspirate as much excess sample as possible, recovering this for future use. The temperature of the DP-stage (and the grid) is kept above the dew-point temperature of the room for all of these steps, to allow a minimal amount of water to evaporate. A temperature offset from the dew point of +8 °C, combined with immediate plunge-freezing after re-aspiration of excess sample, typically results in a good sample thickness for high-resolution structural analysis. If more precision is required, the thickness of the sample film can be optimized by controlled water evaporation using the real-time monitoring system described below. A more extensive discussion of the sample thinning process can be found in the dedicated section 4.3.2.

Protocol 2: Direct sample deposition without re-aspiration

With this protocol, ∼3 nl of sample are directly deposited onto the grid, avoiding the re-aspiration step. The grid temperature is kept at the dew point to avoid water evaporation, and the tiny sample droplet is spread by moving the EM grid underneath the microcapillary tip in a sinusoidal or circular pattern covering an area of approx. 0.5 mm^2. Subsequently, a sample-thinning step must be performed by controlled water evaporation before plunge-freezing. Evaporation is induced by increasing the DP-stage temperature to a value slightly above the dew point of the room (*e.g.*, +2 °C). To obtain reproducible results with these small volumes, the sample thinning process must be supervised by the monitoring system (see dedicated section).

4.3.2 Sample stabilization and thinning by controlled water evaporation

Due to surface tension effects, even extremely small sample aliquots must be thinned for the grids to be usable for cryo-EM. Recently, an interesting method was demonstrated using "self-blotting" grids in combination with ink-jet spotting (Razinkov et al., 2016). Here, we propose a method based on the controlled evaporation of sample water to create thin sample layers. Sample film thickness can be tuned by adjusting the temperature of the DP-stage and the time span before pick-and-plunge-freezing is initiated (see also Supporting Information C.3, section I). The sample is concentrated by water evaporation. This might be desirable

for the protein, but salt concentrations also increase, which can potentially harm protein complexes. Thus, thinning in this way is limited to sample films that are already thin, making the re-aspiration of samples prepared by deposition protocol 1 essential, as demonstrated by Supporting Information C.4. Note that, if necessary, the liquid handling and transfer system supporting the cryoWriter would allow sample conditioning, *e.g.*, salt exchange by a diffusion driven process (Arnold et al., 2016) before cryo-grid preparation.
The cryoWriter setup includes a laser diode (780 nm; Figure 4.1b) and a photo detector to follow the evaporation of sample liquid from the grid in real-time. At 780 nm wavelength, light is not significantly absorbed by water or biological material, making the amount of heat transferred to the sample negligible (Bircher et al., 2013). Nevertheless, changes in the water film thickness due to evaporation has a detectible effect on the amplitude of the signal recorded by the photodetector. Besides changes in light scattering, the transmitted light signal is also affected by interferences between light waves reflected at the surfaces of the thin film (Figure 4.2). As water evaporates, the signal increases approximately linearly,

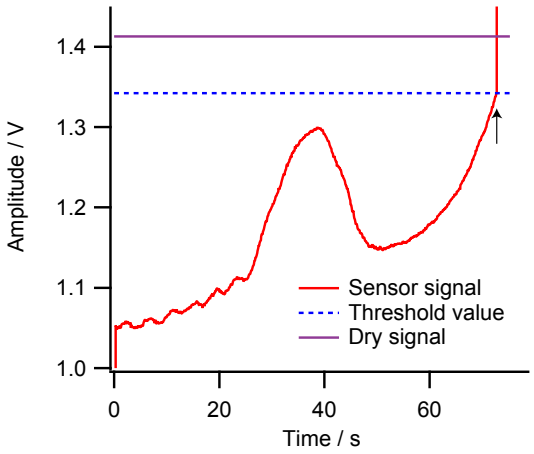

Figure 4.2: *Real-time monitoring of water evaporation from the sample to control the thickness of the vitreous ice layer. The transmitted light of a 780 nm laser is used to register changes in the water-layer thickness before vitrification (see Fig. 1b). The purple (static) line is the signal obtained with the dry grid (dry signal). The red line is the sensor signal recorded after sample deposition during water evaporation (stage temperature 2 °C above the dew point). Empirically, it was found that useable grids are obtained when the sensor signal is about 95% (blue line) of the dry signal. The pick-and-plunge mechanism is triggered when this threshold is reached (indicated by an arrow), leading to the rapid vitrification of the cryo-EM grid (within a few hundred milliseconds). The plot shows the characteristic evolution of the signal over time as sample water evaporates and the very steep increase that occurs as the grid is removed from the optical laser-path (arrow). This graph was chosen for clarity, as it shows a large volume (20 nl) evaporating for a long time at a small offset from the dew point (2 °C). In reality, less sample is deposited (or sample is re-aspirated beforehand), and only the last few seconds of the plot can be recorded.*

until a specific layer thickness is reached where it starts to increase sharply. We attribute this positive peak to constructive interference of the almost perpendicular beam at the layer thickness, $d \simeq \lambda/(2n)$, for wavelength $\lambda = 780$ nm and $n_{780} = 1.329$ (Hale et al., 1973). A negative peak directly follows the positive peak as expected from destructive interference. As detailed in Supporting Information C.3 section II, a laser diode with an emission peak at

around 405 nm instead of at 780 nm was used to prove that the observed signal behavior (Figure 4.2) was primarily due to interference effects. Once a specific user-defined threshold of the signal relative to the absolute signal obtained with the dry grid (see Figure 4.2 for an explanation) is reached, the pick-and-plunge mechanism is triggered by the monitoring system, whereby the cryo-grid is rapidly vitrified.
Note that the "dry signal" depends on the grid type and mesh size. As the difference is significant, a "blank" measurement always needs to be made before sample deposition (Figure 4.2). By contrast, the signal does not depend on the type of sample deposited on a specific grid type/mesh, making it possible to perform screening runs using buffer alone (without sample) to determine the ideal freezing conditions for the experiment.

4.3.3 Proof of concept cryo-grid preparation from different samples

The examples in this and the following section show that the cryoWriter setup can be used to prepare high-quality cryo-EM grids of different biological samples (*e.g.*, soluble or membrane protein particles, filamentous assemblies, viruses, cell lysate) for various purposes, such as structure determination by single particle analysis (demonstrated below) or helical analysis, and single-cell visual proteomics (Engel, 2010). In practice, the choice of the deposition protocol used for a specific sample depends on its properties and the aim of the experiment. The method is not sensitive to the buffer system employed, as shown in later sections.
The use of the cryoWriter and deposition protocol 1 to spread a 20 nl sample volume on a glow-discharged holey carbon film is demonstrated in Figure 4.3. For all preparation steps, the DP-stage temperature was kept 8 °C above the dew point. Subsequently, excess sample was re-aspirated and sample-thinning was performed for 1 s before plunge-freezing. As documented by Figure 4.3a, the sample that remained after re-aspiration formed a homogeneous vitreous ice layer covering a part of the cryo-grid; the periphery of the region is visible and indicated by arrows. The homogeneity of the layer is confirmed by Figure 4.3b, which shows the holey carbon film at higher magnification to demonstrate that the sample layer spans the holes of the carbon support. Figure 4.3c shows the high quality of the apoferritin particles (ring-like appearance) and bacteriophages prepared by this method. The architecture of the bacteriophage tail is revealed (inset). Note the absence of crystalline ice structures, indicating that the sample layer on the grid is indeed vitrified. Further examples are shown in the single particle processing section and in Supporting Information C.4.
The use of the cryoWriter and deposition protocol 2 to distribute 3 nl of sample onto a glow-discharged holey carbon film is demonstrated in Figure 4.4. Sample thinning was performed by monitored water evaporation as detailed in the dedicated section above. Figure 4.4a shows an overview of a typical grid. The area covered by the vitreous sample is generally smaller than the area covered when deposition protocol 1 is used. Furthermore, the thickness of the vitrified sample-layer is not as homogeneous (compare Figure 4.4a and Figures 4.3a and b); although the patterned liquid regions deposited by protocol 2 spread out on the hydrophilic grid, a thickness gradient remains due to the surface tension and because water evaporates faster at the periphery of the wet areas. The lower evaporation rate at the center

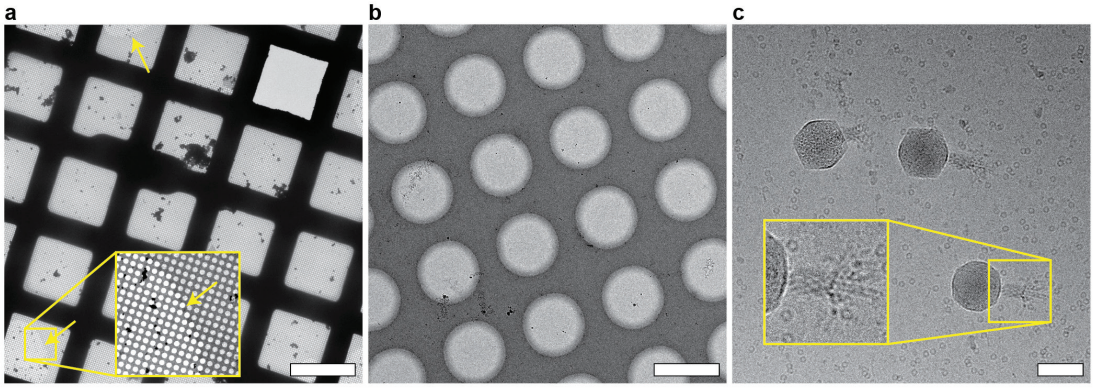

Figure 4.3: *Proof-of-concept data for cryo-EM grid preparation using the cryoWriter device and deposition protocol 1. A total sample volume of 20 nl was applied to a Quantifoil Cu 200 mesh R2/1 grid; excess liquid was re-aspirated to recover as much sample as possible. The DP-stage temperature was 8 °C above the dew point at all times, which resulted in rapid sample thinning; the grid pick-and-plunge mechanism was automatically triggered immediately after re-aspiration of excess sample. (a) Typical overview of a prepared grid showing a thin film of vitreous ice. Yellow arrows indicate its borders. Inset: fourfold enlargement of a border region after contrast adjustment to improve visibility. Note the continuous and homogenous layer of vitreous sample. Scale bar: 100 µm. (b) Higher magnification overview image demonstrating that the sample layer in the holes is homogeneous. Scale bar: 2 µm. (c) Apoferritin particles and bacteriophages in Tris-HCl buffer prepared by this method and imaged at high magnification and defocus to increase contrast. Inset: twofold enlargement of the indicated region showing a bacteriophage tail and a few ring-shaped apoferritin complexes. Scale bar: 80 nm.*

of the sample area is probably a consequence of the larger surface/volume ratio at the droplet periphery, a transiently higher humidity above the grid due to evaporated water and because the less efficient compensation of the evaporation-induced cooling by heat-flow from the grid to the sample droplet in the center.

The thickness gradients observed when protocol 2 is applied to holey carbon films are a drawback. They could be minimized for some samples by using traces of surfactants, or reduced to a lesser extent for all samples by using EM grids covered with thin continuous carbon films (see Supporting Information C.5). However, this is not essential. Cryo-EM can be performed on samples with slightly uneven ice thickness, as demonstrated by Figures 4.4b and c. An image of a 200 kDa membrane protein stabilized with amphipols recorded from a holey carbon cryo-grid prepared using the cryoWriter and protocol 2 is shown in Figure 4.4b. Images of the same protein prepared on thin carbon film for negative-stain TEM and on lacey and holey carbon for cryo-EM using either a Vitrobot plunge-freezer or the cryoWriter, are shown in Supporting Information C.5. Whereas the negative stain image shows intact single particles, degraded particles are found regularly on the grid prepared for cryo-EM by the classic plunge-freezing approach, potentially due to the blotting step. By contrast, the cryo-EM grid prepared with the cryoWriter exhibits a higher protein particle concentration and a higher proportion of homogeneous particles than grids prepared using the classic plunge-freezing approach.

The minute volume consumed when deposition protocol 2 is used, allows cryo-grid prepa-

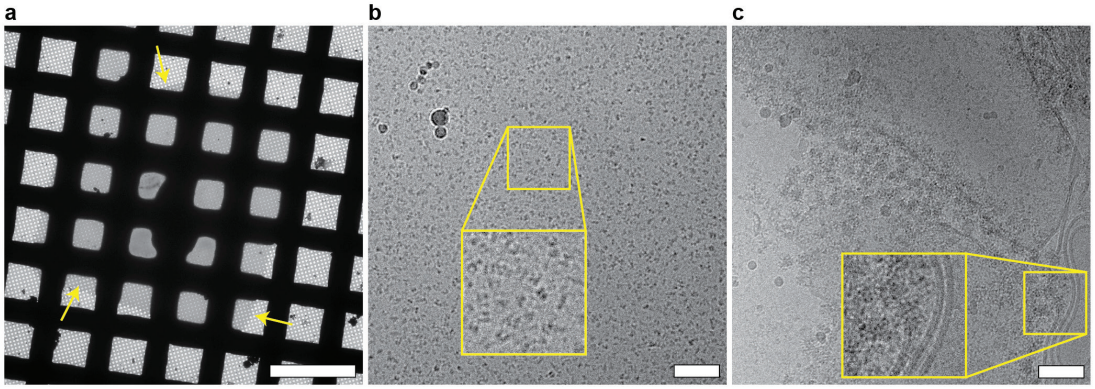

Figure 4.4: *Proof-of-concept data for cryo-EM grid preparation using the cryoWriter device and deposition protocol 2. In each case, a 3 nl sample volume was directly applied to the grid; no sample was re-aspirated. The grid was vitrified after sample thinning by controlled water evaporation. (a) Overview image of a 3 nl sample volume (urease in PBS buffer) in the middle of a Quantifoil Cu 400 mesh R2/2 grid. Note that the layer thickness has a gradient in some regions. The periphery of the vitreous ice is indicated by yellow arrows. Scale bar: 100 µm. (b) Image of a delicate 200 kDa membrane protein reconstituted in amphipols. Inset: twofold enlargement of the indicated region clearly showing the protein particles. Scale bar: 80 nm. See Supporting Information C.5 for a comparison with other sample preparation methods. (c) Example of lossless cryo-grid preparation of the lysate from a single adherent eukaryotic cell. An individual HEK cell growing on a functionalized ITO light microscopy slide was lysed by electroporation and quickly aspirated in a total volume of 3 nl. Subsequently, the lysate was dispensed on the grid using protocol 2 and vitrified. Scale bar: 80 nm.*

ration from samples that are otherwise inaccessible. For example, the lysate of a single eukaryotic cell can be examined. To demonstrate this, adherent HEK 293 cells were cultured on conducting glass slides and an individual target cell was identified in a light-microscope, electroporated and aspirated using a microcapillary as described previously (Arnold et al., 2016; Kemmerling et al., 2013). The same platinum-coated microcapillary was used for electroporation, cell lysate aspiration and dispensing, thus minimizing the exposure of the tiny amount of biological material to surfaces and the resulting loss of cellular components. Lysate deposition using protocol 2 gave high-quality cryo-grids as shown by Figure 4.4c and typical membrane structures with associated proteins are visible. More examples of single cell lysate prepared using sample deposition protocol 2 are shown in Supporting Information C.6.

It's difficult to quantify the amount of water that evaporates before plunge-freezing, despite we can monitor the layer thickness. First, the area covered with sample during the deposition process is larger (approx. 0.5 mm^2) than the vitreous ice area observed in the EM, most prominent using deposition protocol 2 (vitreous sample area approx. 0.1 mm^2; Figure 4.4a). Second, the dry areas of the grid show traces of sample, indicating that salts and protein also spread to these regions and were not collected and concentrated in the remaining thin vitreous layer on water evaporation. This will always be the case when the substrate is hydrophilic. Note that slight water evaporation from the sample is crucial to obtain thin sample layer suitable for cryo-EM in general (see also the discussion).

4.3.4 Single particle analysis

In order to demonstrate the usefulness of the cryoWriter method for high-resolution structural analysis, urease from *Yersinia enterocolitica* bacteria was prepared for cryo-EM using deposition protocol 1, and imaged with a Titan Krios microscope equipped with a DED camera (see Materials and Methods).
Figure 4.5a documents the high quality of the sample grid. Class averages selected from an initial 2D classification are shown in Figure 4.5b. Subsets of particles were selected from the classes generated and used in the final processing steps (Figure 4.5c). Refinement according to the "gold-standard" (R. Henderson et al., 2012; Scheres et al., 2012) yielded a 3D reconstruction of the tetrameric complex at a resolution of 5.03 Å according to the Fourier shell correlation (FSC = 0.143, Supporting Information C.7).

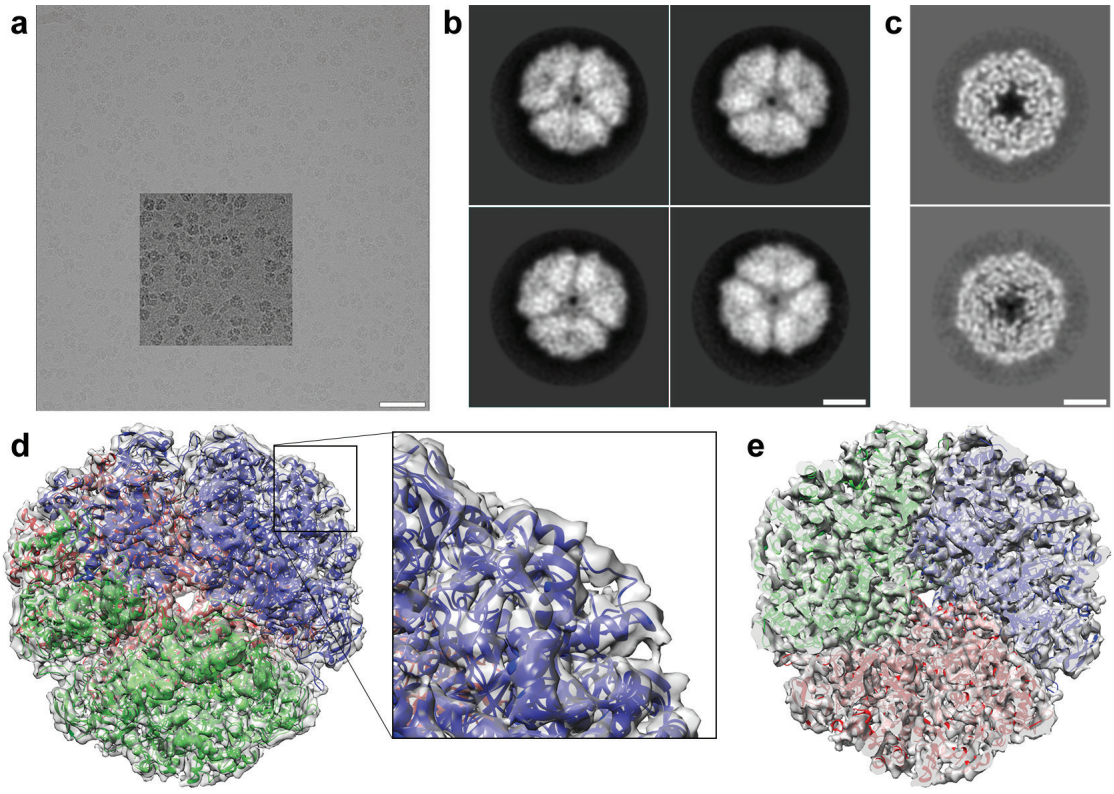

Figure 4.5: *Use of the cryoWriter to prepare samples for high-resolution structural analysis; proof-of-concept. A 20 nl volume of urease in PBS buffer was deposited on a Quantifoil Cu 200 mesh R1.2/1.3 grid using deposition protocol 1. (a) Drift-corrected cryo-EM image of urease particles embedded in vitreous ice. Inset: the particles with increased contrast. Scale bar, 50 nm. (b) 2D class averages including ∼3'400 of the 10'000 particles initially selected. Scale bar, 5 nm. (c) 3D class averages including ∼5'370 of the 8'700 particles identified for further processing. Scale bar, 5 nm. (d) Urease density map at 5.03 Å resolution, viewed perpendicular to its threefold axis; the backbone of the fitted X-ray model is shown (DOI: 10.2210/pdb4z42/pdb). (e) A cross-section of the urease density map and the fitted X-ray model perpendicular to the threefold symmetry axis.*

4.4 Discussion

This work was motivated by the need for improved sample-grid preparation methods for cryo-EM and the need to prepare such grids using minimal amounts of sample (nanoliters). The cryo-EM sample deposition and vitrification tool described here only consumes 3 to 20 nl of sample per grid and can be used together with different types of sample, *e.g.*, single particle preparations of soluble and membrane proteins, viruses and bacteriophages, or whole cell lysate. The setup includes a monitoring system to allow controlled thinning of sample films and the automatic activation of the pick-and-plunge mechanism once a defined threshold is reached. Importantly, freezing conditions and this thickness threshold can be determined using grids prepared with buffer alone instead of the actual sample.

Other important aspects are that the cryoWriter method works with minimal sample loss and does not involve any paper blotting steps. The experience of many laboratories that rely on cryo-grid preparations shows that classic preparation methods can be detrimental to the preservation of delicate protein complexes. This is often attributed to the paper blotting step or to the large surface to volume ratio of the sample film after blotting. The former can rapidly change the buffer characteristics of the sample (salt, pH changes, ions leached from the filter paper) and can also lead to shear forces disturbing long protein assemblies (J. Lee et al., 2012). The latter exposes more protein to a harsh air-water interface during and after blotting. The sample deposition protocols presented here avoid paper blotting entirely. Deposition protocol 1 also minimizes the time the protein remaining on the grid after sample re-aspiration is exposed to the air-water interface; if the DP-stage offset is +8 °C, samples can be vitrified immediately after deposition. Exposure to the air-water interface is longer when deposition protocol 2 is used; sample deposition, spreading, and thinning can take up to 10 s before the grid enters the cryogen. Both deposition protocols also allow the use of additives, such as traces of detergent, that concentrate at the air-water interface and might protect proteins from surface effects. Sample conditioning by a diffusion driven process (Arnold et al., 2016) can be included in the cryoWriter setup, allowing detergent to be rapidly introduced to small sample volumes (< 5 nl) and the preparation of homogeneous grids by protocol 2 (Arnold et al., 2016).

Water evaporation from the sample to obtain thin specimen layers is a critical step during cryo-EM grid preparation. To our experience, water evaporation is also crucial when conventional methods are employed, *i.e.*., in the last stages of paper blotting and in the time interval before plunge-freezing. The question of how much water can be evaporated from a sample without generating harmful conditions for the sample or negatively affecting image quality does not have a general answer. The amount will depend on the protein and the salts present. If the EM images have a grainy background, arising from high salt concentration (see Supporting Information C.4), the cryoWriter protocols can be combined with a conditioning and desalting process described previously (Arnold et al., 2016).

The cryoWriter method promises to significantly shorten the time and effort required to determine suitable freezing conditions. The almost lossless preparation and low sample consumption achieved, will make cryo-EM applicable to the structural analysis of sparsely

available proteins/protein complexes and the content of single cells. This is of particular interest because technical advances in cryo-EM now allow resolutions between 3 and 6 Å to be reached by single particle imaging and the analysis of only a few thousand to a few million protein complexes (Liao et al., 2013), making microfluidic sample preparation methods for structural analysis feasible (Giss et al., 2014).

Acknowledgments

We thank the workshop of the Biozentrum of the University Basel for their support, N. Taylor for his help with image processing, S. Müller for critical discussions and for carefully reading the manuscript, R. Sütterlin for help with cell culturing, A. Fecteau-LeFebvre for technical assistance with EM, J. Senn for assisting with EM data collection, and M. Chami for expert discussions about cryo-EM sample preparation (all from the C-CINA, Biozentrum, University of Basel). We thank A. Engel, emeritus University Basel now University of Delft, Netherlands, for his inspiring conversations. Test samples were kindly provided by P. Ringler, M.-A. Mahi, and T. Schwede (Biozentrum, University of Basel), P. Leiman (Laboratory of Structural Biology and Biophysics, EPFL) and R. Diaz-Avalos (New York Structural Biology Center, USA). The project was supported by the Swiss Nanoscience Institute (SNI, project P1201) and the Swiss National Science Foundation (SNF, project 200021_162521).

Competing financial interests

The authors declare the following competing financial interest: The cryoWriter concept is part of patent application PCT/EP2015/065398 and EP16194230.

Supporting information

Supporting information associated with this article can be found in Appendix C or online at http://dx.doi.org/10.1016/j.jsb.2016.11.002.
Supporting figure C.1 shows the detailed setup of the cryoWriter and sample vitrification process. C.2 shows the control software interface. C.3 discusses the real-time monitoring of water thickness by a 780 nm and a 405 nm laser diode. C.4 shows salt effects caused by incorrect sample thinning. C.5 compares the quality of cryo-EM grid prepared from a membrane protein sample by the classical the cryoWriter methods. C.6 presents single-cell lysate deposited on continuous carbon and holey carbon film. C.7 shows the Fourier shell correlation from single particle reconstruction of urease.

CHAPTER 5

A miniaturized dot-blot platform for single-cell protein analysis

Stefan A. Arnold[a,b], Gregor Dernick[c], Christian Berchtold[d], Goetz Schlotterbeck[d], Henning Stahlberg[a], Thomas Braun[a]

[a] Center for Cellular Imaging and NanoAnalytics (C-CINA), Biozentrum, University of Basel, Switzerland
[b] Swiss Nanoscience Institute (SNI), University of Basel, Switzerland
[c] Discovery Technologies, Pharma Research and Early Development (pRED), F. Hoffmann-La Roche AG, Basel, Switzerland
[d] Institute for Chemistry and Bioanalytics, University of Applied Sciences FHNW, Muttenz, Switzerland

Abstract

Protein analysis of single cells is challenging. The huge dynamic range of expressed proteins coincides with the minute volumes present in single cells. In addition, proteins cannot be amplified like DNA or RNA. Hence, miniaturized devices that prevent sample dilution are fundamental to single-cell protein analysis. Here we present a single-cell reverse-phase protein microarray, which can be seen as a miniaturized dot-blot platform. Adherently grown mammalian cells are observed under the light microscope, individually lysed and aspirated into 5 nl volumes by a microcapillary electrode. The collected cell lysate is directly spotted onto nitrocellulose coated slides and probed with high-quality antibodies against the target proteins of interest.

5.1 Introduction

The stochastic nature of biological processes leads to cellular heterogeneity and phenotypic differences within a population of seemingly identical cells. These differences do not always have a functional significance (Altschuler et al., 2010). If they do, however, impact on life can be dramatic. In cancer, for example, tumor heterogeneity is limiting the efficiency of medical treatments (De Sousa E Melo, Felipe et al., 2013; Janku, 2014). The selective vulnerability of certain neurons observed in many neurodegenerative disorders could also be attributed to cellular heterogeneity (Poulin et al., 2016; Prinz et al., 2011; Y. Wang et al., 2016).
Experiments with single-cell resolution could give valuable insights into such diseases. However, many analytical methods measure only the average of an ensemble. Distinct subpopulations are often obscured by the population average, or their signal is diluted below the detection limit of the analytical method (Buettner et al., 2015; Eberwine et al., 2012; Wilson et al., 2015). Hence, single-cell measurements and the development of appropriate tools has become a major research target in the last few years. It started with the analysis of gene expression and transcription, where polymerase chain reaction (PCR)-based DNA and RNA amplification was readily available even on the microfluidic scale (Kim et al., 2015; M.-C. W. Lee et al., 2014; Patel et al., 2014). Single-cell protein analysis, however, was hindered by the tiny amount of analyte and the lack of a direct amplification technology similar to PCR. Quantitative immunoassays such as enzyme-linked immunosorbent assay (ELISA) require microliter working volumes. A mammalian cell has on average an estimated 100'000 copies of a protein (Schmid et al., 2010). Diluted in 10 µl of buffer, this corresponds to a femtomolar concentration, which is below the picomolar detection limit of most quantitative immunoassays (Tabakman et al., 2011). Not surprisingly, most single-cell protein analyses so far were performed in very small volumes, such as microfluidic droplets, and often included sophisticated means of translating protein concentration to an amplifiable signal, which required complex microfluidic devices and molecular engineering of special probes (Abbaspourrad et al., 2015; Albayrak et al., 2016; Kellogg et al., 2015).
Miniaturization of conventional analysis platforms is not limited to microfluidic devices. A miniaturized single-cell western blot platform was developed for *in situ* lysis of single cells in microwells, followed by electrophoretic separation, immobilization, and antibody probing in a photoactive polyacrylamide gel (Hughes et al., 2014).
Here we present a miniaturized dot-blot platform based on reverse-phase protein array (RPPA) technology (Boellner et al., 2015; Spurrier et al., 2008; Wachter et al., 2015). Single, adherently grown mammalian cells are lysed within milliseconds through a local electric field applied by a microcapillary electrode (Arnold et al., 2016; Kemmerling et al., 2013). The cell lysate is aspirated into the tip of the microcapillary electrode and deposited as a small nanoliter spot on a nitrocellulose (NC) coated glass slide. Subsequently, proteins of interest are labeled with antibodies and analyzed in a microarray scanner.

5.2 Materials and methods

5.2.1 Instrument setup and single-cell RPPA principle

The same instrument that was used for single-cell analysis by electron microscopy (Arnold et al., 2017; Arnold et al., 2016) is also used for single-cell RPPA. However, instead of writing the sample on an EM grid, it is spotted on an NC coated glass slide. The setup is illustrated in Figure 5.1. Inside the live-cell incubator stage (1) an indium tin oxide (ITO) coated glass slide is placed. On the ITO slide a polydimethylsiloxane (PDMS) Petri dish (2) is holding an adherently growing cell culture. A microcapillary electrode (3) is used to lyse and aspirate individual cells from the cell culture and spot the collected lysate on the adjacent microarray slide (4). The microarray slide is made of glass, with 16 pads of NC film coated on top. NC is commonly used for protein immobilization on microarrays. The porous microstructure of NC efficiently adsorbs and stabilizes proteins. Target proteins in the cell lysate are labeled in a two-step process as depicted in Fig. 5.1. The cell lysate spots are first incubated with primary antibodies that bind specifically to the proteins of interest. Subsequently, secondary antibodies with a fluorescent label for detection are added. These antibodies are specifically chosen to label the primary antibodies' Fc domain, which is constant within the same animal class. The labeled slide is then scanned at specific wavelengths to excite the selected fluorophores.

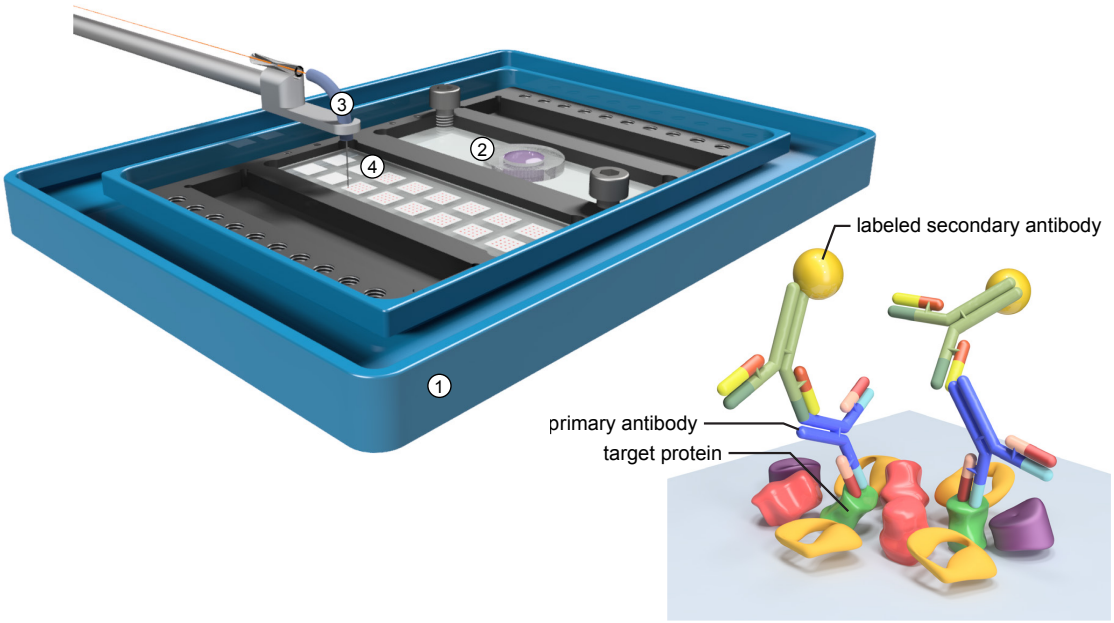

Figure 5.1: *Illustration of the single-cell RPPA setup. In a live-cell incubator stage (1) cells are grown in a PDMS well on an ITO slide (2), lysed and aspirated with a microcapillary electrode (3), and spotted on the adjacent microarray slide (4). Bottom right: RPPA principle – the lysate spots are incubated with primary, target specific antibodies. Fluorescently labeled secondary antibodies are used to bind to the primary antibodies' Fc domain.*

5.2.2 Cell lysis and spotting

Cell culturing, lysis, and aspiration of lysed HEK 293 cells was performed as described previously in chapter 2 and 3 (Arnold et al., 2016; Kemmerling et al., 2013). For semi-automated cell lysis and deposition, an openBEB macro script (D.12, Appendix D) was used to support the user during the experiment. Spot positions, lysis parameters, flow rates, and volumes for aspiration and deposition were initially defined by the user. After manual positioning of the microcapillary above a target cell, the macro was started. First, the user was asked to define the spot position on the NC membrane. Next, the microcapillary tip was moved 200 µm aside and a picture of the cell was taken. The microcapillary was then again placed above the cell and the voltage pulse was triggered to break the cell membrane. Immediately after the voltage pulse, the cell was aspirated into the microcapillary by the syringe pump. Afterwards, the microcapillary was again moved aside and a user input was requested to visually confirm that lysis and aspiration was successful. In case lysis was not successful, the macro could be stopped and restarted here. If it worked, the macro script continued. A snapshot of the cell remnants was taken, and the sample was deposited at the previously defined location on the NC pad.
For high-throughput spotting, the semi-automated macro script was replaced with a fully automated, but less accurate protocol (D.13, Appendix D). Cells were now grown to confluence on the ITO surface and a regular array of positions was defined on the cell culture. Due to the confluence of the cell culture, most positions would target at least one cell. After defining all other parameters and positions, the macro was started and up to 192 spots were deposited on NC. A washing break after every 4th spot was set to prevent clogging of the microcapillary tip (D.11, Appendix D). To wash the microcapillary, the tip of the microcapillary was inserted into the opening of a slightly larger tubing, immersed in a bath of detergent (1% Alconox, Alconox Inc., USA). Through the large tubing, detergent was flushed in and out, causing a high flow of detergent along the tip of the microcapillary. In parallel, detergent was also aspirated and flushed inside the tip of the microcapillary. In the end, the tip was flushed with clean system liquid (ddH_2O) before a new cell was targeted.

5.2.3 Buffers

PBS buffer (Dulbecco's Phosphate Buffered Saline, 2.7 mM KCl, 1.5 mM KH_2PO_4, 136.9 mM NaCl, 8.9 mM $Na_2HPO_4 \bullet 7H_2O$, pH 7.4, Sigma Aldrich, Switzerland) or TBS buffer (Tris Buffered Saline, 0.05 M Tris and 0.15 M NaCl, pH 7.6, Sigma Aldrich, Switzerland) supplemented with Tween20 (Sigma Aldrich, Switzerland) are denoted as PBS-T and TBS-T, respectively, whereas the percentage of Tween20 is stated, *e.g.* 0.01%.
Blocking and assay buffer (B&A buffer) consisted of a 1:1 mixture of LiCor ODYSSEY blocking buffer (927-40000, LI-COR Biotechnology GmbH, Germany) and PBS-T 0.2%. A 1:10 dilution of B&A buffer in PBS-T 0.1% was used for washing. The final wash in a 50 ml Falcon tube was done in TBS-T 0.1%.

5.2.4 Antibodies

Several antibodies were used throughout the single-cell RPPA development. They are listed in Table 5.1 below.

Primary antibodies

Target	Host	Catalogue No.
h-Pan-Actin	Mouse	Millipore NG1848416
HSP60	Mouse	Millipore MAB3514
h-GAPDH	Rabbit	Abcam ab37168

Secondary antibodies

Target	Host	Label	Catalogue No.
Mouse IgG	Goat	IRDye 800	Li-Cor 926-32210
Rabbit IgG	Goat	Alexa647	Invitrogen A21245

Table 5.1: *The listed antibodies were used for various RPPA experiments. The antibodies were diluted in assay buffer to the final concentration of 1 μg/ml for incubation.*

5.2.5 RPPA protocol

The printed NC slides (UniSart® 3D slide, Sartorius AG, Germany) were placed in a 16-well incubation chamber (ProPlate 16 Well Slide Module 204862, Grace Bio-Labs, USA) and blocked for 10 min at room temperature with B&A buffer. Subsequently, the buffer was removed and 100 μl of primary antibody solution were added to each well and incubated for 18 h at room temperature. Afterwards, the wells were washed with 200 μl of wash buffer, followed by incubation with secondary antibodies for 1 h. After the incubation, the wells were washed twice with wash buffer. In the end, the slide was removed from the incubation chamber and placed in a 50 ml Falcon tube filled with TBS-T 0.1% for a final wash and subsequently dried with a nitrogen-jet. The full protocol is summarized in Table 5.2.

5.2.6 RPPA analysis

Different microarray scanners were used to scan the processed slides: InnoScan1100AL (Innopsys, France) with 10 μm/pixel at 532 nm and 635 nm; InnoScan710AL (Innopsys, France) with 10 μm/pixel at 785 nm; MS 200 Microarray Scanner (Roche NimbleGen, USA) with 10 μm/pixel at 532 nm and 635 nm. The obtained images were processed with GenePix Pro 6.0 software (Molecular Devices, LLC, USA). The results were exported and analyzed with TIBCO Spotfire software (TIBCO, USA). Graphs were plotted in Igor Pro (WaveMetrics Inc., USA).

#	Step	Buffer/Reagent	Time/Comments
1)	Blocking	B&A buffer*	10 min, 100 µl/well
2)	Incubation	Primary AB in B&A buffer**	18 h; 100 µl/well
3)	Wash	Wash buffer	10 min; 200 µl/well
4)	Incubation	Secondary AB in B&A buffer	1 hour; 100 µl/well
5)	Wash	Wash buffer	10 min; 200 µl/well
6)	Wash	Wash buffer	5 min; 200 µl/well
7)	Wash	TBS-T 0.1%	4x shake in 50 ml Falcon tube
8)	Dry	Nitrogen-jet	Until dry

* Insert slide into reusable 16-well incubation chamber (ProPlate 16 Well Slide Module 204862, Grace Bio-Labs, USA).
** Seal with tape (ProPlate SealStrip 204874, Grace Bio-Labs, USA).

Table 5.2: *Protocol for spotting and developing reverse-phase protein microarrays on nitrocellulose substrates.*

5.3 Results and discussion

First tests with single-cell RPPA that showed promising results were reported by Kemmerling and Arnold (Kemmerling et al., 2013; see also Appendix A). Since then, the single-cell lysis instrument was further developed and liquid handling capabilities were greatly improved to nanoliter precision (Arnold et al., 2017; Arnold et al., 2016). These developments helped to further investigate the potential of single-cell RPPA. The first questions to be answered were technical in nature (sample carry-over, sensitivity, array processing, etc.) and went hand in hand with further developments of the setup, *e.g.*, to improve sample deposition in order to spot regular arrays.

5.3.1 Liquid handling accuracy

The liquid handling accuracy and reproducibility was tested by spotting different volumes of a fluorescent solution on a clean glass slide (Figure 5.2). Multiple 4x4 arrays with increasing spot volume from 2 nl to 13 nl were spotted with an aqueous 10 nM sulforhodamine b solution. The slide was scanned at 533 nm and the spot intensity was plotted against the spotted volume. As shown in Figure 5.2a, the signal intensity increases linearly with spot volume. Figure 5.2b also shows well ordered spots, which facilitates automated data analysis. A coffee ring effect can be observed on the dried spots. This, however, is due to spotting on an untreated glass surface and has not been observed on NC or hydrogel coated slides.

5.3.2 Sample carry-over and spreading on NC

When cells are collected and spotted with the same sampling device, it must be ensured that the total sample is deposited and nothing is lost or carried over from one spot to the next. To investigate sample carry-over, 5 nl of cell lysate were aspirated, and subsequently, three

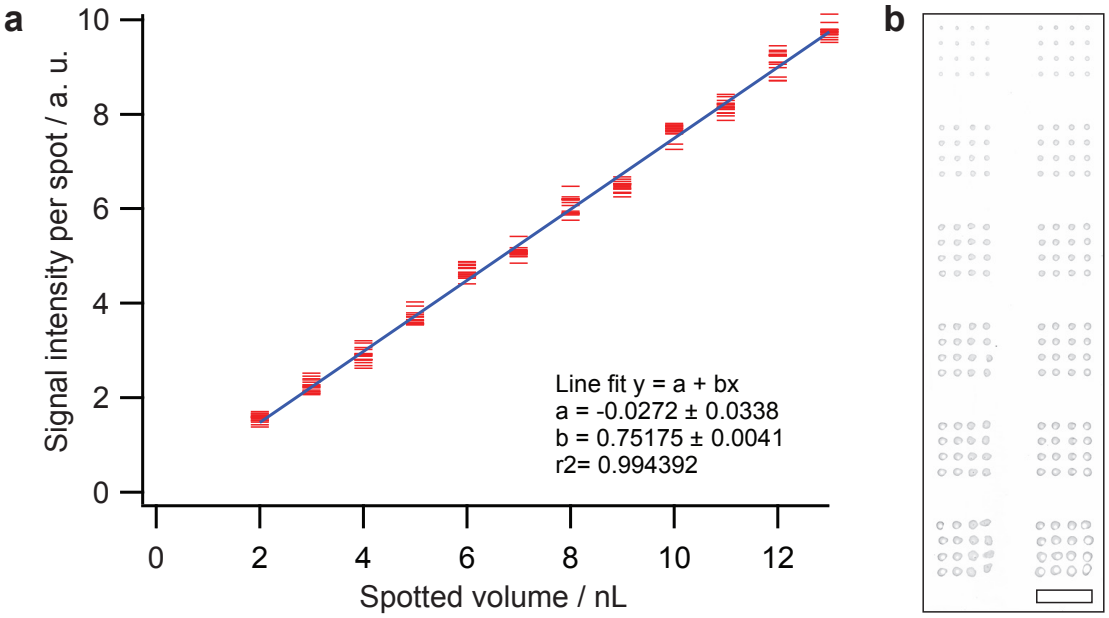

Figure 5.2: *(a) Multiple arrays of 4x4 spots of 10 nM sulforhodamine b solution were spotted on a clean glass slide. The spotted volume was increased by 1 nl with every new array (from 2 nl to 13 nl). The spotted volume was plotted against signal intensity. (b) Inverted image of the scanned slide, showing the increasing spot size and total signal intensity with increasing spot volume. Scale bar is 5 mm.*

spots of 5 nl were dispensed one after another. Probing the spots against actin revealed a significant amount of sample carry-over on the second spot (red line in Figure 5.3a). This was to be expected and can be explained by two effects: (i) When switching from aspiration to dispensing mode, there is a small loss in piston stroke due to the backlash in the gears of the syringe pump. According to the manufacturer, the backlash of a new unit lies between 7 and 12 µm. For a syringe with a barrel diameter of 0.46 mm, this translates to a reduction of 1–2 nl on the first deposition after a change of flow direction. (ii) Sample can diffuse into the system liquid, or adhere to the capillary wall, causing a slight carry-over.

Due to these effects, the spot volume should be larger than the initially aspirated volume. In the next experiment, the volume of the first spot was increased threefold (blue line in Figure 5.3a), and it was shown that the complete sample was now contained in the first spot.

The difference in signal intensity between the two experiments can be explained as follows: (i) the first experiment contained sample spots consisting of multiple (up to 6) cell lysates, which results in a higher overall signal intensity and a larger standard deviation. In the second experiment, only one cell was lysed, aspirated, and deposited per spot. (ii) The first experiment was performed in PBS buffer, whereas the second experiment was performed in cell culture medium. The high protein content in cell culture medium could have blocked some of the binding sites of the target protein, leading to a decreased signal intensity.

An adverse effect of larger spot volumes is the increased spot size on the NC membrane, which requires a larger array spacing and reduces the data density. In addition, to obtain a high signal-to-noise ratio, the sample should be very concentrated in a confined spot.

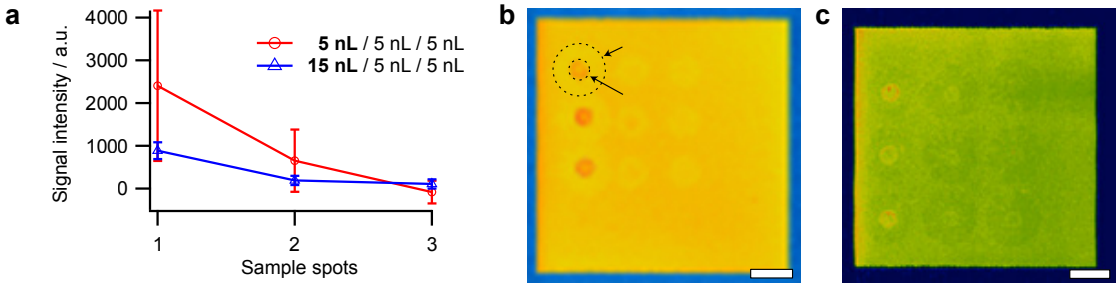

Figure 5.3: *(a) Deposition of three spots (cell lysate followed by two wash fractions). Red line (circles) is 5 nl per spot, blue line (triangles) is 15 nl lysate spot, followed by two 5 nl wash fractions. (b) and (c) NC membrane with array of spots, first column sample, second and third column wash fractions. (b) 5 nl spots of 5 nl aspirated cell lysate. (c) 15 nl spots of 5 nl aspirated lysate. Protein quickly absorbs at the center of the spot (inner ring, long arrow), whereas buffer solution can spread further away (outer ring, short arrow). Scale bar 1 mm.*

Fortunately, proteins are quickly absorbed by the NC membrane, and even though the sample buffer spreads far on the NC membrane, the proteins remain concentrated in a small area at the center of the spot. This is shown in Figure 5.3b and c with pads of the NC membrane containing a 3x3 array of spots with a 1.2 and 1.5 mm spacing, respectively. Each row is a single experiment. The first column holds the sample spot, followed by two washing fractions in columns two and three. Figure 5.3b corresponds to the first experiment with 5 nl sample spots, Figure 5.3c to the second experiment with the three times larger first spot. Arrows indicate two rings, a high intensity inner ring containing most of the target protein and a halo-like outer ring of sample buffer. Note that the spot size is not considerably affected by a larger deposited sample volume.
As a rule of thumb, it was decided to deposit three times the aspirated volume in future experiments. This should ensure that loaded sample is deposited on a single spot and not retained in the microcapillary and flushed away during cleaning.

5.3.3 Single-cell RPPA with housekeeping protein actin

Housekeeping proteins (Ferguson et al., 2005), such as actin or glyceraldehyde 3-phosphate dehydrogenase (GAPDH), are highly abundant in cells and therefore a good starting point for single-cell RPPA. First experiments with actin were already performed in an earlier stage (refer to the supporting information of chapter 2, appendix A). To test the single-cell resolution of the RPPA method with the improved setup, the lysate of one to six cells was collected and spotted on a NC membrane. Actin was again chosen as target protein. Figure 5.4 shows the number of cells dispensed in each spot vs. the total fluorescence intensity. The size of the lysed cells is not taken into consideration here. However, the actin concentration likely scales with the volume of the cell. Hence, in future experiments, cell size should also be measured and considered in the analysis.

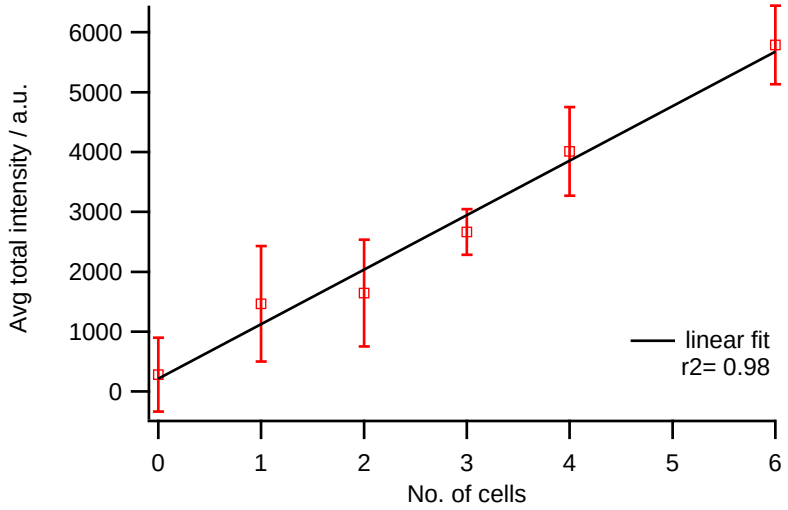

Figure 5.4: *One to six cells were lysed and aspirated together and dispensed as spots on an NC pad. After incubation with an anti-actin antibody and a fluorescently labeled secondary antibody, the slide was scanned. The total fluorescence intensity was plotted against the number of lysed cells dispensed in each spot.*

5.3.4 Multiple target analysis

In a standard forward phase protein array, different target antibodies can be spotted to capture a broad range of target proteins. However, the analysis of multiple proteins in a single-cell lysate spot is more difficult. In a first experiment, single-cell sample fractionation was tested (Fig. 5.5). Therefore, one to five adherent HEK 293 cells were lysed together and aspirated with buffer in a total volume of 50 nl. Subsequently, the 50 nl were deposited as

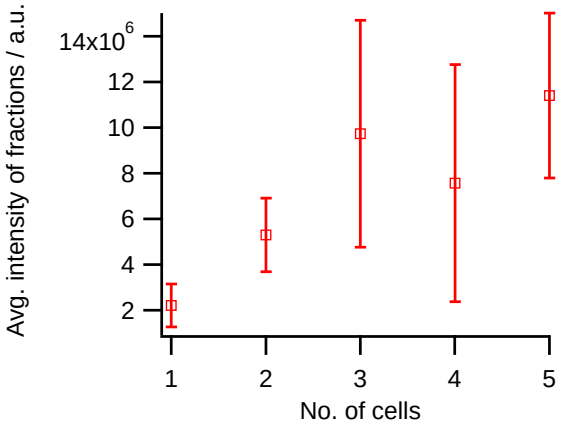

Figure 5.5: *One to five cells were lysed and aspirated together, and spotted as 9 individual spots (fractions). The average signal obtained from each fraction is plotted for each number of lysed cells. The spots were analyzed for actin. An increase in total signal intensity is observed with the number of lysed cells. However, the variability from spot to spot is very high, as revealed by the standard deviation (error bars).*

nine 5 nl spots on a 3x3 array and labeled for actin. The analysis revealed a large variation from spot to spot as shown by the high error bars (standard deviation) in Figure 5.5.
It is known, that mixing at low Reynolds numbers (Bruus, 2008), which is often the case in microfluidic channels and microcapillaries, is difficult and slow. In addition, lysed cells are not a very homogeneous sample, but rather a mix of cytosolic proteins, ruptured organelles, and larger membrane patches. Hence, the collected cell lysate does probably not mix well within the aspirated 50 nl plug, which would explain the large differences of the individual fractions.

GAPDH/HSP60 assay development

As an alternative, the use of differently labeled secondary antibodies was tested. The goal was to detect multiple target proteins on a single spot, by incubating the sample with different primary antibodies, and subsequently distinguishing them with differently labeled secondary antibodies. To this end, an assay development was performed to find the ideal combination of antibodies for parallel measurement of HSP60 and GAPDH. As primary antibodies, a mouse anti-HSP60 and a rabbit anti-GAPDH antibody were used. Anti-mouse-(800 nm) and anti-rabbit-(647 nm) antibodies served as secondary antibodies. Due to the host specificity, only anti-rabbit labeled GAPDH should be seen in the red channel (635 nm), whereas only anti-mouse labeled HSP60 should be seen in the infrared channel (785 nm). This was achieved, as shown in Figure 5.6. It shows a slide scanned in two different channels (635 nm and 785 nm) and incubated with multiple combinations of antibodies. HSP60 and GAPDH signals can be measured independently in two different channels without any cross-reaction. Hence, the GAPDH signal could be used to normalize the HSP60 signal, allowing to measure heat-shock or stress-induced changes in the cells (see below).
However, as revealed in Figure 5.6, NC exhibits strong autofluorescence at 635 nm (which is even stronger at 533 nm). Therefore, other microarray substrates, such as hydrogel coatings (NEXTERION® Slide H, SCHOTT Technical Glass Solutions GmbH, Germany) could be used alternatively.

5.3.5 Towards high throughput

For statistically significant data collection, hundreds of cells need to be lysed and spotted. This is only realistically feasible with a fully automated protocol. With the help of image analysis and particle recognition tools delivered by LabVIEW, automated cell targeting could be developed in the future. In a first approach, a much simpler alternative was tested. Therefore, an array of positions was defined across a confluent cell culture and macro script D.13 (Appendix D) was used to automatically collect and spot cells from these positions.
A total of 190 spots were printed within 70 min. The printed slide was incubated with anti-HSP60 and anti-GAPDH antibodies to see how the cells developed during the 70 min of sample collection in PBS buffer at room temperature. By dividing the GAPDH signal with the

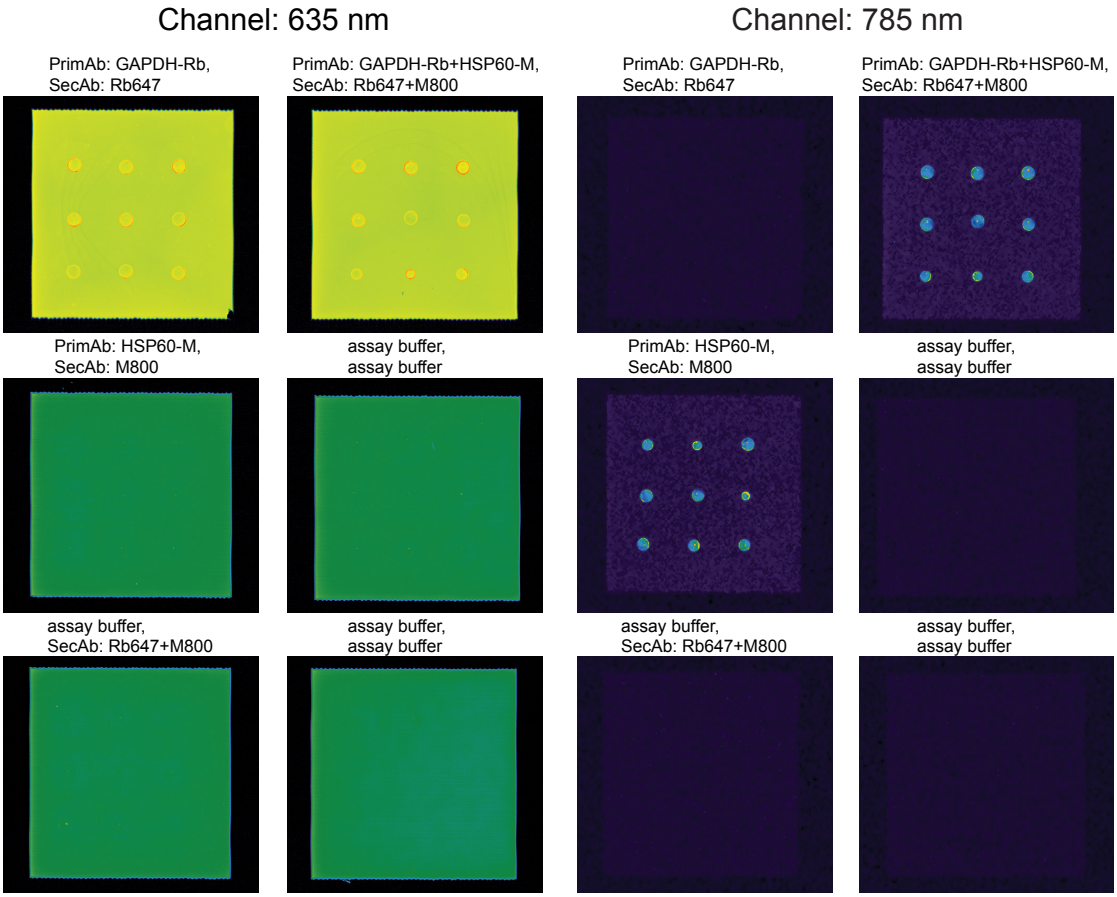

Figure 5.6: *Assay development for HSP60 and GAPDH analysis. A single or a few HEK 293 cells were lysed and deposited as spots on a NC membrane. The printed slide was incubated with primary antibodies against HSP60 and GAPDH expressed in different host species (mouse and rabbit). Subsequently, the slide was incubated with secondary antibodies against rabbit and mouse, with red and infrared fluorescent labels, respectively. In the red channel (635 nm), only the GAPDH signal is measured against a strong NC background. In the infrared channel (785 nm), only the HSP60 signal can be observed, with a much better signal-to-noise ratio due to the lower background fluorescence in the infrared.*

HSP60 signal, a stress-induced change occuring over time might be revealed. As shown in Figure 5.7, slide 1 shows a clear decrease in the mean signal intensity of the GAPDH/HSP60 signal in the first ten minutes of the experiment. A decrease of the GAPDH/HSP60 signal would suggest an increasing expression of HSP60, and hence, a response of the cells against some external factors (buffer change, pH change, temperature change, *etc.*). The results were not as clear for slide 2. A well defined external stress factor (*e.g.* driving a controlled heat ramp, releasing a drug) might give a clearer picture in the future, whether GAPDH can be used as an internal control. However, even the expression of housekeeping proteins can vary significantly in certain biological contexts (Ferguson et al., 2005). Hence, a good understanding of the functions of such housekeeping proteins is required, and depending on the experiment, a different type should be chosen.

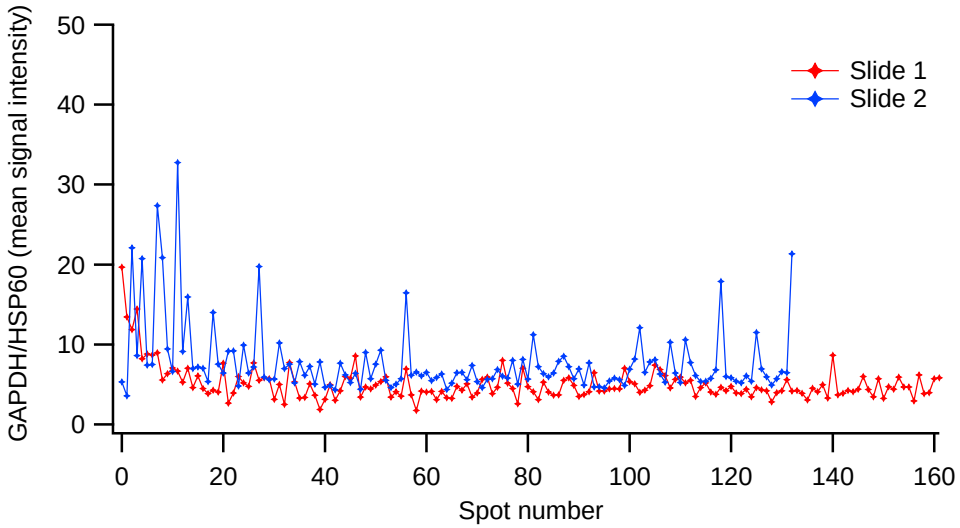

Figure 5.7: *The mean signal intensities of GAPDH divided by HSP60. GAPDH is used as a positive control. There seems to be some change in HSP60 levels at the beginning of the experiment (at least for slide 1), indicating an increased stress-induced expression of HSP60.*

5.4 Conclusion and outlook

Single-cell protein analysis requires miniaturized experimental designs to prevent dilution of the sample. Here we have presented a miniaturized dot-blot, or reverse-phase protein array, which can measure protein concentrations at the single-cell level. This was shown for heat-shock protein HSP60, as well as for actin and GAPDH. Although all three proteins are abundant in cells, the technique has the potential to detect also less abundant proteins, and further experiments are planned to detect α-synuclein in single neuron-like cells. In order to detect such less abundant proteins, single-cell reverse-phase protein arrays might need additional sensitivity. In this respect, different strategies to enhance microarray sensitivity have already been demonstrated. Near-infrared fluorescence signals were enhanced up to 100-fold by preparing protein microarrays on a nanostructured, plasmonic gold film (Tabakman et al., 2011). Alternatively, using advanced, so-called surface-enhanced Raman scattering (SERS) probes, immunoassays with limits of detection in the femtomolar range were reported (Chang et al., 2016). And last, signal amplification was also achieved by sequentially incubating fluorescently labeled secondary antibodies that were reactive against each other (Brase et al., 2010). These and future developments will further improve the sensitivity of reverse-phase protein arrays, and single-cell analysis will largely benefit from it.

Chapter 6

Interfacing single-cell lysis with liquid chromatography-mass spectrometry

Christian Berchtold[a,1], Stefan A. Arnold[b,c,1], Gregor Dernick[d], Henning Stahlberg[b], Thomas Braun[b], Goetz Schlotterbeck[a]

[a] Institute for Chemistry and Bioanalytics, University of Applied Sciences FHNW, Muttenz, Switzerland
[b] Center for Cellular Imaging and NanoAnalytics (C-CINA), Biozentrum, University of Basel, Switzerland
[c] Swiss Nanoscience Institute (SNI), University of Basel, Switzerland
[d] Discovery Technologies, Pharma Research and Early Development (pRED), F. Hoffmann-La Roche AG, Basel, Switzerland
[1] Authors contributed equally

Abstract

The analysis of metabolites collected from a single cell requires extremely sensitive instruments, because the total quantity is very low and, in contrast to DNA and RNA, metabolites cannot be further amplified. Mass spectrometry is one of the most sensitive analytical tools available, and hence, a method of choice for many single-cell analysis applications. Because cell lysate is a complex mixture of metabolites, proteins, lipids, *etc.*, physical separation of its contents can increase the selectivity and sensitivity of the applied analysis method. At last, interfacing single-cell sampling with the appropriate mass spectrometry device can be challenging. Here we demonstrate the use of a thin layer chromatography device for the extraction and analysis of nanoliter-sized samples from polymer slides. This development will allow the deposition of single-cell samples for off-line analysis by liquid chromatography-mass spectrometry.

6.1 Introduction

The analysis and quantification of metabolites at the single-cell level is extremely challenging. Metabolite concentration in a cell ranges from 10^{-6} mM to a few mM for highly abundant metabolites, such as glutamate (Bennett et al., 2009; Chen et al., 2016; Park et al., 2016). For a mammalian cell with a volume of a few picoliter, this corresponds to an absolute number of molecules on the order of a few thousand to a billion molecules, which makes the detection of low abundant metabolites very challenging.
Mass spectrometry (MS) has become an established tool for the highly sensitive detection of analytes. Continuous improvements in MS instrumentation has enabled the detection of analytes at the single-cell level (Fessenden, 2016). In addition, a variety of ways exists for how sample is introduced into mass spectrometers, which enables many different interfaces and approaches for single-cell sample delivery, such as matrix-assisted laser desorption/ionization (MALDI) or (nano-)electrospray ionization (nano-ESI) (Heinemann et al., 2011).
The first step in single-cell analysis is isolating a specific cell for analysis. With suspension cell cultures, cytometry is commonly used for cell isolation, and individual cells can quickly be deposited and prepared for MALDI-MS (Amantonico et al., 2010; Ibanez et al., 2013). Adherent cell cultures are more difficult to handle, but offer additional opportunities, such as live-cell imaging of interacting cells. Extraction of adherent cells in vitro is often done by nano-ESI. The same nano-ESI emitter tip is first used to penetrate and sample a cell, before it is used to spray the sample into the MS device (Rubakhin et al., 2011). Alternatively, a microfluidic probe, directly coupled to the ESI emitter, is used to probe individual cells and deliver the sample to the emitter in real time (Pan et al., 2014). These approaches, however, require a direct link between cell sampling and the MS device. If the mass spectrometer is located remotely, a transfer system similar to a MALDI plate is required.
Previously, we have demonstrated an instrument for single-cell lysis of adherent cells by microcapillary electrodes (Arnold et al., 2016; Kemmerling et al., 2013). Because this instrument is able to collect single-cell lysate in nanoliter volumes, only diluting the sample a thousandfold, it is extremely versatile and can be combined with various analysis methods. This versatility was now further explored by combining the instrument with liquid chromatography (LC)-MS. Chromatographic separation helps to discriminate isomers, and hence provides additional selectivity and sensitivity. In combination with ESI-MS, chromatographic separation can further enhance the sensitivity by reducing ion suppression effects (Annesley, 2003).
The first challenge was to interface two remotely located instruments, *i.e.* the cell lysis setup and the LC-MS instrument. Removing a loaded microcapillary from the cell lysis setup and inserting it into the high-performance liquid chromatography (HPLC) system proved difficult and inept for multiple sample analysis. Hence, a transfer method based on thin layer chromatography (TLC) was invented. With this method, an array of samples can be spotted on a polymer slide. The slide is then transferred to the MS lab, where the sample spots are eluted and fed into the LC-MS instrument by the TLC device.

6.2 Materials and methods

Cyclic olefin copolymer (COC) microscope slides were obtained from microfluidic ChipShop GmbH, Germany. Polyether ether ketone (PEEK) and polytetrafluoroethylene (PTFE) slides were donated by the mechanical workshop at Hoffmann-La Roche AG, Switzerland.
Test samples used for system characterization (all from Sigma Aldrich, Switzerland) are listed in Table 6.1. Solvents used for experiments were ddH_2O, methanol, isopropanol, and acetonitrile, all supplemented with 0.1% formic acid (HPLC grade, Sigma Aldrich, Switzerland).

6.2.1 Instrument setup

Liquid handling and sample deposition is performed with a previously described setup (Arnold et al., 2016; Kemmerling et al., 2013). To introduce the sample into the LC-MS instrument, a new interface was developed, as illustrated in Figure 6.1. The sample is first spotted onto a plastic slide (1), dried, and stored under argon gas. This slide is then transported to the mass spectrometry facility, where it is placed on a TLC system (CAMAG, Switzerland). The TLC extraction head (2) is pressed on the slide, forming a small chamber around the sample spot. The seal is pressure-tight up to 400 bar and allows to elute the sample from the surface with the appropriate solvent. The TLC extraction head inlet is connected to an HPLC pump (Agilent 1100, Agilent Technologies AG, Switzerland) via a 6-port, 2-position valve (3). Through the same valve, the extraction head outlet is connected to an LC column

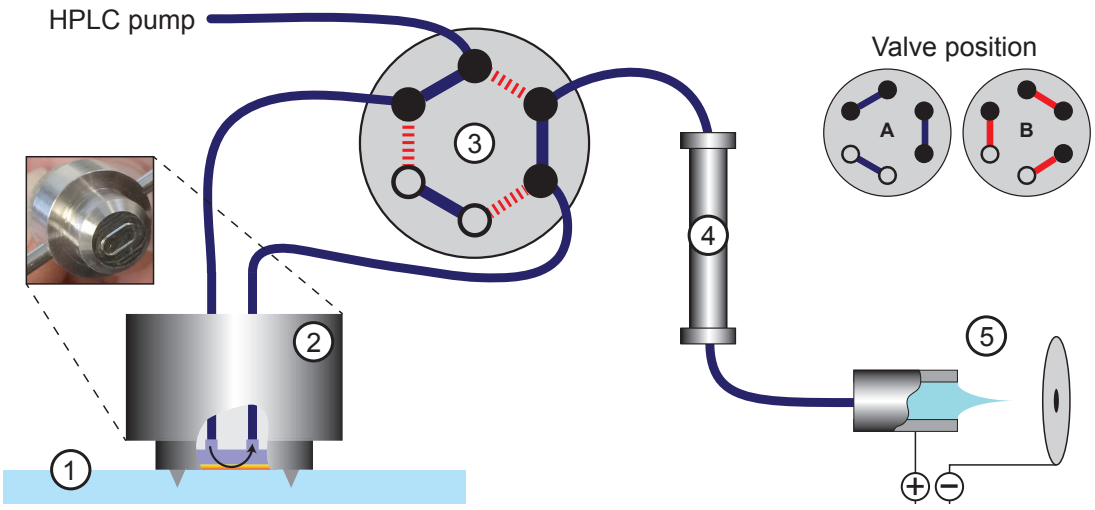

Figure 6.1: *Schematic drawing of the single-cell LC-MS interface. An array of cell lysate is spotted on a COC plastic slide (1). The TLC extraction head (2) is pressed on the COC slide forming a small pressure-tight chamber around the sample spot. The extraction head inlet is connected via a 6-port valve (3) to a standard HPLC pump. The outlet is connected via another set of ports to a liquid chromatography column (4). After sample extraction, the valve is switched and elution buffer from the HPLC machine is directly pumped through the column. The separated sample is fed into the electrospray ionization capillary of the mass spectrometer for analysis (5).*

(4, Waters Atlantis T3 column, 100 Å, 3 µm, 2.1 mm X 100 mm, Waters GmbH, Germany). Electrospray ionization (5) is used to couple liquid chromatography with mass spectrometry (LTQ-Orbitrap XL, Thermo Scientific, USA). Valve position A is used for sample extraction from the slide with the LC column in line. Position B is the standard connection, where the HPLC autosampler is connected with the column, bypassing the extraction head, *e.g.*, for pre-conditioning, sample separation and transfer to the mass spectrometer. For non-targeted analysis and for the basic evaluation of the system, a generic gradient was used.

6.2.2 LUHMES batch cell lysate

Lund human mesencephalic (LUHMES) cells are used to study neurodegenerative diseases, as they can be differentiated to post-mitotic cells that show biochemical, morphological and functional features of dopaminergic neurons (X.-M. Zhang et al., 2014). LUHMES cells were cultured and differentiated following a published protocol (Scholz et al., 2011). To prepare batch lysate, the cells cultivated in a T-25 flask were washed with PBS (Dulbecco's Phosphate Buffered Saline, 2.7 mM KCl, 1.5 mM KH_2PO_4, 136.9 mM NaCl, 8.9 mM $Na_2HPO_4 \bullet 7H_2O$, pH 7.4, Sigma Aldrich, Switzerland) and lysed with a solution of 8 M urea, 75 mM NaCl, in 50 mM Tris buffer, pH 8.2, supplemented with protease inhibitor cocktail (complete mini, Roche, Switzerland), 1 mM β-glycerophosphate, 1 mM sodium orthovanadate, 10 mM sodium pyrophosphate, and 1 mM phenylmethylsulfonyl fluoride (PMSF), all from Sigma Aldrich, Switzerland. 50 µl aliquots of batch lysate at a concentration of ∼5 mio cells/ml were stored at -20 °C. To print slides, an aliquot was diluted in 150 µl H_2O, yielding a concentration of ∼1250 cells/µl.

6.3 Results and discussion

6.3.1 Handover substrates

To hand over the sample from the single-cell lysis instrument to the LC-MS device, a suitable slide substrate was needed. The main requirements were material softness for proper sealing with the TLC extraction head, and chemical persistence against common solvents. Tests with the TLC device were performed with COC, PEEK, and PTFE slides. All materials were washed with water, acetonitrile, and isopropanol. As shown in Figure 6.2, no significant contamination was found compared to a blank test without a slide. Sealing on all substrates was sufficient up to 400 bar. The tests were performed without an LC column, with mass range 50-2000 m/z positive and negative mode. In the end, COC was chosen for further experiments due to its availability and material transparency, which also facilitated finding the sample spots by eye. Other materials were not tested further.

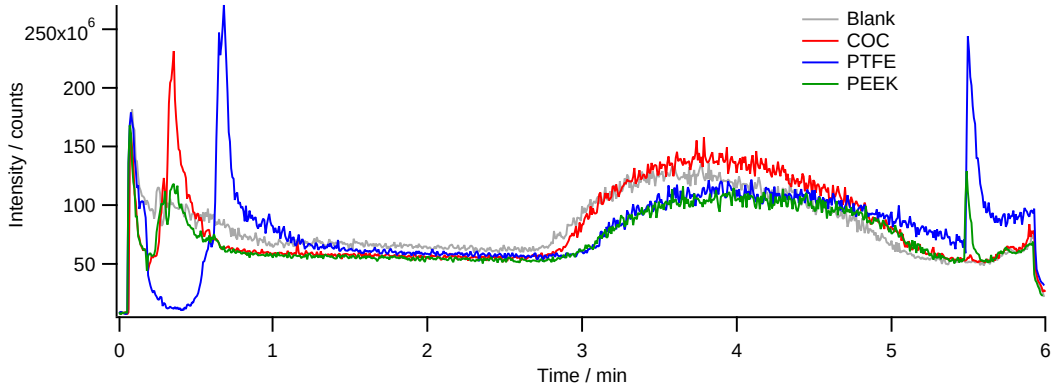

Figure 6.2: *Testing of different materials (COC, PTFE, and PEEK) against chemical persistence to solvents and presence of plasticizers. No significant contamination was found and all materials were sealing sufficiently up to 400 bar. Full scan orbit-trap (resolution 7500). Blank = valve in position B, no extraction over slide. Gradient 100% H_2O, 0.1% formic acid, to 100% acetonitrile/isopropanol, 0.1% formic acid.*

6.3.2 Setup characterization

A mixture of typical metabolites and drugs across a wide logP range (see Table 6.1) was spotted on COC slides (5, 10, 20, and 40 nl/spot) and extracted by the TLC/LC-MS setup. The extraction of the dried sample spots with the TLC/LC-MS setup was characterized

Compound	$[M+H]^+$	LogP	concentration (µg/ml)	retention time (min) injected	slide	LOD (pg) injected	slide
Alanine	90.0544	-2.85	0.488	0.44	0.67	24.4	24.4
Aspartate	134.0442	-3.89	0.192	0.45	0.67	34.8	9.7
Glutamic acid	148.0599	-3.69	0.497	0.46	0.68	24.84	24.9
Valine	118.0857	-2.26	0.250	0.67	0.85	12.5	12.5
Glutamine	147.0759	-3.64	0.492	0.68	0.67	24.25	24.6
Nicotine	163.1224	1.1	0.101	0.83	0.83	5.05	5.05
Adenosine	268.1035	-1.2	0.789	2.26	-	39.4	-
Phenylalanine	166.0857	-1.38	0.410	3.21	-	24.6	-
Acetaminophen	152.0701	0.46	0.392	4.45	4.55	39.2	19.6
Sulfadimethoxine	311.0803	1.08	0.725	6.92	7.02	36.25	36.3
Carbamazepine	237.1017	2.3	0.153	7.47	7.55	30.6	7.65
Testosteron	289.2157	3.32	0.112	8.56	8.63	56	22.4
Diclophenac	296.0234	3.9	0.228	9.48	9.57	22.8	91.2

Table 6.1: *List of the tested metabolites and drugs. A sample mix was spotted on COC slides and eluted with the TLC interface into the LC-MS. For comparison, the same sample mix was directly injected into the LC-MS instrument. The samples were measured in full scan mode. Additional sensitivity could be obtained by measuring in a targeted, MRM mode. Retention times as well as limit of detection (LOD) for directly injected samples and samples eluted from slide are shown. A signal-to-noise ratio of three was used to estimate LOD. The LogP value is a measure of a compounds lipophilicity or hydrophobicity. The tested molecules are spread across a broad range of LogP values.*

and compared to conventional, direct injection of 1 µl volumes of sample into the LC-MS instrument. A typical peak broadening for the early eluting peaks was observed with spotted samples. This was expected due to the additional dwell volume of the TLC/LC-MS interface. Although there was a slight loss in area and some metabolites were either not stable under dried conditions (Adenosine, Phenylalanine), it was clearly shown that the COC-TLC interface is capable of transmitting metabolites into the mass spectrometer also in a quantitative way.

A second example is shown in Figure 6.3, where dopamine and glutamic acid were measured in multiple reaction monitoring (MRM) mode. A mixture containing 52 pg glutamic acid and 72 pg dopamine was directly injected into the LC-MS instrument (red graph). The same amount of sample was spotted on COC and extracted with the TLC interface (blue graph). Peak broadening was observed for the dopamine peak of the COC eluted sample, however, the peak area remained about the same.

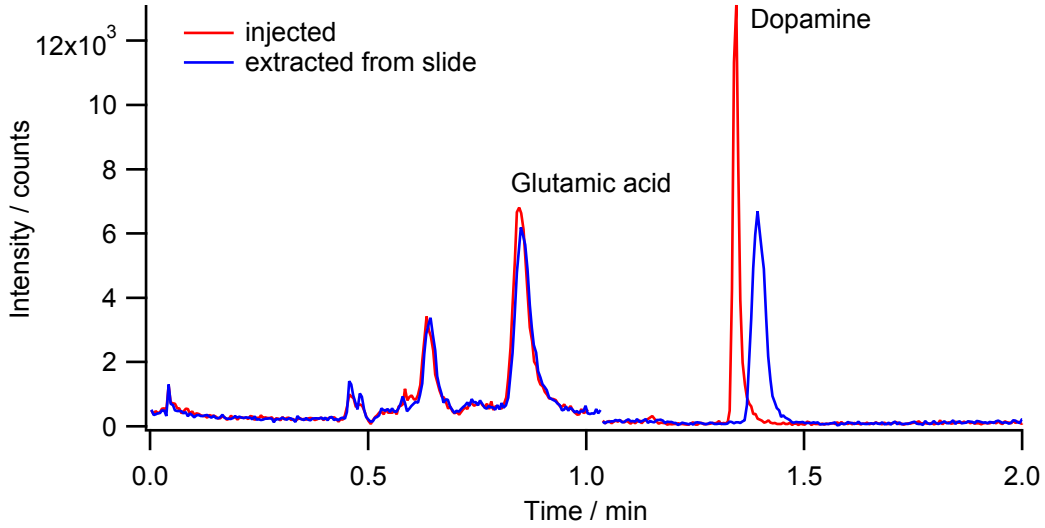

Figure 6.3: *Mixture of 72 pg dopamine and 52 pg glutamic acid, injected (red), and extracted from COC slide (blue).*

To test the setup with a complex sample, batch lysate obtained from LUHMES cells was diluted to a concentration corresponding to ∼1250 cells/µl. Small volumes of 2, 4, 6,..., 18 nl were spotted on COC. The spots were eluted using the TLC interface and fed into the LC-MS device, where a targeted mode was used to detect glutamic acid. As shown in Figure 6.4, the peak area increased linearly with the deposited spot volume. Theoretically, the smallest spot contained only lysate from 2–3 cells. Since glutamic acid, or glutamate, is one of the most abundant metabolites in cells (Bennett et al., 2009), it could be expected to be detectable at the single-cell level. Although cells were thoroughly washed with phosphate buffer prior lysis, additional control experiments will be needed to exclude that traces of glutamic acid were also introduced by the original cell medium. In addition, the used lysis buffer based on 8 M urea is not ideal for mass spectrometry, as urea causes a lot of ion suppression. An alternative lysis buffer might further increase the sensitivity. Nevertheless, the experiment showed that

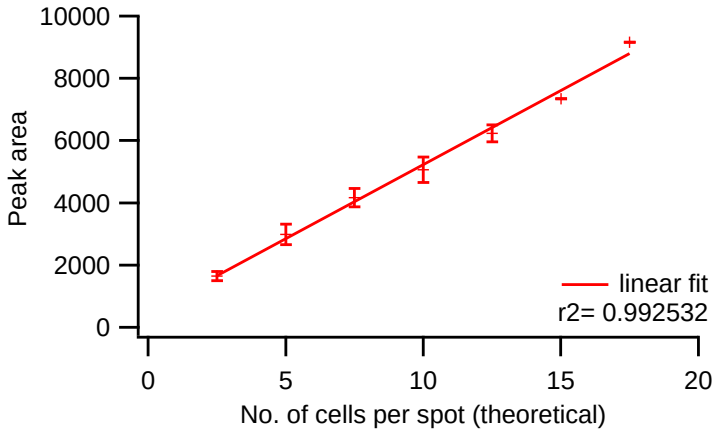

Figure 6.4: *Glutamic acid found in samples from spotted batch lysate. The smallest spot (2 nl) corresponds to an estimated number of 2.5 cells. Error bars are standard deviation.*

the TLC/LC-MS interface is also working with more complex samples and can potentially reach single-cell sensitivity. With further optimization of the setup and instrumentation, even less abundant metabolites should be detectable at the single-cell level in the future.

6.4 Conclusion

A novel interface was presented that couples live-cell imaging and single-cell lysis to liquid chromatography and mass spectrometry. This represents a first step towards the metabolomic analysis of single cells by LC-MS. It was shown that similar results were obtained compared to conventional sample injection. In addition, the new handover platform allows to separate cell sampling and MS analysis, facilitating the collaboration between cell biologists and mass spectrometry operators. By including a chromatographic separation, further selectivity and sensitivity is gained. However, to enable true single-cell analysis, a significant enhancement in sensitivity will be required. This might be achieved by optimizing multiple parameters. The TLC interface is not yet optimized for small volumes and high pressure. A capillary with smaller inner diameter (*e.g.* 10 µm) might reduce peak broadening. The TLC extraction head could be miniaturized to optimize the sample transfer. Also the slides could be optimized specifically for the TLC interface. Small sample wells could be preformed on the slide to accommodate the sample and fit with the extraction head.
Automation of the TLC interface for sample positioning and extraction would facilitate the analysis of multiple samples. An LC column of smaller inner diameter (maybe even in the µm scale) might also reduce the dwell volume and enhance sensitivity. Other means for increasing the sensitivity would be the use of a highly specific MS/MS mode and an ion trap with a longer accumulation time, or using the latest generation MS device.
Finally, the handover platform could be extended to complementary analysis methods. A slide surface functionalized with capturing antibodies, for example, might allow the subsequent measurement of metabolites and proteins in the same sample spot.

Chapter 7

Conclusion and outlook

A large part of this thesis was aimed at developing novel sample preparation methods for electron microscopy, thus enabling single-cell analysis by EM.
First, a single-cell lysis device based on irreversible electroporation with a microcapillary electrode was developed. This enabled targeted lysis and aspiration of single mammalian cells from tissue cultures. The volumes aspirated by the microcapillary were on the order of a few hundred nanoliters, and standard EM sample preparation was used to prepare the lysate for negative stain EM.
In a next step, the liquid handling and cell sampling device was refined and single cells were now collected in volumes as small as three nanoliters. These small volumes required new sample preparation methods for negative stain EM. A new method was developed, allowing the conditioning and nearly lossless preparation of nanoliter samples for negative stain EM by a diffusion-driven exchange of salt ions and negative stain at the tip of the microcapillary. As an example, it was shown that lysate from heat-shocked cells contained higher levels of heat shock proteins than control cells. Because sample preparation from nanoliter volumes without paper blotting was also promising for single-particle cryo-EM, the method was further developed to allow cryogenic sample preparation. A dew point stage was built to keep the deposited nanoliter samples from evaporating. And an automated, rapid plunge-freezing apparatus was engineered. Single-cell lysate and protein particles were successfully prepared for cryo-EM using this new instrument.
The improved single-cell sampling device also opened new possibilities for alternative and complementary single-cell analysis methods that required highly concentrated samples. Miniaturized dot-blot experiments with single-cell lysate spots were developed based on reverse-phase protein array technology. As proof-of-concept, protein expression levels of different housekeeping proteins were measured in single cells.
At last, the same instrument was combined with liquid chromatography-mass spectrometry for metabolite analysis. Since the mass spectrometer was located remotely, a new handover interface was designed. Plastic slides served as carrier for arrays of nanoliter-sized sample spots. Using a thin-film chromatography device, the dried sample spots could be eluted from the carrier surface and fed into the LC-MS instrument. A proof-of-concept study demonstrated the utility of this new interface, although single-cell sensitivity was so far only reached for

the most highly abundant metabolites.

Many different methods were presented in this thesis, however, they all share the same instrument. Future improvements of this instrument will be of benefit for all developed methods. Most important, the instrument should be further automated to increase reproducibility and make the individual methods accessible for other, less trained users, *e.g.*, to perform single-particle cryo-EM work. The openBEB macro language seems to be an ideal tool to automate certain processes in LabVIEW. Further improvements and new features are to be expected from an updated version of openBEB.
Further, the complete instrument should be enclosed in a humidity controlled chamber for better reproducibility of EM grid preparation, especially for cryo-EM. But also the drying of sample spots on nitrocellulose or COC slides is likely influenced by humidity, although difficult to judge to what extend. Nevertheless, these methods might benefit from more controlled environmental parameters as well.
Future developments will also involve the integration of a microfluidic protein isolation and purification step based on functionalized magnetic (nano)particles. This will allow the purification and isolation of target proteins from a few lysed cells, taking EM sample preparation again one step further towards a fully miniaturized EM pipeline.
In parallel, development of quantitative EM should also be addressed. With the new tools for lossless sample preparation of defined nanoliter volumes, small sample spots can be deposited on large, electron transparent substrates, such as Si_3N_4 membranes, that are free of obstructing grid bars. Once the disturbing coffee-ring effect, caused by aggregation of particles at the edge of a drying droplet, can be reduced, the complete sample can be imaged in the electron microscope using automated data collection. Such a development would turn the lyse-and-spread visual proteomics approach into a truly quantitative method.
The work on complementary single-cell analysis methods, namely protein microarrays and liquid chromatography-mass spectrometry, should be continued. Protein microarrays can deliver additional proof for visual proteomics studies, *e.g.*, by confirming increased expression levels of certain proteins. They can also help to identify the best antibodies for protein isolation. In addition, proteins that are too small for EM can be detected by immunolabeling on microarrays. At last, proteomics data could be complemented with metabolomics data obtained from mass spectrometry. It might even be possible to detect metabolites and target proteins sequentially on a single-cell spot. A functionalized sample carrier with capturing antibodies could be used to immobilize target proteins in a sample spot. After eluting the metabolites, the sample carrier could be incubated with labeled antibodies against the protein of interest and analyzed like a normal protein microarray.

Closing remarks

Looking back at the past four years, I can conclude that the EM field is experiencing an exciting time. Increasing numbers of high-resolution protein structures are solved with cryo-EM. Data collection and image processing become more automated and usable by a broad community.

And as a result, more and more people are jumping on the train. Single-particle projects that were impossible ten years ago, are becoming routine work. And new projects with smaller, more complex, or more heterogeneous protein particles will continue to push the boundaries of this technology. It is fair to assume, that in the future, further progress can be expected on all levels, from sample preparation, to EM and camera hardware, data processing and image analysis. After years of deep slumber, it will be exciting to see where this field is headed to in the years to come.

APPENDIX A

Supporting information: Chapter 2

A.1 Software implementation

The control software was implemented in LabVIEW in an object-oriented way and can be called as a plug-in to the openBEB software framework (www.openBEB.org). All components of the system are addressed in a single user interface, which is shown in Supplemental Figure A.1.

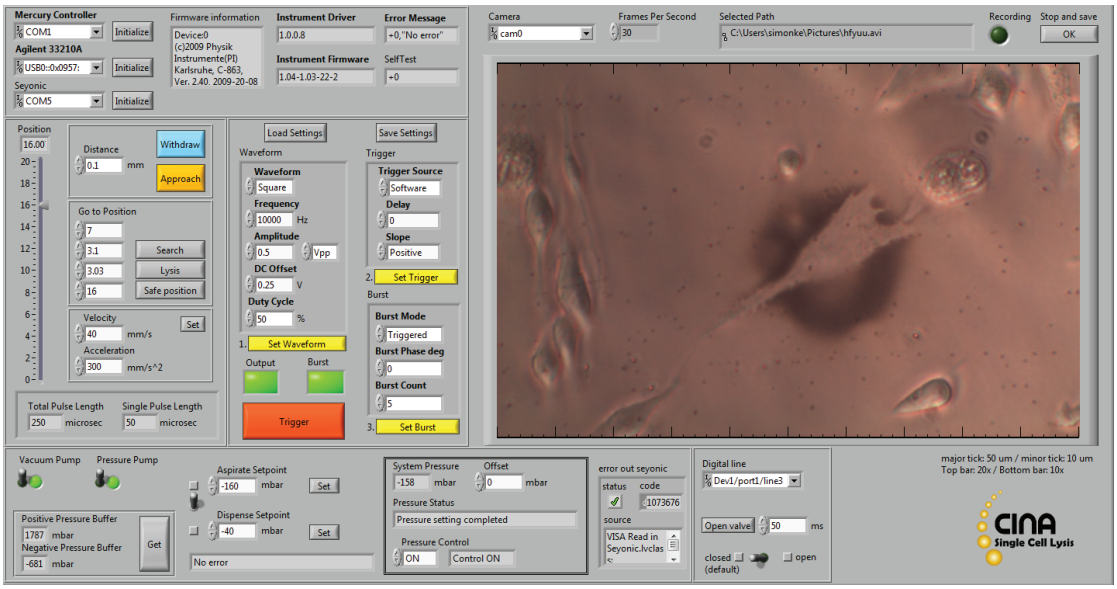

Figure A.1: *Single-cell lysis software user interface. Stepper motor, function generator, pressure, shutter valve, and video recording are controlled from a single user interface.*

The stepper motor can be moved up and down (approach/withdraw) with sub-micrometer precision. In addition, three different values can be assigned for specific positions (e.g., safe, search, or lysis position). Motor speed and acceleration can be changed if needed. The function generator panel is on the right hand side of the motor control panel. The different parameters (e.g., waveform, frequency, amplitude, burst mode, etc.) can be set and saved to an .xml file. The trigger button starts the electric pulse. A live image from the camera with

a default frame rate of 30 frames/s is shown next to the function generator panel. Video recording is started and paused by pressing the record button. Scale bars for the two objective lenses of the employed optical microscope (10x and 20x) are displayed at the top and bottom of the live image. The pressure control panel is in the lower region of the interface. On the left, the vacuum and pressure pumps can be switched on and off. The pressure status of the positive and negative pressure buffer is displayed below the two switches. A switch allows the user to quickly select one of the two pressure values (aspirate/dispense). Additional information, such as the system pressure, or whether pressure adjustments are in progress or completed, are shown to the right (black box). The remaining panel controls the solenoid valve, which is normally closed. The switch allows to open this valve for a defined period of time or continuously.

A.2 Buffers

The ability of the set-up to achieve single-cell lysis was tested in different buffers (Supporting Figure A.2). In terms of lysis parameters, the conductive buffers PBS and HEPES behaved similarly (Supporting Figure A.2B-D). However, the electric parameters had to be adjusted to achieve cell lysis in low-conductivity isotonic sucrose buffer. The application of five 100 μs DC square pulses with amplitudes of 40 V to the gold-coated microcapillary was required to achieve lysis. The fields generated were higher than those used in PBS or HEPES buffer, and needed to be applied for a significantly longer time. As a result, some of the cells surrounding the target cell were also affected and showed morphological changes (Supporting Figure A.2E and F).

A.3 Finite element analysis

Finite element analysis (FEA) using an axisymmetric time-dependent model in COMSOL Multiphysics was used to simulate the electrical field and the temperature rise induced by the electrical pulses applied to the microcapillary electrode.
The electric current and heat transfer modules in COMSOL were used for modeling. Parameters of the model included a gold microcapillary tip with 50 μm outer diameter (40 μm inner diameter), immersed in PBS buffer with an electrical conductivity of 1.67 S/m (Gielen et al., 2010). In the model, the conductive tip was placed 20 μm above the indium tin oxide (ITO) ground electrode and a potential of 10 V or 20 V was applied to the electrode by means of a square function (5 x 50 μs square pulses). Material properties used in the simulations were either from the COMSOL material library or reported elsewhere (Tolk et al., 2012; Yagi et al., 2005).
The simulations also provide an estimation of the temperature rise in the buffer solution, containing the cells, due to Joule heating (Erickson et al., 2003). The model implicated the heating caused by the electrical pulses as well as heat dissipation. Heat dissipation, as expected, mainly occurred through the electrodes, which have a high thermal conductivity.

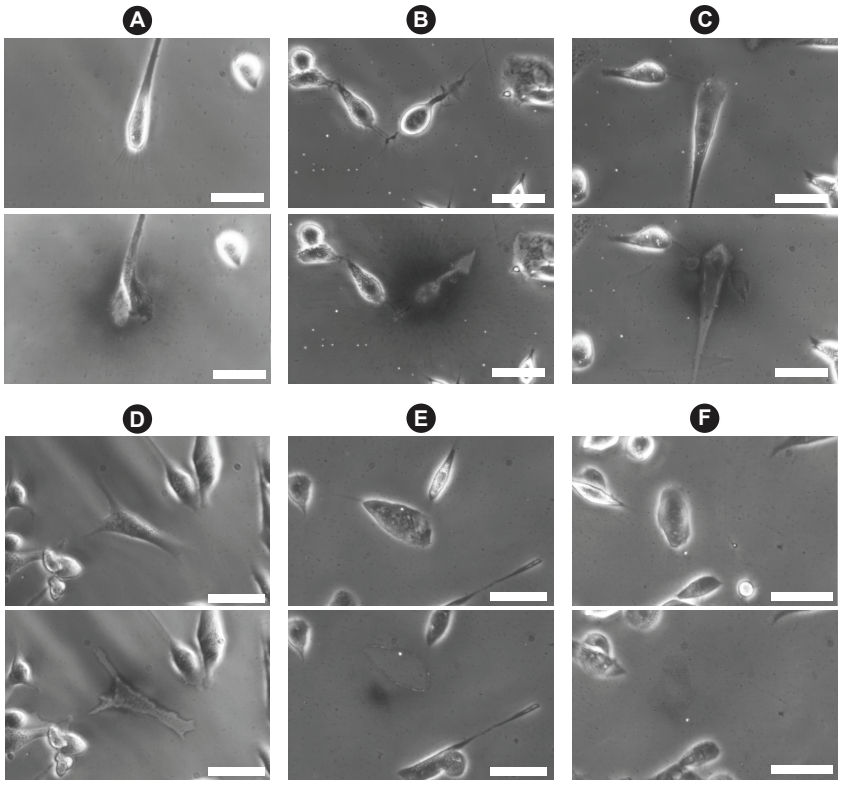

Figure A.2: *Light microscopy images of individual adherent BHK cells in PBS (A-C), HEPES buffer (D) and isotonic sucrose buffer (E, F) before (top rows) and after (bottom rows) lysis. Scale bars: 50 µm. (A) After a burst of electrical pulses has been applied, the targeted cell shows a necrotic morphology. (B-D) After a burst of electrical pulses and subsequent aspiration, only ghost imprints of the targeted cells remain; the surrounding cells are not affected. (E,F) Lysis in low-conductivity isotonic sucrose buffer. Longer electrical pulses with higher amplitudes had to be applied to achieve lysis. This also affected the surrounding cells, which showed a change in morphology.*

Convective heat dissipation was neglected due to the small Rayleigh numbers defined by the micrometer dimensions of the problem (Guyon et al., 2001). The temperature changes in the fluid are a function of time, applied voltage, and thermal and electrical properties of buffer and electrodes that alter heat generation and sinking. Supporting Figure A.3 shows the predicted temperature distribution at the end of the fifth 10 V pulse (see also Supporting Figure A.4). Voltages greater than 10 V were only applied to compensate for electrode aging. As heating can be harmful to cells and proteins, simulations were used for estimating the spatial temperature distribution throughout the model as a result of Joule heating. The simulations using a worst-case scenario (5 x 50 µs DC square pulse with an amplitude of 20 V over a 20 µm gap), predict a maximum temperature of approximately 75 °C in PBS (Supporting Figure A.4). However, temperatures above 40 °C only occur for 1 ms, and 20 V amplitudes were only used to compensate for electrode ageing. For amplitudes of 10 V reflecting the standard conditions the simulation predicts a much lower maximum temperature that stays well below 40 °C (Supporting Figure A.4), which was found to be the onset temperature of thermal protein denaturation in mammalian cells (Bischof et al., 2005). However, the

transition temperatures, *Tm*, at which half the protein content is denatured, vary from 40–90 °C for different proteins (Lepock, 2003). Moreover, these values are mostly derived on the

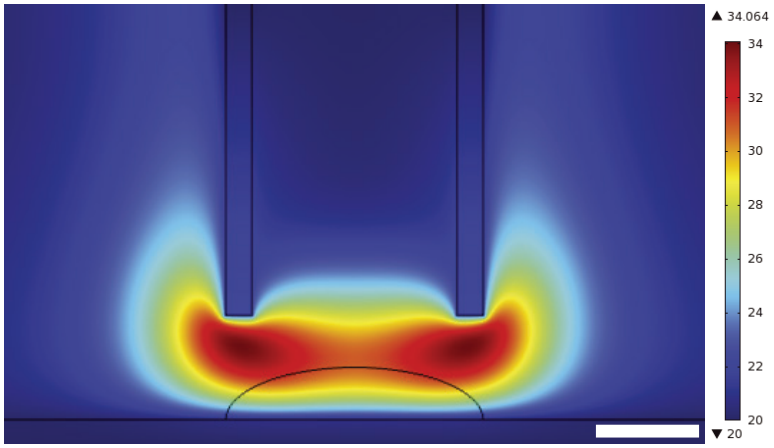

Figure A.3: *Temperature distribution results from simulations in °C; Scale bar: 20 µm. The simulation considered the effect of Joule heating and conductive heat dissipation. The color map indicates the temperature distribution at the end of the fifth 50 µs, 10 V DC square pulse (time point 0.45 ms of the simulation; see Supporting Figure A.4) when the maximal temperature in the worst-case scenario occurs. The simulations reveal a maximum temperature of 34 °C in close vicinity to the microcapillary electrode tip, where the electric field has its highest strength. The profile of a cell (curved black line) placed on the bottom electrode (ITO) was added to the model in order to estimate the average values within this region.*

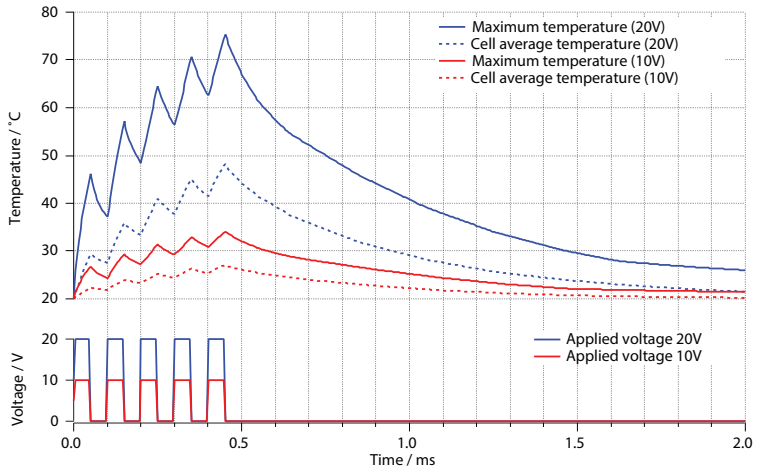

Figure A.4: *Temperature changes predicted by FEA. The solid lines (top panel) show the variation of the maximum temperature in the solution over time as result of the electric pulses (bottom panel) applied via the gold-coated microcapillary. Typical experiments for cell lysis were performed with voltages of maximally 10 V. However, to compensate for electrode erosion, voltages up to 20 V were applied in rare cases. The uppermost temperature reached was about 75 °C for amplitudes of 20 V (blue solid line) and about 34 °C for amplitudes of 10 V (red solid line). The dotted lines show the average temperature within the cell region (indicated in Supporting Figure A.3 and A.4) over time. The maximum average temperature within the cell region is 48 °C for amplitudes of 20 V (blue dotted line) and about 27 °C for amplitudes of 10 V (red dotted line). (bottom panel) Plot of the electric pulses applied to the microelectrode tip; five DC square pulses with amplitudes of 20 V (blue) and 10 V (red) and a pulse duration of 50 µs.*

basis of equilibrium thermodynamics by differential scanning calorimetry (DSC) and do not reflect the effects of short heat pulses on proteins. In addition to the short peak-temperature durations demonstrated by the model, the estimated average temperatures within the cell region are much lower than the maximum temperatures (Supporting Figure A.3 and A.4).

A.4 Test proteins

A.4.1 Temperature-dependent enzymatic activity of HRP

Horseradish peroxidase (HRP) conjugated goat anti-mouse IgG (8.5 mg/ml, A2554, Sigma, Switzerland) was diluted to 0.85 µg/ml in PBS and heated to 40 °C, 60 °C and 80 °C for 30 min, while the control sample remained on ice. After dilution of the treated samples to 8.5 ng/ml with PBS, the enzymatic activity of HRP was analyzed by enhanced chemiluminescence (ECL) on a dot plot (Supporting Figure A.5A). The results shown in Supporting Figure A.5 illustrate the strong decrease of the enzymatic activity of HRP with temperature. At 40 °C a significant decrease in the enzymatic activity was observed, indicating that the temperature sensitivity of HRP is suitable to further characterize our setup. The complete loss of the

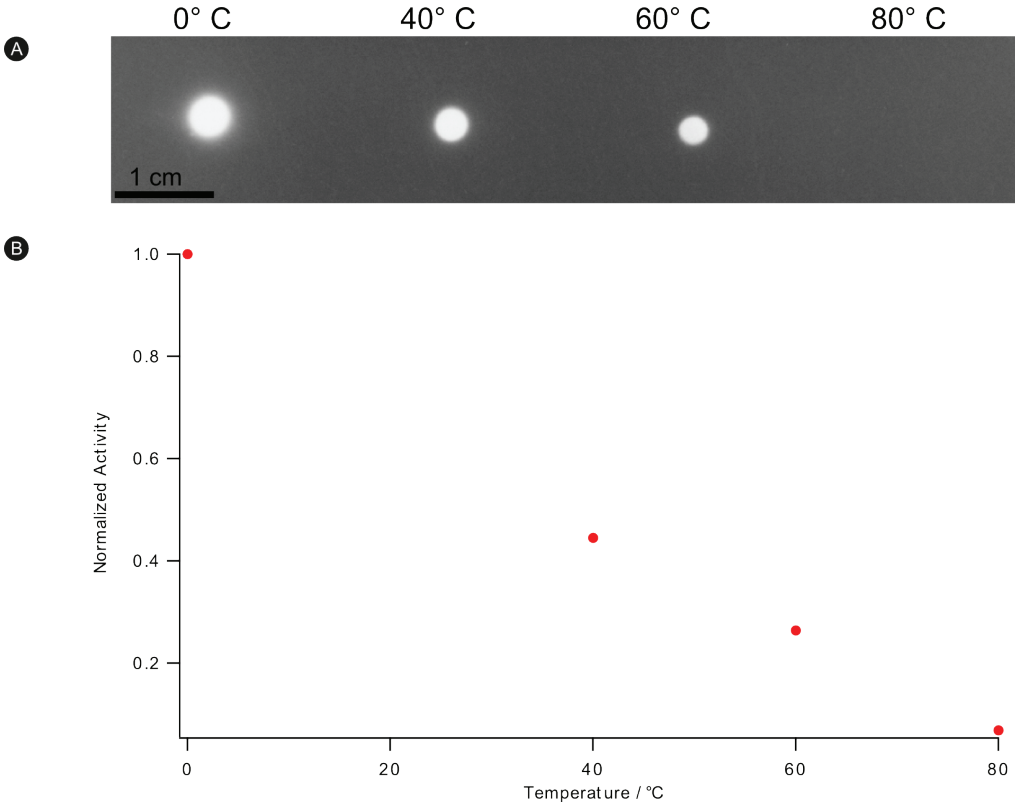

Figure A.5: *Temperature dependence of the enzymatic activity of HRP. (A) The enzymatic activity of HRP in the heated samples was analyzed by ECL on a dot plot. (B) The detected intensities were normalized with respect to the control sample and show a strong decrease with temperature and completely disappear at 80 °C.*

enzymatic activity at 80 °C is in good accordance with previous studies showing that the cofactor (heme) of the active site is depleted above 74 °C (Chattopadhyay et al., 2000).

A.4.2 Structural preservation of F-actin

Synthetic F-actin was chosen as a test sample to further investigate the effects of electrical pulses on sensitive supramolecular assemblies. 2 µl of 0.1 mg/ml F-actin (polymerized from G-actin; 8101-01, Hypermol, Germany, with polymerization buffer PolyMix; 5000-01, Hypermol, Germany) sample was placed onto an ITO coated glass slide, and the microcapillary electrode was placed in the drop, about 20 µm above the glass slide. Different voltages (6 V, 10 V, 14 V, 20 V, 30 V and 40 V), each with a burst count of 5 and a single pulse length of 50 µs were applied. 1 µl was removed from the treated sample droplet, diluted to 0.01 mg/ml

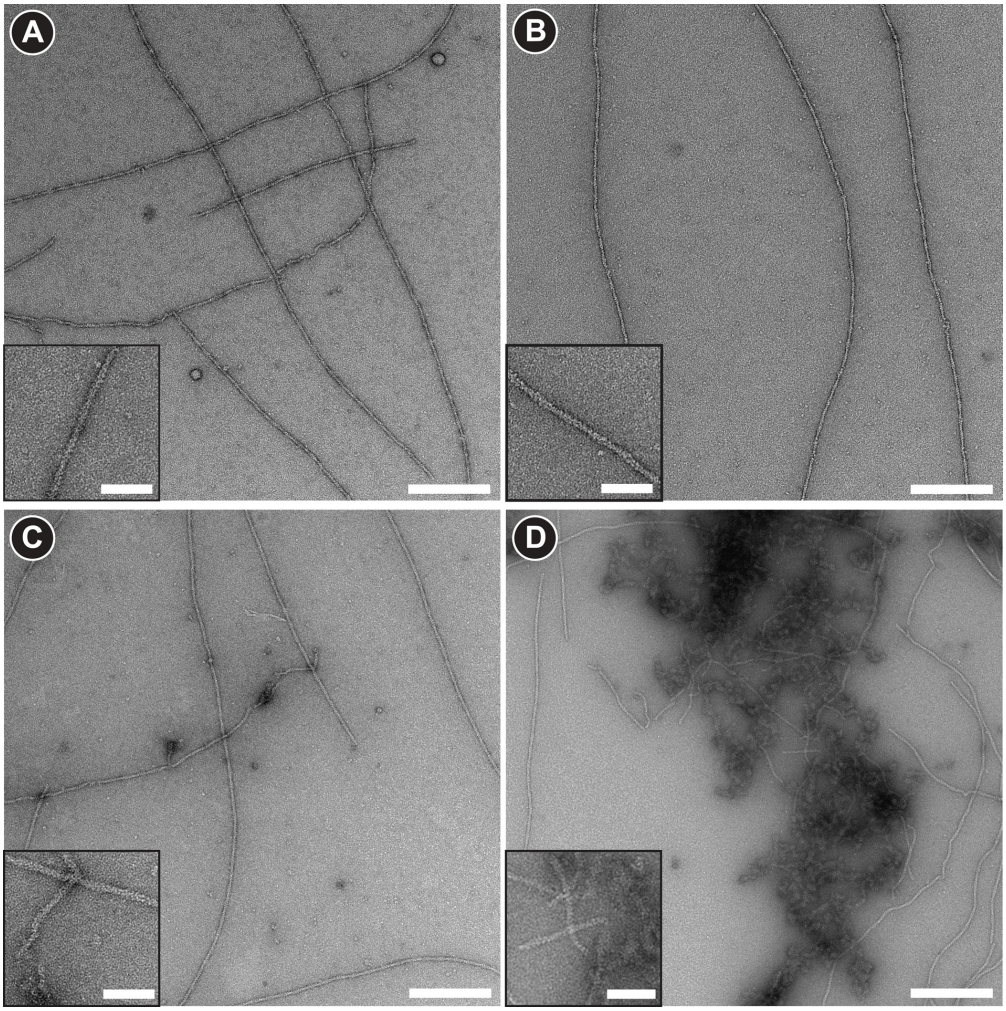

Figure A.6: *Actin filaments exposed to different voltages in the setup. The TEM micrographs illustrate the observed tendency of actin filaments treated with (A) 0 V, (B), 10 V (C) 20 V and (D) 40 V. Scale bars: 200 nm; insets 50 nm.*

in PolyMix buffer, adsorbed onto an EM grid and negatively stained with 2% uranyl acetate without washing.
The visual inspection of the samples with TEM did not reveal obvious structural differences, due to the treatment, up to 14 V. Compared to the untreated control sample the structural details in the samples exposed to 6 V, 10 V and 14 V were preserved and no signs of protein denaturation were detected (Supporting Figure A.6A and B). At 20 V the signs of structural damage such as filament fractionation, were rarely observed (Supporting Figure A.6C) and became more frequent at 40 V. At 40 V, protein denaturation and aggregation was observed (Supporting Figure A.6D).

A.5 Lysis and aspiration movies of fluorescently labeled cells

Human embryonic kidney (HEK 293) cells were cultured and prepared similarly to the BHK cells described in the manuscript, except that they were grown in Eagle's minimal essential medium (EMEM) supplemented with 1% non-essential amino acids, 2 mM glutamine and 10% fetal bovine serum.
For the fluorescence experiments, cells growing inside a miniaturized Petri dish were gently washed 2x with pre-warmed PBS and 200 µl of 2 µM calcein acetoxymethylester (calcein AM) (Invitrogen, US) in PBS solution was added to the miniaturized Petri dishes. The cells were incubated for 30 min at 37 °C. Electroporation was performed as described in the manuscript, and the subsequent aspiration was performed with a delay of approximately 1.5 sec (see supplementary movies).

A.6 Reverse phase protein array

HEK 293 cells were cultured, prepared as described in the previous paragraph. Electroporation and aspiration was performed as described in the manuscript. Inside the miniaturized Petri dishes one culture was growing on a bare ITO surface and a second culture was growing on a collagen coated ITO surface. Collagen coating has been performed as described previously (Harnett et al., 2007).
For the collection of samples with more than one cell, a cluster of cells (up to 23) was lysed and aspirated simultaneously. Subsequent to aspiration the samples were spotted onto a nitrocellulose membrane-coated microscope slide (16-pad FAST slide, Maine Manufacturing, Sanford, Maine, USA).
For a dilution series of batch lysed cells, HEK 293 cells were detached, counted and lysed in batch by sonification. Afterwards the batch lysate was diluted in PBS to give an equivalent of 330, 3300 and 33000 cells and 1 µl was spotted on the nitrocellulose membrane-coated microscopy slides by hand.
The assay procedure followed in principle as described before (Dernick et al., 2011). In brief, the slides were blocked in LiCor Odyssey blocking buffer for 10 min and then incubated with an anti-actin antibody (Millipore, #NG1848416, diluted 1:1000 in 10% LiCor Odyssey

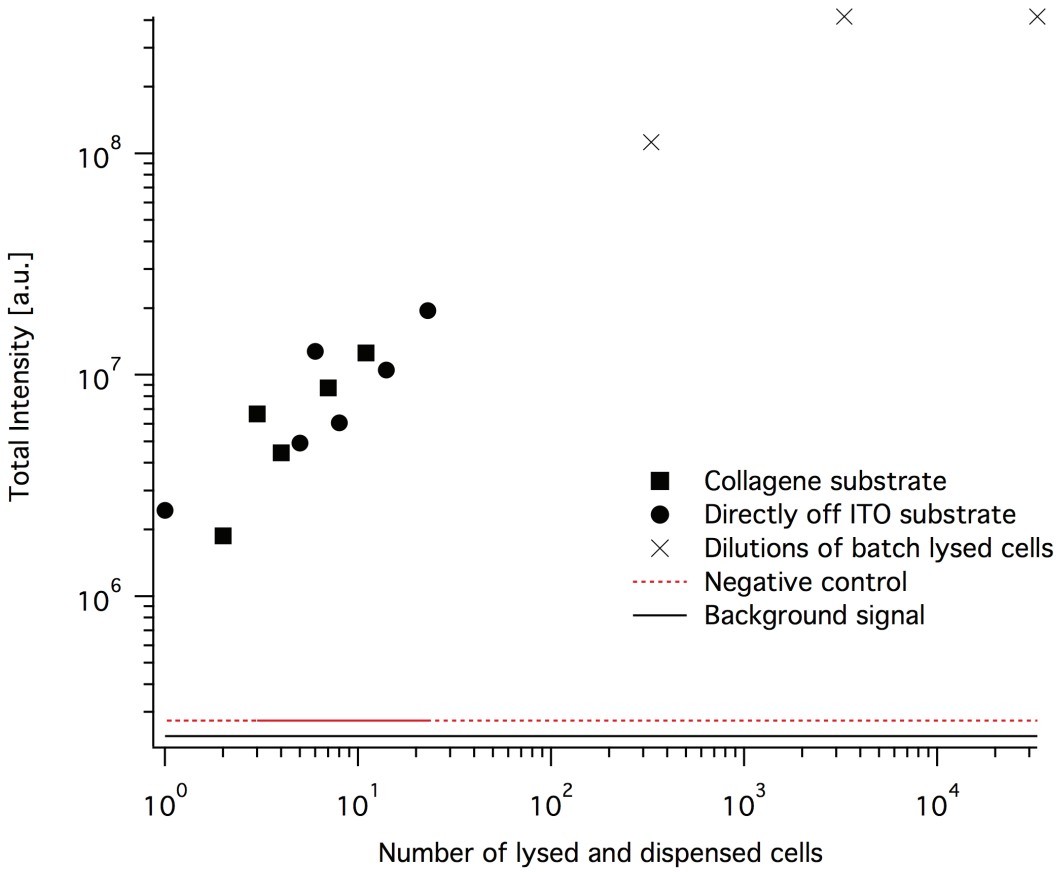

Figure A.7: *Cell lysis and reverse phase protein array. Individual cells were lysed and dispensed as spots on a nitrocellulose membrane-coated microscope slide. After incubation with an anti-actin antibody and a fluorescently labeled secondary antibody the slide was scanned. The total fluorescence intensity was plotted against the number of lysed cells dispensed in each spot.*

blocking buffer (=assay buffer), 24 h room temperature) washed three times 5 min in assay buffer. Then the slide was incubated with a fluorescently labeled secondary antibody (LiCor anti-mouse-IRDye800, 1 µg/ml in assay buffer, 1h at room temperature), washed three times 5 min in assay buffer and blown dry. The slide was imaged in a LiCor Odyssey infrared fluorescence scanner in the 800 nm channel with intensity 4, quality low, resolution 21 µm. Quantification of spot intensities was done in GenePix Pro 6.0 (Molecular Devices, Sunnyvale, CA, USA) with variable spot diameters. The total spot intensity was reported in Supporting Figure A.7.

APPENDIX B

Supporting information: Chapter 3

B.1 Effect of different desalting times

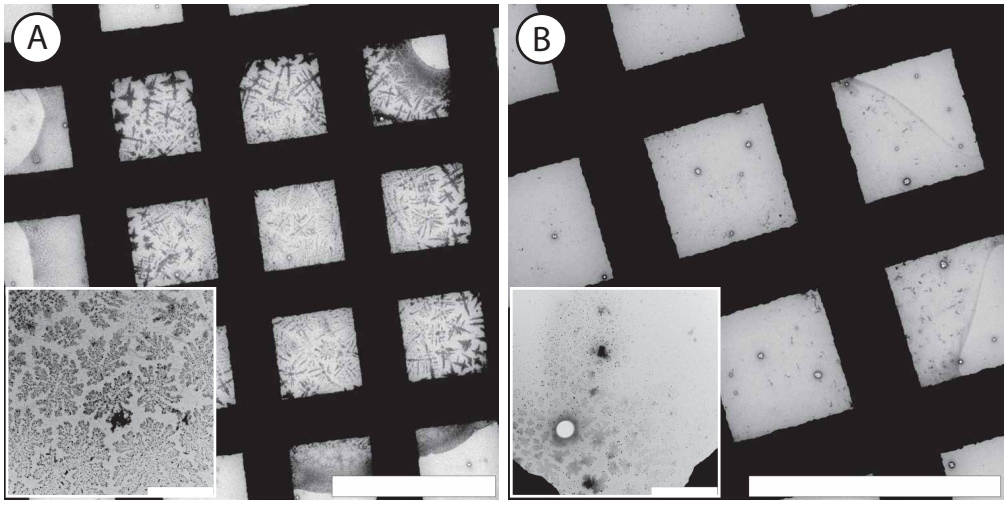

Figure B.1: *Desalting of a single-cell lysate sample. A microcapillary loaded with 5 nl of single-cell lysate was dipped into a reservoir of NanoVan 2%. A) 3 min immersion with the sample plug isolated from the system liquid (H_2O) by a 50 nl air plug, thus preventing desalting via the system liquid. The deposited spot from 5 nl sample volume shows a very high density of salt crystals; B) 7 min immersion with the sample plug in direct contact with the system liquid (H_2O), thus allowing diffusion of salt ions into the system liquid. Only a few salt crystals formed when the deposited 5 nl sample spot dried, mainly at the edges of the deposited spot. Scale bars: 200 µm for the overview and 5 µm for the insets.*

B.2 Quantification of sample loss

To compare the simulation with an experiment, 5 nm gold beads (supplied by Cell Microscopy Center, Department of Cell Biology, University Medical Center Utrecht, The Netherlands), diluted in 50 mM volatile ammonium bicarbonate (ABC) buffer, were used as a test sample to compare a conditioned sample spot with a directly deposited, non-conditioned sample spot. Since the deposition and drying of sample spots is influenced by the salt concentration of the sample, great care was taken to ensure that the conditions were almost identical for both deposited spots. Therefore, we first aspirated 200 nl of ABC buffer into the microcapillary before

loading 5 nl of Nanogold, to prevent desalting of the sample during dialysis. Conditioning was performed for 10 min by immersing the tip of the microcapillary into a reservoir of ABC buffer. Meanwhile, a slot grid with three large windows (Formvar/Carbon Type-B, Triple Slot, Copper, #01816, Ted Pella Inc., USA) was glow discharged for 30 s. After conditioning, 5 nl

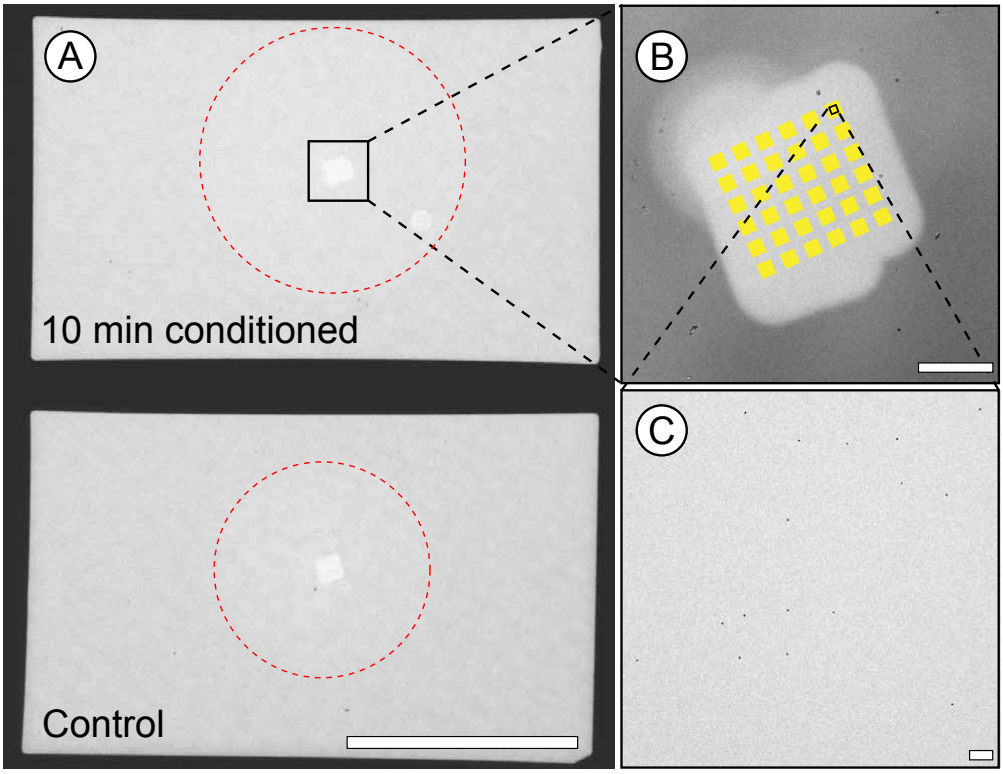

Figure B.2: *Quantification of particle amount by EM. A) Top: Overview of a slot grid after image acquisition (brighter areas are due to electron beam). Bottom: Control experiment (no conditioning) and positive control were applied in individual grid windows. Scale bar corresponds to 500 µm. B) A higher magnification image showing the area indicated in A), to illustrate the particle quantification approach (see text above). Scale bar: 20 µm. C) An even more magnified view of one of the yellow areas in B). At this magnification, individual gold particles can be recognized and their density per surface area can be evaluated. Scale bar: 100 nm.*

were deposited onto the center window of the slot grid. Next, the microcapillary was flushed with 1 µl of system liquid and 50 nl of fresh ABC buffer were aspirated before the next 5 nl of Nanogold sample was aspirated. This time the microcapillary was directly positioned over one of the two free slots on the still freshly glow discharged slot grid and 5 nl were deposited. Supporting Figure B.2 shows the particle counting approach used for the control experiments. A total of 6x6 images with a size of 4.7 µm x 4.7 µm (magnification 25 000x) were recorded from each window with deposited sample, using a Philipps CM10 electron microscope (see Materials and Methods). Subsequently, the gold particles in the images were counted by a particle-counting algorithm (LabView, National instruments). The results performed with two different nozzle geometries (inner diameter of 30 µm or 40 µm, respectively) are shown in Table S2 and compared to the FEM simulations (see main manuscript).

Experiment	FS360-250-40	Simulation	FS360-100-30	Simulation
Conditioning 10'				
Avg. no of particles	106.6		72.3	
Std. Dev.	17.7		9.8	
Negative control				
Avg. no of particles	206.5		94.4	
Std. Dev.	26.5		18.4	
Loss	**48.4%**	**60.9%**	**23.4%**	**18.2%**

Table B.1: *Observed numbers of gold particles per grid square (corresponding to 1600 μm^2) prepared after 10-min diffusion (top) or without diffusion (bottom). The relative loss due to diffusion is listed in the last row, which is compared with FEM simulated values (see main text). Two types of microcapillaries were used for the experiments, of 360 μm outer and 250 μm respectively 100 μm inner diameters, and 40 μm respectively 30 μm tip inner diameters. The measured loss values are approximately in range with simulated values.*

B.3 Direct deposition of nanocrystals without conditioning

Supporting Figure B.3 demonstrates the need for conditioning of 3D crystals prior to EM grid preparation.

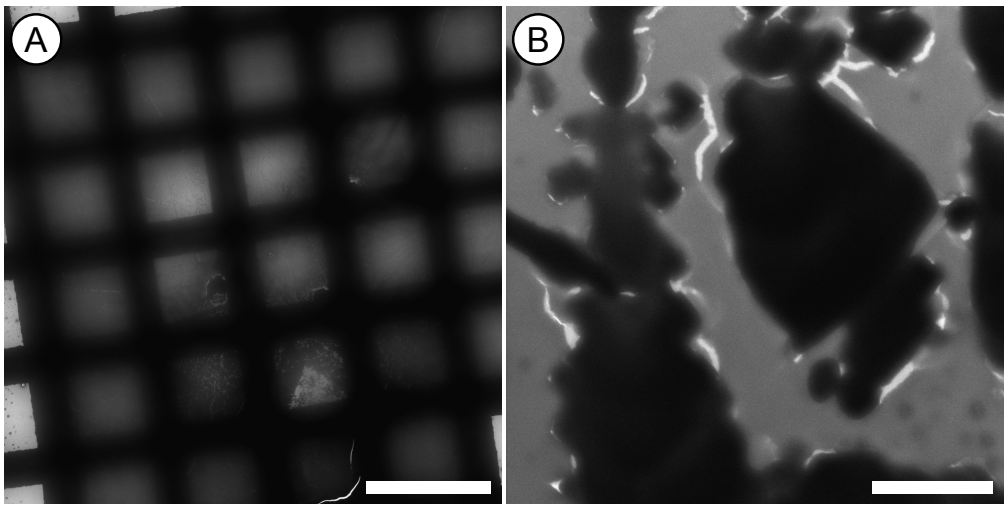

Figure B.3: *Direct deposition of nanocrystal solution without conditioning. A) Overview. Scale bar: 200 μm. B) Enlargement of electron-dense material. Scale bar: 5 μm.*

APPENDIX C

Supporting information: Chapter 4

C.1 cryoWriter: Detailed setup description and sample vitrification

The CryoWriter setup is illustrated in Supporting Figure C.1. It has a temperature-controlled stage (1) that is maintained close to the dew point (DP-stage). A combined temperature and humidity sensor (UFT75-AT, Sensor-Tec, Germany) continuously determines the dew point of the room, and a water-cooled Peltier element regulated by a Peltier controller (Cooltronic GmbH, Switzerland) is used to adjust the temperature of the DP-stage accordingly. The electron microscopy (EM) grid (previously glow-discharged for 30 sec in air plasma), is held by tweezers (2) that are fixed to an adapter (3). Rotation of a finger screw on the adapter opens and closes the tweezers allowing the grid to be gripped and held. An electromagnet (MMT Magnettechnik GmbH & Co. Germany) (4) holds the tweezers in the horizontal position, and the tweezers are cooled via two small Peltier elements mounted on it. The electromagnet is fixed to a precision kinematic mount (5) (KS05K/M, Thorlabs GmbH, Germany), which itself is mounted on a manual z-axis stage. Thus, the grid held by the tweezers can be aligned and placed flat (horizontally), with the holy carbon side up, in a slot in the DP-stage. The slot has a small hole (2 mm diameter) at its center to allow the passage of a laser beam (see below). Except in this region, the outer rim and the lower surface of the grid are in direct contact with the stage material. The DP-stage itself is mounted on a motorized stage (Prior Scientific, UK) (6), allowing the positioned grid and tweezers to be moved on a horizontal plane. A second adapter with another permanent magnet inserted (7) is connected to a large solenoid (8) (HD8286-R-F, Kuhnke, Germany) via a pivot. This adapter can rotate freely around its pivot axis, but is held in a horizontal orientation by a small permanent magnet (9). The large solenoid has a hub length of 30 mm and is controlled by a solenoid controller (MST-1630.001/002, Tremba GmbH, Germany) in such a way that the solenoid is actuated when a secondary circuit is closed (10).
A fused silica microcapillary (New Objective, USA) (11) mounted on an assembly of linear stages (M-404.2PD and M-414.3PD, Physik Instrumente, Germany), is connected to a high-precision syringe pump (Cetoni GmbH, Germany) (not shown). The microcapillary is used to aspirate sample from a storage container, e.g., PCR tubes, well plates etc., or from a lysed single cell (Arnold et al., 2016), and dispense it onto the grid on the DP-stage. Since the DP-stage is mounted on a motorized stage, the grid can be moved while the sample is being

dispensed, allowing it to be distributed across a wider area of the grid, if required. Two CCD cameras (not shown) allow direct observation of sample deposition and spreading (side view and tilted top view, see Supporting Figure C.2). The microcapillary is retracted once this is complete.

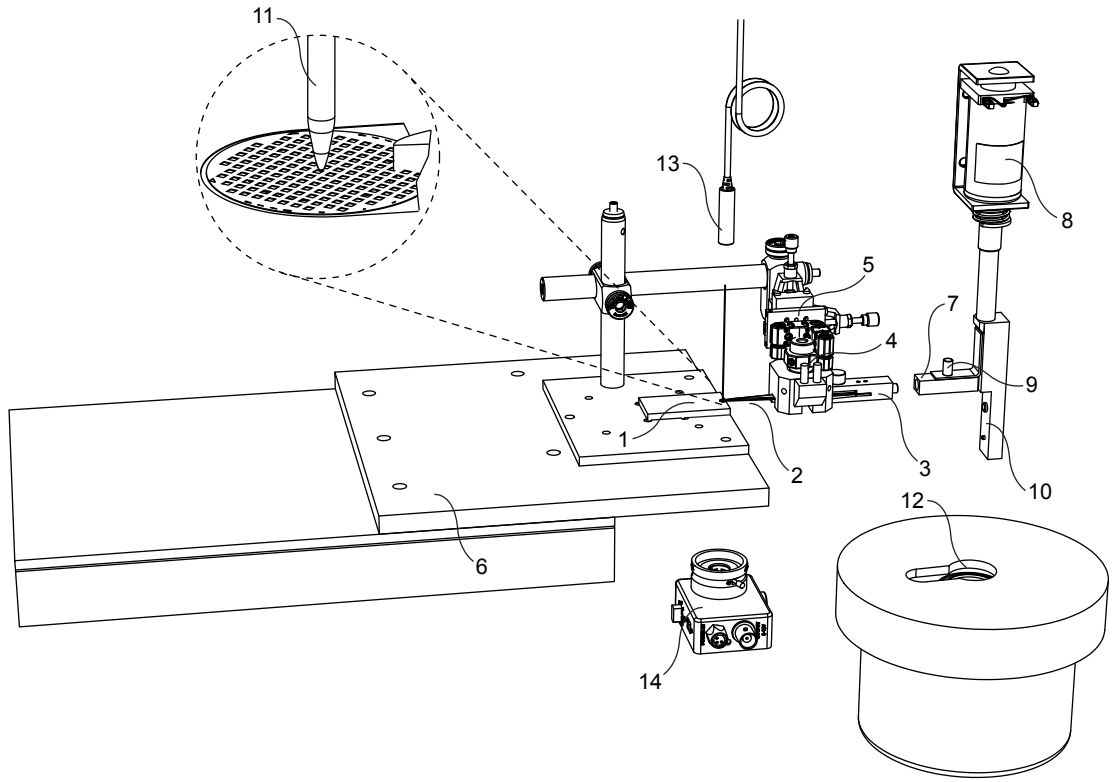

Figure C.1: *Schematic representation of the cryo-plunging device and its working principle. (1) Temperature-controlled dew point stage (DP-stage); (2) tweezers; (3) adapter holding the tweezers with magnet inserted at the other end; (4) electromagnet; (5) kinematic stage; (6) xy-motorized stage; (7) second adapter with magnet inserted; (8) solenoid with 30 mm hub; (9) small permanent magnet; (10) secondary electrical circuit to trigger the solenoid; (11) microcapillary; (12) cryogen container with lid; (13) laser diode; (14) photodetector.*

After sample deposition, evaporation of the liquid is controlled by the temperature of the DP-stage and can be monitored using a laser diode (λ=780 nm, CPS192, Thorlabs GmbH, Germany) (13) and a photodetector (photodiode PDA100A, Thorlabs GmbH, Germany) (14) with a manual aperture (SM1D12SZ, Thorlabs, Germany). The laser diode is mounted above the DP-stage, illuminating the area of the grid where sample was deposited. The photodetector is positioned underneath the DP-stage in the optical path of the laser diode. Sample vitrification proceeds automatically when the laser signal registered by the monitoring system reaches a defined threshold or after a pre-set time defined by the user (see main text). Injection of the grid into the cryogen is triggered when the electromagnet (4) is turned off

and the two magnets inside adapters (3) and (7) snap together, withdrawing the tweezers and grid from the DP-stage. The newly-formed assembly falls into the vertical position due to its increased weight. When the assembly reaches the vertical position, it automatically closes the secondary circuit (10), which triggers the large solenoid. The 30-mm solenoid hub shoots the EM grid and the tip of the tweezers into the cryogen (12) (a mixture of ethane and propane (40:60) liquefied in a standard cryogen container from Vitrobot, FEI, USA with a custom-made Styrofoam lid to minimize ice contamination during plunge-freezing). Only a few hundred milliseconds pass from the moment the electromagnet (4) is turned off until the grid is immersed in the cryogen. The tweezers can now easily be removed from the assembly by hand (magnetic connection) and the grid can be placed in a grid-storage box immersed in liquid nitrogen and subsequently transferred to a storage Dewar or directly into a cryo-equipped electron microscope for observation.

C.2 cryoWriter: Control software

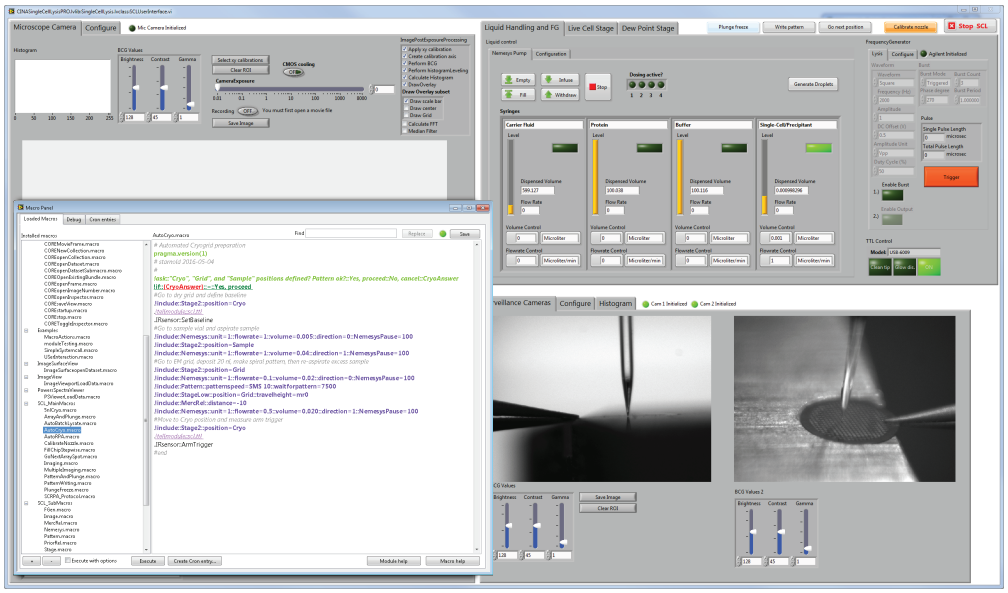

Figure C.2: *Control software showing the liquid handling control plug-in (top right), surveillance camera views of the microcapillary and the EM grid during sample deposition (bottom right), and the macro panel (left) for automation.*

All instrument modules are controlled via National Instruments LabVIEW software (Elliott et al., 2007). The openBEB framework (www.openbeb.org) is used to load each instrument program as an independent plug-in (Ramakrishnan et al., 2014). Many experimental steps, such as sample loading, deposition, and cryo-injection have been automatized using the macro language of openBEB. Supporting Figure C.2 shows a screenshot of the control software, including the macro window for process automation.

C.3 Real-time monitoring of water thickness by a 780 nm laser diode

If the grid and stage are kept at the dew point temperature, the relative humidity (rH) of the microenvironment in proximity to the grid is 100%. To prevent water condensation and allow controlled evaporation of sample water from the grid surface, the stage temperature needs to be slightly above the dew point temperature, e.g., the temperature offset is chosen to give 90% rH at the grid surface.

(I) rH of the DP-stage/grid microenvironment and sensitivity to rH of the room

Calculations show that for small offsets from the dew point temperature (e.g., +2 °C), the rH of the DP-stage microenvironment is linearly dependent on the stage temperature over room rHs ranging from 20% to 90% at a room temperature of 23 °C (Supporting Figure C.3a). Further, the temperature offset needed to create a 90% rH microenvironment on the stage, varies by less than 0.3 degrees for room rHs ranging from 20% to 90% at 23 °C (Supporting Figure C.3b). Thus, the cryoWriter procedure is not sensitive to rH changes in the room, and the system does not necessarily require a humidity-controlled chamber, however, this might be desirable for future applications.
The rH at temperature *T*, *rH(T)*, was calculated as follows:

$$rH(T) = 100 \cdot \frac{E(RT)}{E_S(T)} = e^{17.62\left(\frac{RT}{243.12+RT} - \frac{T}{243.12+T}\right)} \cdot rH(RT)$$

$$\text{with} \quad E(RT) = E_S(RT) \cdot \frac{rH(RT)}{100} \quad \text{and} \quad E_S(T) = 611.2e^{\frac{17.62T}{243.12+T}}$$

Where *E(RT)* and $E_S(T)$ are the actual vapor pressure (in Pascal) at room temperature *RT* and the maximum (saturated) vapor pressure at temperature *T*, respectively, as described by the Magnus formula (Alduchov and Eskridge, 1996).
In agreement with the above conclusions, when larger sample volumes were deposited by protocol 1, it generally sufficed to determine the time lag required between sample deposition and pick-and-plunge freezing using buffer aliquots (see proof-of-concept experiments in the main text; Section 4.3.3), the degree of thinning did not need to be monitored experimentally.

(II) Dependence of laser transmission on sample-layer thickness

The cryoWriter setup allows, water evaporation to be experimentally monitored by an optical system consisting of a 780 nm laser diode and a photodetector. This is an alternative to determining the time lag resulting in useable vitreous layers by trial and error and is particularly important for deposition protocol 2. The transmission of an almost perpendicular laser beam through the grid is measured (see Figure 4.1 of main text and Supporting Information C.1.

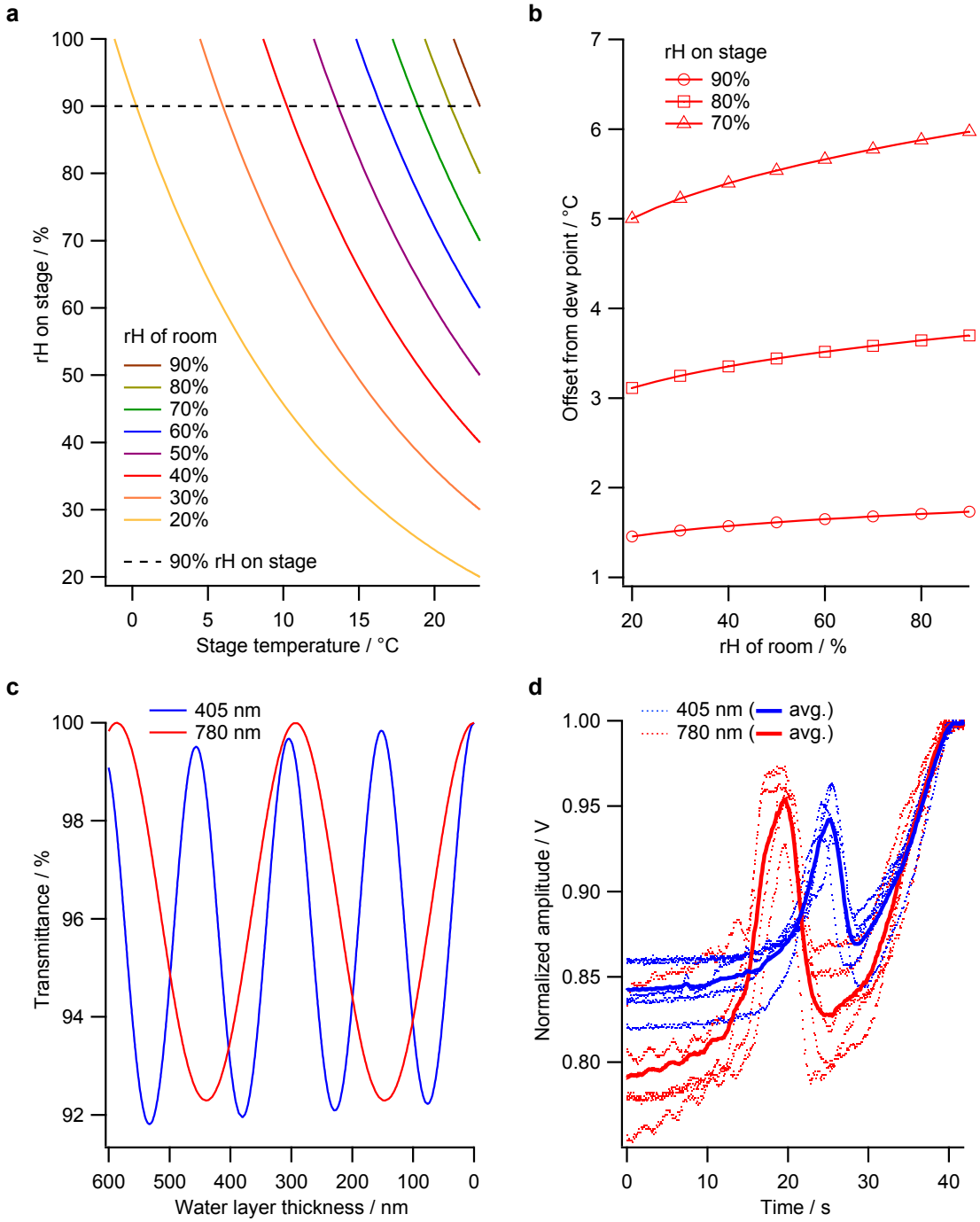

Figure C.3: *(a) The DP-stage temperature vs. the relative humidity (rH) of the stage/grid microenvironment, plotted for eight different room rHs at a room temperature of 23 °C. For small positive offsets from the dew point temperature (e.g., +2 °C), the plots are approximately linear and have similar slopes for all eight scenarios.*

(continued)

(b) Dependence of the offset from the dew point temperature needed to create three different rH microenvironments on the DP-stage vs the rH of the room at 23 °C. The offset needed to create a 90% rH microenvironment on the DP-stage varies by less than 0.3 degrees when the room rH changes from 20% - 90%. (c) Simple simulation of the transmittance of ideal coherent blue (405 nm) or infrared (780 nm) laser light incident perpendicular to a layer of water. The transmittance is plotted against the thickness of the water layer (Concise Macleod software, Thin Film Center Inc., USA). (d) Normalized amplitude vs time for the complete evaporation of a 20 nl water spot deposited on a glow discharged EM grid (Quantifoil Cu 200 mesh, R2/1) measured with an infrared (red line, $\lambda = 780$ nm) or a blue laser (blue line, $\lambda = 405$ nm). The grid was kept 3 °C above the dew point. Several independent experiments were carried out (n=5; dotted lines) on different grids for both wavelengths and the average results were calculated (solid lines). Note, that the clarity of the interference pattern suffers (i) due to the bad coherence length of the laser diodes used, (ii) imprecise tilt geometry of the laser relative to the grid, and (iii) the non-uniform film thickness on the illuminated area.

Changes in film thickness due to evaporation affect the amplitude of the signal recorded by the photodetector (Figure 4.2 of main text). To confirm that these signal changes are dominated by interference effects as suggested in the main text, the transmitted signal was measured for laser diodes emitting at different wavelengths (780 nm and 405 nm). As expected from interference theory (Supporting Figure C.3c), the two patterns were qualitatively the same and the positive peak of the blue laser signal was shifted towards thinner water layers (Supporting Figure C.3d).

C.4 Salt effects caused by incorrect sample thinning

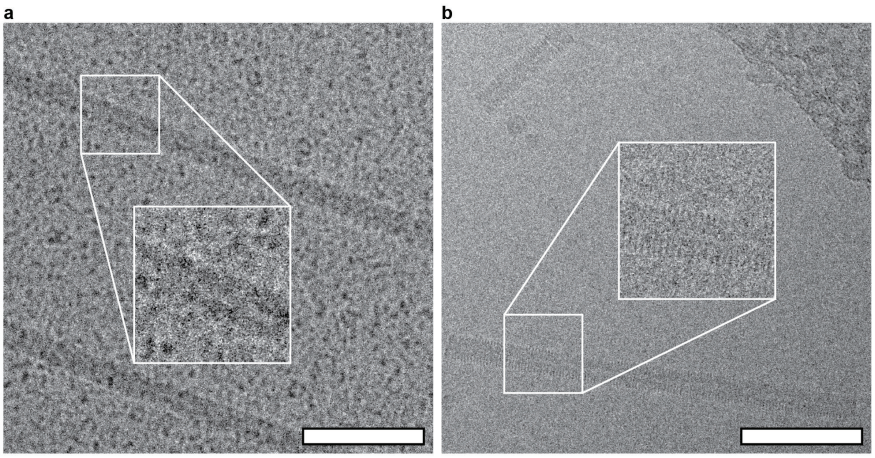

Figure C.4: *Demonstration of salt effects occurring when too much water evaporates during sample thinning. Tobacco mosaic virus (TMV) samples in PBS containing 0.1% decyl-β-D-maltopyranoside (DM) were prepared for cryo-EM using the cryoWriter and deposition protocol 2; (a) Incorrect sample thinning, too much sample was left on the grid and/or not spread wide enough before thinning. As a result, small salt crystals (high contrast) are visible in the background and the resolution of the repeating structure of TMV is diminished. (b) Correct sample thinning. The 23 Å repeat of TMV is clearly visible in the raw image and the vitrified ice background has low contrast. This image also shows that the cryoWriter can be used to prepare cryo-EM grids from samples containing detergent. Insets in (a) and (b): two-fold enlargement of the indicated region. Scale bars: 80 nm.*

C.5 Comparison with classical preparation method of a membrane protein

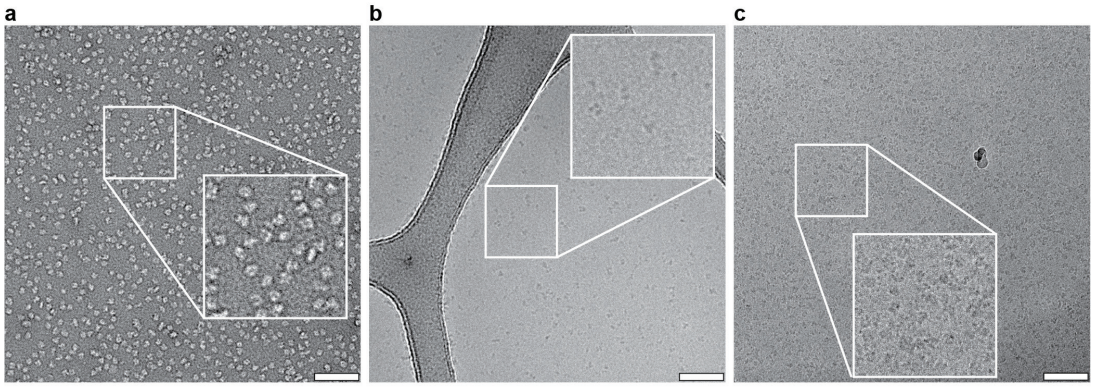

Figure C.5: *200 kDa membrane protein reconstituted in amphipols. The sample was prepared for microscopy in different ways. The cryo-EM grids were prepared on the same day. The same sample stock of the reconstituted protein in HEPES buffer complemented with 5 µM sodium azide was used throughout. (a) Negatively stained grid; 2% uranyl acetate. (b) Cryo-EM grid prepared using a classic Vitrobot plunge-freezer. The protocol used with the Vitrobot was as follows: 300-mesh Lacey copper grids were glow discharged for 60 s and fed into the Vitrobot for plunge-freezing in liquid ethane: amount of protein sample loaded, 2.5 µl; wait time, 5s; blotting force, 1; blotting time, 3 s; blotting paper, Whatman #1 qualitative; nominal relative humidity 100% (measured relative humidity at grid position: 85%), chamber equilibrated at 10 °C. (c) Cryo-grid (Quantifoil 200 mesh, R2/2) prepared using cryoWriter protocol 2; 3 nl sample volume. Insets: two-fold enlargement of the indicated regions. Scale bars: 80 nm.*

C.6 Cryo-EM grid preparation with continuous carbon film coated grids vs. holey carbon film only

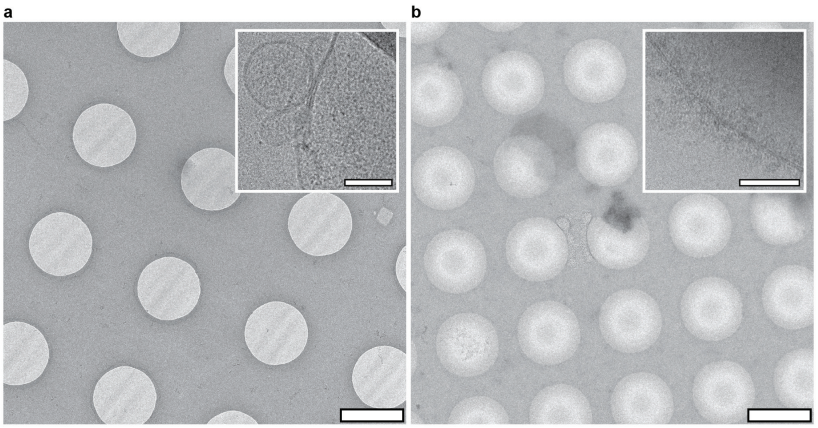

Figure C.6: *Single-cell lysate deposited with protocol 2. (a) Holey carbon grid with additional layer of continuous carbon (Quantifoil 200 mesh R2/2). Note the slight wrinkles of the continuous carbon layer and the otherwise homogeneous ice layer. (b) Holey carbon grid without continuous carbon film (Quantifoil 200 mesh R2/1). Note the gradients within the holes. Insets show typical membrane patches found in single-cell samples. Scale bars represent 2 µm for overview and 80 nm for insets.*

C.7 Fourier shell correlation

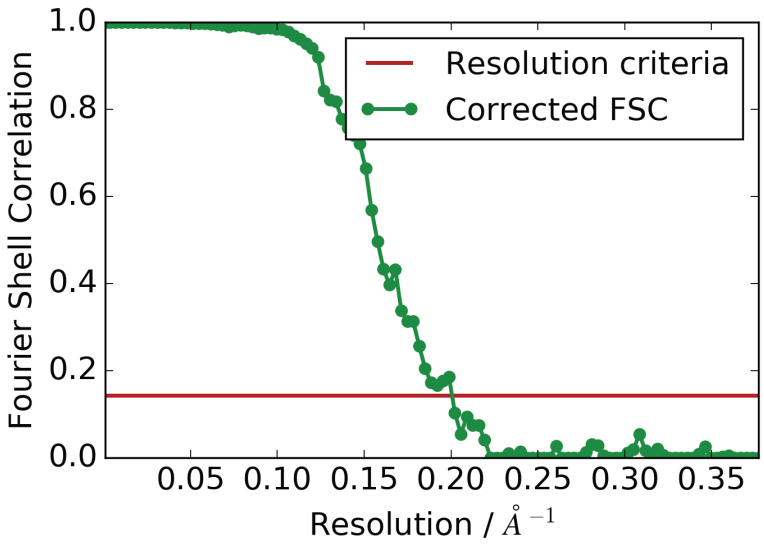

Figure C.7: *The corrected Fourier Shell Correlation (FSC) curve after the final sharpening of the urease map. According to the "gold-standard" the frequency at which FSC = 0.143 indicates the resolution of the 3D reconstruction. Here, the corresponding spatial frequency is 0.199 Å^{-1}, giving an estimated resolution of 5.03 Å.*

APPENDIX D

openBEB macro scripts

D.1 openBEB modules and plugins

The functionality of openBEB (Ramakrishnan et al., 2014) can be extended by plug-ins. A plug-in can provide an arbitrary number of modules. Modules are pieces of program that can be accessed by a macro language and that are used for example to control a specific hardware. Technically, they are queued state-machines of a specific structure. The modules involved in the single-cell lysis, sample deposition, and cryoWriter setup are summarized in Table D.1.

Module name	Description
SCL.miccamera	Light microscope camera.
SCL.surveillancecamera	Surveillance cameras installed in the setup.
SCL.stage	All mechanical stages.
SCL.frequencygenerator	Voltage pulse generation for single-cell lysis.
SCL.nemesys	Liquid handling.
SCL.dpstage	Dew point stage and temperature control.
SCL.ttl	TTL switches used to trigger electromagnet or LED lights.

Table D.1: *The modules provided by the single-cell lysis (SCL) plug-in. The individually programmed modules are used to control all types of hardware embedded in the single-cell lysis setup and sample preparation platform.*

D.2 The openBEB macro language

The openBEB macro language is used to access the modules listed above and to execute certain actions, such as moving the stage or dispensing a sample. A short overview of the most frequently used special characters and functions of the macro language is given in Table D.2 below. For a comprehensive documentation of openBEB and the openBEB macro language, visit openBEB.org.
A module is addressed with the *!tellmodule* command. By using the indentation ".", a block of commands can be send to the selected module. The *!default* command is used to define

Character	Explanation
#	Indicates comments.
!	Defines commands for the macro-interpreter.
{variable}	The {} indicate the name of a variable.
.	Used for indentation of blocks, *e.g.*, after an !if statement.
::	used to separate commands, parameters, etc.
—	—
!default	Defines a variable with a default value.
!ask	Opens a dialog window, variables can be selected with answer.
!if	If statement.
!do	Executes a block of commands in a loop.
!calc	Environment for simple calculations.
!include	Embedds an other macro, *e.g.*, a repetitive sub-macro.
!tellmodule	Sends the subsequent block of commands to the addressed module.
!waitmodule	Creates a rendezvous request at the end of the module queue.

Table D.2: *The most commonly used characters and commands of the openBEB macro language and their function.*

variables, such as flow rate, or volume, as shown in the example code D.1 below. Execution of the code would run the consumer loop "*Dispense*" of the *SCL.examplemodule* module and set values for the variables *flow rate* and *volume*. Variables further allow the embedding of macros within other macros by the *!include* command. For example, the small macro script below can be integrated in another script with the command *!include::Example::flowrate=5::volume=5*. Repeatedly used snippets of code are thus written as sub-macros for fast and easy integration in larger scripts. A full summary of all sub-macros is given in the next section.

```
1  #Variables
2  !default::flowrate=1
3  !default::volume=1
4  #Commands
5  !tellmodule::SCL.examplemodule
6  .Dispense::{flowrate}::{volume}
```

Macro script D.1: *Example.macro*

D.3 Sub-macros

D.3.1 Frequency generator

The frequency generator (33220A, Agilent, Switzerland) can be triggered with macro script D.2. The parameters however, such as frequency or amplitude, need to be set in the user interface. A pause time can be chosen to wait for a certain time after a trigger.

```
#Variables
!default::FGenPause=500
#Commands
!tellmodule::SCL.FrequencyGenerator
.SendTrigger
.!waitmodule
.!wait::{FGenPause}
```

Macro script D.2: *FGen.macro*

D.3.2 Image acquisition

Macro script D.3 is useful for taking snapshots on the light microscope camera. The image name is a variable that can be set in the macro, the index is automatically added to the name.

```
#Variables
!default::name=Test
#Commands
!tellmodule::SCL.MicCamera
.setFileseriesDescriptor::LocationName::{name}
.setFileseriesDescriptor::Index::{index}
.SaveImage
```

Macro script D.3: *Image.macro*

D.3.3 Liquid handling

The Nemesys syringe pump (Cetoni GmbH, Germany) is controlled with macro script D.4. The dispensing unit, flow rate, dispensing volume, and flow direction (aspiration=1 or infusion=0) can be set in the macro. The *.Status* command keeps the module in a for loop until the dispensing volume has been reached. This is required for multiple dispensing runs, otherwise, the last dispensing command would overwrite all previous ones.

```
#Variables
!default::unit=0
!default::flowrate=1
!default::volume=1
!default::direction=0
!default::NemesysPause=0
#Commands
!tellmodule::SCL.nemesys
.MacroDosing::{unit}::{flowrate}::{volume}::{direction} #
   DosingUnit::FlowRate::TargetVolume::Infuse(0) or Withdraw
   (1)
.Status::{unit}
.!waitModule::SCL.nemesys::-1
.!wait::{NemesysPause}
```

Macro script D.4: *Nemesys.macro*

D.3.4 Stages

The instrument has 4 axes (xy-microscope stage, z-axis stage, plus an additional x-axis stage). The z- and x-axis stages are controlled by Mercury controllers (C-863, Physik Instrumente GmbH, Germany). The microscope stage (Prior Scientific, UK) is controlled by a separate controller. Both controllers are included in the *SCL.stage* module.

Relative movement

Macro script D.5 is used to move the microscope stage a specific distance relative to the current position.

```
#Variables
!default::stepsX=500
!default::stepsY=500
!default::PriorPause=500
#Commands
!tellmodule::SCL.Stage
.PRIORgoRelativeXYposition::{stepsX}::{stepsY}
.getStatus
.!waitmodule
.!wait::{PriorPause}
```

Macro script D.5: *PriorRel.macro*

This relative movement can also be used to program and trigger a pattern, *e.g.*, to spread a sample across a surface by moving back and forth in x and y. Macro script D.6 shows an example where two different patterns, a snake-like and a spiral pattern, can be selected. The patterns are illustrated in Figure D.1.

```
#Variables
!default::steps=10
!default::xrange=100
!default::yrange=100
!default::pattern=spiral #Alternative: snake
!default::patternspeed=SMS 10
#Commands
!tellmodule::SCL.Stage
.sendCommandPrior::{patternspeed}
.!if::{pattern}::=::snake
..!do::{steps}::index
...!calc::x={xrange}::0
#Calculate index%2, i.e. index even or odd.
...!calc::m={index}/2::0
...!calc::p={index}-(2*{m})::0
#Check if index%2 = 0
...!if::{p}::=::0
....!calc::x=(-1)*{xrange}::0
...PRIORgoRelativeXYposition::{x}::{0}
...getStatus
...PRIORgoRelativeXYposition::{0}::{yrange}
...getStatus
.!if::{pattern}::=::spiral
..!do::{steps}::index
...!calc::x={xrange}::0
...!calc::y={yrange}::0
#Calculate index%2, i.e. index even or odd.
...!calc::m={index}/2::0
...!calc::p={index}-(2*{m})::0
#Check if index%2 = 0
...!if::{p}::=::0
....!calc::x=(-1)*{xrange}::0
....!calc::y=(-1)*{yrange}::0
...!calc::x=({index}+1)*{x}::0
...!calc::y=({index}+1)*{y}::0
...PRIORgoRelativeXYposition::{x}::{0}
...getStatus
...PRIORgoRelativeXYposition::{0}::{y}
...getStatus
.sendCommandPrior::SMS 100
```

Macro script D.6: *Pattern.macro*

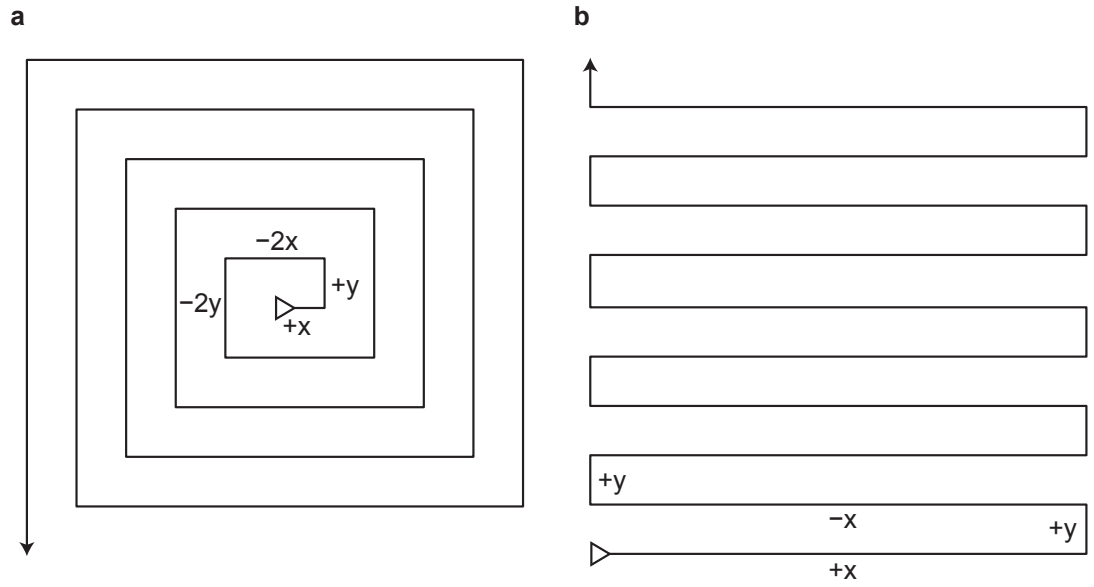

Figure D.1: *Two different patterns for spreading sample across an EM grid. (a) Spiral pattern and (b) snake pattern.*

The same relative movement can also be sent to the Mercury controllers. In macro D.7 the z-axis is moved relative to its current position.

```
#Variables
!default::distance=500
#Commands
!tellmodule::SCL.Stage
.MercMoveRelativeZ::macro::{distance}
.getStatus
.!waitModule::SCL.Stage::-1
```

Macro script D.7: *MercRel.macro*

Absolute movement (x_1,x_2,y,z)

To move the microcapillary tip to a new position, macro scripts D.8 and D.9 are used. The two scripts are very similar, depending on the targeted positions, one or the other might be safer to use. The position to move to is defined as a variable *{position}*. Both macros first retract the z-axis to the (safe) home position, before getting the new coordinates and starting to move towards the new position. Here, the two macros differ. Macro D.8 first moves the additional x-axis stage to its new x_2-coordinate. Once the new position is reached, the microscope stage is moved to its new position (x_1,y). This procedure, however, can be dangerous. The microcapillary tip is mounted on the additional x-axis and is moved

with it. Under certain circumstances, the microcapillary and its holder can crash into parts installed on the microscope stage, if both stages are not moved simultaneously. Therefore, it is generally safer to move both stages at the same time. This is done with macro D.9. In the last step, both scripts work the same again, *i.e.* the z-axis is moved to its final position.

```
#Variables
!default::position=Test
#Commands
!tellmodule::SCL.Stage
.MercGoHomeZ
.getStatus
.WritePositionFromTable::{position}
.MercMoveAbsoluteX
.getStatus2
.goAbsoluteXYZPosition
.getStatus
.!waitmodule
```

Macro script D.8: *Stage.macro*

```
#Variables
!default::position=Test
#Commands
!tellmodule::SCL.Stage
.MercGoHomeZ
.getStatus
.WritePositionFromTable::{position}
.MercMoveAbsoluteX
.goAbsoluteXYPosition
.getStatus2
.getStatus
.goAbsoluteXYZPosition
.getStatus
.!waitmodule
```

Macro script D.9: *Stage2.macro*

Macro script D.10 is used in situations, where it is not required to retract the z-axis all the way to the home position in order to move to a new position. When printing an array of spots for example, it is much faster to move only a few hundred µm up, since the positions are all on the same slide. A travel height is set by sending a *move relative* command to the Mercury controller (mr-400, in counts, *i.e.* 1 mm = 4000 counts).

```
#Variables
!default::position=Test
!default::travelheight=mr-400
#Commands
!tellmodule::SCL.Stage
.WritePositionFromTable::{position}
.GoPositionSpecificTravelHeight::macro::{travelheight}
.getStatus
.!waitModule
```

Macro script D.10: *StageLow.macro*

D.3.5 Microcapillary tip washing

The microcapillary tip is prone to contamination, especially during single-cell handling. Periodic tip washing can prevent cross-contamination and clogging of the tip. The macro script D.11 can be embedded as a sub-macro in larger scripts, *e.g.*, in macro script D.13. Two syringe pump dosing units are required. One unit belongs to the microcapillary setup, the second unit is part of the wash station. The wash station consists of a small reservoir with a Teflon tubing, which is connected to the second dispensing unit. The microcapillary can be inserted into the opening of the Teflon tubing. The second dispensing unit is then used to pump a detergent solution through the Teflon tubing in and out of the reservoir, causing a high flow rate at the outlet of the tubing and around the microcapillary tip.
Besides a number of dispensing volumes, the rate at which the microcapillary tip should be cleaned is defined in the macro. Using the *!calc* function, the *modulo* of index/rate is calculated, where index represents the current spot number. If $mod = 0$, it is time for a washing step, and the tip is moved to the wash station, where the washing protocol is initiated.

```
#Variables
!default::rate=4
!default::vol1=50
!default::vol2=0.02
!default::vol3=0.04
!default::vol4=0.06
#
!calc::m={i}/{rate}::0
!calc::w={i}-({rate}*{m})::0
#
#Check if mod(i,rate) = 0
!if::{w}::=::0
#
#If true, go to washing position
.!include::Stage::position=Wash
#
```

```
#Start washing sequence
.!tellmodule::SCL.nemesys
..MacroDosing::0::1500::{vol1}::1 #MacroMode::DosingUnit::
   FlowRate::TargetVolume::Infuse(0) or Withdraw(1)
..MacroDosing::1::5::{vol2}::0 #Dispense XX nl
..Status::1
..MacroDosing::1::5::{vol3}::1 #Aspirate XX nl
..Status::1
..MacroDosing::1::5::{vol4}::0 #Dispense XX nl
..Status::1
..Status::0
..MacroDosing::0::1500::{vol1}::0 #MacroMode::DosingUnit::
   FlowRate::TargetVolume::Infuse(0) or Withdraw(1)
..MacroDosing::1::5::{vol2}::0 #Dispense XX nl
..Status::1
..MacroDosing::1::5::{vol3}::1 #Aspirate XX nl
..Status::1
..MacroDosing::1::5::{vol4}::0 #Dispense XX nl
..Status::1
..Status::0
..!waitmodule
#Move up
.!tellmodule::SCL.Stage
..MercGoHomeZ
..getStatus
```

Macro script D.11: *AutoRPPAsub.macro*

D.4 RPPA macro scripts

The working principle of these macro scripts are detailed in section 5.2.2.

D.4.1 Semi-automated RPPA experiment

```
!input::Where should I deposit your cell? (CAUTION: the
   position must exist!)::RPPApos
!include::PriorRel::stepsX=-100::stepsY=0::PriorPause=0
!include::Image::name={RPPApos}_A
!include::PriorRel::stepsX=100::stepsY=0::PriorPause=500
!include::FGen::FGenPause=500
!include::Nemesys::unit=1::flowrate=2::volume=0.005::
   direction=1::NemesysPause=100
!include::PriorRel::stepsX=-100::stepsY=0
!ask::Was it successful?::Yes, proceed::No, cancel::
   LysisAnswer
!if::{LysisAnswer}::=::Yes, proceed
.!include::Image::name={RPPApos}_B
.!include::Stage::position={RPPApos}
.!include::Nemesys::unit=1::flowrate=20::volume=0.015::
   direction=0::NemesysPause=1000
.!include::MercRel::distance=200
```

Macro script D.12: *SingleCellRPPA.macro*

D.4.2 Automated RPPA experiment

```
!ask::"Buffer" and "Wash" positions defined? Image folders?::
   Yes, proceed::No, cancel::RPAAnswer
!if::{RPAAnswer}::=::Yes, proceed
.!do::96::index
#Increment index by one
..!calc::i={index}+1::0
#go to flushing position inside PDMS well but high above
   cells.
..!include::StageLow::position=Buffer::travelheight=mr-20000
#flush 10 nl and aspirate 5 nl (get air and sample out of
   nozzle, aspirate 5 nl to swich pump mode and make
   aspiration of cell more effective.
..!include::Nemesys::unit=1::flowrate=10::volume=0.01::
   direction=0::NemesysPause=100
..!include::Nemesys::unit=1::flowrate=2::volume=0.005::
   direction=1::NemesysPause=100
#go to cell target, stay inside PDMS well (no travel height:
   mr-0)
..!include::StageLow::position=cell_A{i}::travelheight=mr-0
```

```
#move to the side, take snapshot, move on top, send trigger,
   aspirate cell, move aside, take snapshot
..!include::PriorRel::stepsX=-100::stepsY=0::PriorPause=0
..!include::Image::name=cell_A{i}_A
..!include::PriorRel::stepsX=100::stepsY=0::PriorPause=500
..!include::FGen::FGenPause=500
..!include::Nemesys::unit=1::flowrate=5::volume=0.005::
   direction=1::NemesysPause=500
..!include::PriorRel::stepsX=-100::stepsY=0
..!include::Image::name=cell_A{i}_B
#Move with minimal travel height to the RPA slide and deposit
    spot
..!include::StageLow::position=RPA_{i}::travelheight=mr-20000
..!include::Nemesys::unit=1::flowrate=5::volume=0.015::
   direction=0::NemesysPause=100
#Take an image of the deposited spot
..!tellmodule::scl.surveillancecamera
...WriteToImage
#Start washing protocol if mod(i,rate)=0
..!include::AutoRPPAsub::rate=4::vol1=50::vol2=0.02::vol3
   =0.06::vol4=0.06 #Needs positions Wash and Buffer
#Go to wash position when loop has ended
!include::Stage::position=Wash
```

Macro script D.13: *AutoRPPA*

D.4.3 Automated spotting of sample(s)

Macros script D.14 is used to automatically print a whole slide with one or multiple samples. It is mainly used for batch lysate of cells and RPPA assay development. The number of spots to be printed is defined at the beginning of the macro script. Next, the number of spots that should be printed in one go are defined, *e.g.*, 16 for a complete 4x4 array. *sampleload* defines the volume of sample that should be loaded in order to print a series of spots. *sampletrash* is the volume that will go to waste after the series of spots has been deposited. It's function is to trash the remaining sample inside the microcapillary, as well as to flush the microcapillary with system liquid. *vol* defines the volume for each spot. Further, two options exist: *IncreaseVolume* can be set to *yes*. This will increase the spot volume after each series of spots, *e.g.*, by 1 nl. If *MultipleSamples=yes*, a different sample will be loaded after each series of spots, creating arrays of different samples.

```
#Variables
!default::spots=224
!default::rate=16
!default::sampleload=0.3
!default::sampletrash=0.3
!default::vol=0.01
!default::IncreaseVolume=no
!default::MultipleSamples=no
#
!ask::"Trash", "SampleA1...n", "AboveA1...n", and "RPA_1...n"
    positions defined?::Yes, proceed::No, cancel::RPAAnswer
!if::{RPAAnswer}::=::Yes, proceed
#go to flushing position above first sample.
.!include::Stage::position=AboveA1
#flush 5 nl.
.!include::Nemesys::unit=1::flowrate=1::volume=0.005::
   direction=0::NemesysPause=100
#go into first sample tube.
.!include::StageLow::position=SampleA1::travelheight=mr-0
#Aspirate sample and quickly infuse a few nl to switch pump.
.!include::Nemesys::unit=1::flowrate=1::volume={sampleload}::
   direction=1::NemesysPause=100
.!include::Nemesys::unit=1::flowrate=1::volume=0.005::
   direction=0::NemesysPause=100
.!include::Stage::position=RPA_1
#Start loop
.!do::{spots}::index
#Increment index by one
..!calc::i={index}+1::0
#Move to the RPA slide and deposit 16 spots
..!include::StageLow::position=RPA_{i}::travelheight=mr-300
..!include::Nemesys::unit=1::flowrate=5::volume={vol}::
   direction=0::NemesysPause=100
#Abort loop if all spots are complete.
..!breakif::{i}::=::{spots}
#
#Calculate mod(i,rate), i.e. the rate (in terms of sample
   spots) at which the nozzle should be cleaned and/or fresh
   sample loaded.
..!calc::m={i}/{rate}::0
..!calc::w={i}-({rate}*{m})::0
#
#Check if mod(i,rate) = 0
..!if::{w}::=::0
...!calc::j=1::0
...!if::{MultipleSamples}::=::yes
....!calc::j={i}/{rate}+1::0
```

```
...!calc::k={i}+1::0
#If needed, increase spot volume for the next array of spots.
...!if::{IncreaseVolume}::=::yes
....!calc::vol=0.002+{i}/(1000*{rate})
....!calc::j=1::0
#If true, flush to trash
...!include::Stage::position=Trash
#flush nozzle.
...!include::Nemesys::unit=1::flowrate=5::volume={sampletrash
   }::direction=0::NemesysPause=100
#go above next sample tube and dispense 5 nl
...!include::Stage::position=AboveA{j}
...!include::Nemesys::unit=1::flowrate=1::volume=0.005::
   direction=0::NemesysPause=100
#Go into sample tube.
...!include::StageLow::position=SampleA{j}::travelheight=mr-0
#Aspirate sample and switch pump by infusing 5 nl.
...!include::Nemesys::unit=1::flowrate=1::volume={sampleload
   }::direction=1::NemesysPause=100
...!include::Nemesys::unit=1::flowrate=1::volume=0.005::
   direction=0::NemesysPause=100
#Move to next spot position
...!include::Stage::position=RPA_{k}
#
#If all spots are made, go to trash and end macro.
.!include::Stage::position=Trash
.!include::Nemesys::unit=1::flowrate=5::volume={sampletrash
   }::direction=0::NemesysPause=100
```

Macro script D.14: *SlideSpotter.macro*

D.5 cryoWriter macro scripts

D.5.1 Plunge-freezing trigger

Macro script D.15 is used at the final step of plunge-freezing. After the sample was deposited and thinned, the macro is executed. First, a screen shot of the grid on the dew point stage is taken. Parameters, such as date and time, room temperature, relative humidity, dew point, and stage temperature are burned into the image. Next, the microcapillary is retracted and the stage is moved to the plunge-freezing position. Once the position is reached, the electromagnet holding the tweezers is turned off using a TTL switch, and the tweezers are released for plunge-freezing. Finally, the large x-axis stage is moved to its home position, making more space for manual grid handling.

```
#Commands
!tellmodule::scl.surveillancecamera
.WriteToImage
!tellmodule::SCL.Stage
.PRIORwriteXYPosition::Cryo
.goAbsoluteXYposition
.getStatus
.!waitmodule
.!wait::-1
!tellmodule::scl.ttl
.Magnet::macro::OFF
!tellmodule::SCL.Stage
.MercGoHomeX
```

Macro script D.15: *PlungeFreeze.macro*

D.5.2 Automated cryo-grid preparation

Macro script D.16 was written to test a fully automated cryo-plunging protocol. Three positions need to be defined: The sample location, the grid, and the "*Cryo*" position for measuring laser intensity and releasing the tweezers. The macro always asks first, whether these positions are defined, *i.e.* the sample must be present, the grid held by tweezers and positioned on the dew point stage. If approved, the stage is moved to the "*Cryo*" position to get a reference signal of the dry grid on the photo detector. Subsequently, the sample is loaded and deposited on the grid. After deposition, a pattern is started to spread the sample across a larger area. Once the pattern is finished, the microcapillary is again centered and slightly lowered to re-aspirate any excess sample. In the last step, the stage is moved again to the "*Cryo*" position, and the release trigger is armed. The release of the tweezers is triggered when the laser signal amplitude reaches a defined threshold level.

```
#Commands
!ask::"Cryo", "Grid", and "Sample" positions defined? Pattern
    ok?::Yes, proceed::No, cancel::CryoAnswer
!if::{CryoAnswer}::=::Yes, proceed
#Go to dry grid and define baseline
.!include::Stage2::position=Cryo
.!tellmodule::scl.ttl
..IRsensor::SetBaseline
#Go to sample vial and aspirate sample
.!include::Nemesys::unit=1::flowrate=1::volume=0.005::
   direction=0::NemesysPause=100
.!include::Stage2::position=Sample
.!include::Nemesys::unit=1::flowrate=1::volume=0.04::
   direction=1::NemesysPause=100
#Go to EM grid, deposit 20 nl, make spiral pattern, then re-
   aspirate excess sample
```

```
.!include::Stage2::position=Grid
.!include::Nemesys::unit=1::flowrate=0.1::volume=0.02::
   direction=0::NemesysPause=100
.!include::Pattern::steps=10::xrange=100::yrange=100::
   patternspeed=10
.!include::StageLow::position=Grid::travelheight=mr0
.!include::MercRel::distance=-10
.!include::Nemesys::unit=1::flowrate=0.5::volume=0.020::
   direction=1::NemesysPause=100
#Move to Cryo position and measure arm trigger
.!include::Stage2::position=Cryo
.!tellmodule::scl.ttl
..IRsensor::ArmTrigger
```

Macro script D.16: *AutoCryo.macro*

D.6 Live-cell imaging

This script is used to take snapshots on the microscope camera at different positions, *e.g.*, within a cell culture or microfluidic device. All positions are placed in a for loop and imaged consecutively. The last position is usually off chip, to prevent photo-toxicity or bleaching effects during imaging intervals. The interval is set by the *!wait* command, causing the system to wait for a defined time between iterations.

```
#Commands
!do::90::index
.!include::Stage::position=pos1
.!include::Image::name=pos1
.!include::Stage::position=pos2
.!include::Image::name=pos2
.!include::Stage::position=pos3
.!include::Image::name=pos3
.!include::Stage::position=pos4
.!include::Image::name=pos4
.!include::Stage::position=off
.!wait::600000# in ms (600000 = 10 min)
```

Macro script D.17: *Imaging.macro*

D.7 System macros

D.7.1 System calibration

The calibration routine helps to keep stored positions valid, even after a microcapillary exchange. The tip of a (newly inserted) microcapillary is first roughly centered over the 20x objective of the microscope with the help of the linear x-axis stage and the manual y-axis stage. Next, the tip is slowly lowered until it gently touches the surface of a standard microscopy slide inserted in the setup. The tip can now be exactly centered in the camera window. Macro script D.18 then retracts the z-axis by 4 cm, and defines the new coordinates as home position for the x- and z-Mercury controller.

```
#Commands
!tellmodule::SCL.Stage
.MercMoveRelativeZ::macro::40000
.getStatus
.MercCalibrateAll
```

Macro script D.18: *Calibrate.macro*

D.7.2 Quick position change

Switching to a new position, by double-clicking on a stored position in the user interface, is always accompanied by a full retraction of the z-axis. This additional travel prevents crashes of the microcapillary, but also causes a certain time delay. For short range movements on flat surface, macro script D.19 was written. In a dialog window, the new position can be entered, and the setup will move to its new destination with the z-axis only slightly retracted (as defined in the macro script).

```
#Commands
!input::Where should I go next? (CAUTION: the position must
   exist!)::NEXT
!include::StageLow::position={NEXT}::travelheight=mr-300
```

Macro script D.19: *GoNextArraySpot.macro*

D.7.3 System shut-down

To exit the instrument software, all modules need to be individually stopped and closed. The macro script D.20 performs this task. Notice, the mercury stages are also send back to their home position. This is important, because upon power-up, the mercury controller sets the current position as new home position.

```
LogComment::Stop SCL plug-in
#
#UserInteraction (if requested)
!semaphore::acquire
!default::interaction=ask
!if::{interaction}::=::ask
.!ask::Are you sure you want to close the single cell lysis
   software?::Quit SCL::Cancel::stopControl
#If flag is not ask, automatically quit SCL
!if::{interaction}::!=::ask
.!store::stopControl=Quit SCL
#
#Check, if openBEB really should be quit
!if::{stopControl}::=::Quit SCL
.!tellmodule::SCL.MicCamera
..stopCamera
..stopModule
#
.!tellmodule::SCL.Stage
..MercGoHomeZ
..getStatus
..MercGoHomeX
..getStatus2
..!waitmodule
..MercStop
..PRIORstopCommunication
..stop
#
.!tellmodule::SCL.FrequencyGenerator
..StopCommunication
..StopModule
#
#.!tellmodule::SCL.Dispenser
#..SeyonicStopCommunication
#..StopModule
#
.!tellmodule::SCL.TTL
..StopModule
#
.!tellmodule::SCL.SurveillanceCamera
..stopCamera
..stopModule
#
.!tellmodule::SCL.nemesys
..CloseDevice
#
.!tellmodule::SCL.DPStage
..StopSensor
#
!semaphore::release
```

Macro script D.20: *StopSCL.macro*

List of abbreviations

(nano)-ESI	(nano)-electrospray ionization
ABC	ammonium bicarbonate buffer
AM	ammonium molybdate
BHK	baby hamster kidney
COC	cyclic olefin copolymer
cryo-EM	cryo electron microscopy
CTF	contrast transfer function
ddH_2O	double-distilled water
DED	direct electron detection/detector
DM	decyl-β-d-maltopyranoside
DP-stage	dew point stage
DSC	differential scanning calorimetry
ECL	enhanced chemiluminescence
ED	electron diffraction
EM	electron microscopy
ET	electron tomography
FEA/M	finite element analysis / method
FEG	field emission gun
FS	fused silica
FS(OD)-(ID)-(Tip)	fused silica capillary with outer, inner, and tip diameter
FSC	fourier shell correlation
GAPDH	glyceraldehyde 3-phosphate dehydrogenase
HEK cells	human embryonic kidney cells
HEPES	4-(2-hydroxyethyl)-1-piperazineethanesulfonic acid
HPLC	high-performance liquid chromatography
HRP	horseradish peroxidase
HSP60	heat-shock protein 60
ID	inner diameter
ITO	indium tin oxide

LD	laser diode
LOD	limit of detection
LUHMES cells	Lund human mesencephalic cells
MALDI	matrix-assisted laser desorption/ionization
MCE	microcapillary electrode
MRM	multiple reaction monitoring
MS	mass spectrometry
NC	nitrocellulose
NHS	N-Hydroxysuccinimide
NMR	nuclear magnetic resonance
OD	outer diameter
OM	optical microscope
PBS	phosphate-buffered saline
PDMS	polydimethylsiloxane (SYLGARD®184)
PE	polyethylene
PEEK	polyether ether ketone
PMSF	phenylmethylsulfonyl fluoride
PTFE	polytetrafluoroethylene
RPPA	reverse-phase protein arrays
SCL	single-cell lysis
SERS	surface-enhanced Raman scattering
SNR	signal-to-noise ratio
TEM	transmission electron microscopy
TLC	thin layer chromatography
TMV	tobacco mosaic virus
TRiC/CCT	TCP-1 ring complex, or chaperonin containing TCP-1
Tris	tris(hydroxymethyl)aminomethane
UA	uranyl acetate

List of symbols

λ	wavelength
d	film thickness
$E_S(T)$	maximum (saturated) vapor pressure (in Pascal) at temperature T
E(RT)	actual vapor pressure (in Pascal) at room temperature
n_{780}	refractive index at wavelength of 780 nm
rH	relative humidity
RT	room temperature in °C
T	temperature in °C

Bibliography

Abbaspourrad, A., Zhang, H., Tao, Y., Cui, N., Asahara, H., Zhou, Y., Yue, D., Koehler, S. A., Ung, L. W., Heyman, J., Ren, Y., Ziblat, R., Chong, S., and Weitz, D. A. (2015). "Label-free single-cell protein quantification using a drop-based mix-and-read system". *Sci. Rep.*, 5, 12756.

Aebersold, R. and Mann, M. (2003). "Mass spectrometry-based proteomics". *Nature*, 422 (6928), 198–207.

Aebi, U., Millonig, R., Salvo, H., and Engel, A. (1986). "The three dimensional structure of the actin filament revisited". *Ann. N.Y. Acad. Sci.*, 483 (1), 100–119.

Aebi, U. and Pollard, T. D. (1987). "A glow discharge unit to render electron microscope grids and other surfaces hydrophilic". *J. Electron Microsc. Tech.*, 7 (1), 29–33.

Albayrak, C., Jordi, C. A., Zechner, C., Lin, J., Bichsel, C. A., Khammash, M., and Tay, S. (2016). "Digital Quantification of Proteins and mRNA in Single Mammalian Cells". *Mol. Cell*, 61 (6), 914–924.

Altschuler, S. J. and Wu, L. F. (2010). "Cellular heterogeneity: do differences make a difference?" *Cell*, 141 (4), 559–563.

Amantonico, A., Oh, J. Y., Sobek, J., Heinemann, M., and Zenobi, R. (2008). "Mass spectrometric method for analyzing metabolites in yeast with single cell sensitivity". *Angewandte Chemie. International Edition*, 120 (29), 5462–5465.

Amantonico, A., Urban, P. L., Fagerer, S. R., Balabin, R. M., and Zenobi, R. (2010). "Single-cell MALDI-MS as an analytical tool for studying intrapopulation metabolic heterogeneity of unicellular organisms". *Anal. Chem.*, 82 (17), 7394–7400.

Annesley, T. M. (2003). "Ion Suppression in Mass Spectrometry". *Clin. Chem.*, 49 (7), 1041–1044.

Arnold, S. A., Albiez, S., Bieri, A., Syntychaki, A., Adaixo, R., McLeod, R. A., Goldie, K. N., Stahlberg, H., and Braun, T. (2017). "Blotting-free and lossless cryo-electron microscopy grid preparation from nanoliter-sized protein samples and single-cell extracts". *J. Struct. Biol.*, 197 (3), 220–226.

Arnold, S. A., Albiez, S., Opara, N., Chami, M., Schmidli, C., Bieri, A., Padeste, C., Stahlberg, H., and Braun, T. (2016). "Total sample conditioning and preparation of nanoliter volumes for electron microscopy." *ACS Nano*, 10 (5), 4981–4988.

Baker, L. A. and Rubinstein, J. L. (2010). "Chapter fifteen – radiation damage in electron cryomicroscopy". *Methods Enzymol.*, 481, 371–388.

Bantscheff, M., Schirle, M., Sweetman, G., Rick, J., and Kuster, B. (2007). "Quantitative mass spectrometry in proteomics: a critical review". *Anal. Bioanal.Chem.*, 389 (4), 1017–1031.

Beck, M., Malmström, J. A., Lange, V., Schmidt, A., Deutsch, E. W., and Aebersold, R. (2009). "Visual proteomics of the human pathogen Leptospira interrogans". *Nat. Methods*, 6 (11), 817–823.

Beck, M., Topf, M., Frazier, Z., Tjong, H., Xu, M., Zhang, S., and Alber, F. (2011). "Exploring the spatial and temporal organization of a cells proteome". *J. Struct. Biol.*, 173 (3), 483–496.

Bennett, B. D., Kimball, E. H., Gao, M., Osterhout, R., van Dien, S. J., and Rabinowitz, J. D. (2009). "Absolute metabolite concentrations and implied enzyme active site occupancy in Escherichia coli". *Nat. Chem. Biol.*, 5 (8), 593–599.

Best, C., Nickell, S., and Baumeister, W. (2007). "Localization of protein complexes by pattern recognition". *Methods Cell Biol.*, 79, 615–638.

Bhardwaj, R., Fang, X., and Attinger, D. (2009). "Pattern formation during the evaporation of a colloidal nanoliter drop: a numerical and experimental study". *New J. Phys.*, 11 (7), 075020.

Bircher, B. A., Lang, H.-P., Duempelmann, L., Gerber, C., and Braun, T. (2013). "Photothermal excitation of microcantilevers in liquid: effect of the excitation laser position on temperature and vibrational amplitude". *Micro & Nano Letters*, 8 (11), 770–774.

Bischof, J. C. and He, X. (2005). "Thermal stability of proteins". *Ann. N.Y. Acad. Sci.*, 1066, 12–33.

Boellner, S. and Becker, K.-F. (2015). "Reverse Phase Protein Arrays-Quantitative Assessment of Multiple Biomarkers in Biopsies for Clinical Use". *Microarrays (Basel, Switzerland)*, 4 (2), 98–114.

Booth, C. R., Meyer, A. S., Cong, Y., Topf, M., Sali, A., Ludtke, S. J., Chiu, W., and Frydman, J. (2008). "Mechanism of lid closure in the eukaryotic chaperonin TRiC/CCT." *Nature structural & molecular biology*, 15 (7), 746–753.

Brase, J. C., Mannsperger, H., Frohlich, H., Gade, S., Schmidt, C., Wiemann, S., Beissbarth, T., Schlomm, T., Sultmann, H., and Korf, U. (2010). "Increasing the sensitivity of reverse phase protein arrays by antibody-mediated signal amplification". *Proteome science*, 8, 36.

Brody, J. P. and Yager, P. (1997). "Diffusion-based extraction in a microfabricated device". *Sensors and Actuators a-Physical*, 58 (1), 13–18.

Brody, J. P., Yager, P., Goldstein, R. E., and Austin, R. H. (1996). "Biotechnology at low Reynolds numbers". *Biophys. J.*, 71 (6), 3430–3441.

Brown, R. B. and Audet, J. (2008). "Current techniques for single-cell lysis". *Journal of The Royal Society Interface*, 5 (Suppl 2), S131–S138.

Bruus, H. (2008). *Theoretical Microfluidics*. Oxford University Press.

Buettner, F., Natarajan, K. N., Casale, F. P., Proserpio, V., Scialdone, A., Theis, F. J., Teichmann, S. A., Marioni, J. C., and Stegle, O. (2015). "Computational analysis of cell-to-cell heterogeneity in single-cell RNA-sequencing data reveals hidden subpopulations of cells". *Nat. Biotechnol.*, 33 (2), 155–160.

Callaway, E. (2015). "The revolution will not be crystallized: a new method sweeps through structural biology". *Nature*, 525, 172–174.

Cascio, P., Call, M., Petre, B. M., Walz, T., and Goldberg, A. L. (2002). "Properties of the hybrid form of the 26S proteasome containing both 19S and PA28 complexes". *EMBO J.*, 21 (11), 2636–2645.

Castro-Hartmann, P., Heck, G., Eltit, J. M., Fawcett, P., and Samsó, M. (2013). "The ArrayGrid: A methodology for applying multiple samples to a single TEM specimen grid". *Ultramicroscopy*, 135, 105–112.

Chang, H., Kang, H., Ko, E., Jun, B.-H., Lee, H.-Y., Lee, Y.-S., and Jeong, D. H. (2016). "PSA Detection with Femtomolar Sensitivity and a Broad Dynamic Range Using SERS Nanoprobes and an Area-Scanning Method". *ACS Sensors*, 1 (6), 645–649.

Chattopadhyay, K. and Mazumdar, S. (2000). "Structural and conformational stability of horseradish peroxidase: effect of temperature and pH". *Biochemistry*, 39 (1), 263–270.

Chen, W. W., Freinkman, E., Wang, T., Birsoy, K., and Sabatini, D. M. (2016). "Absolute Quantification of Matrix Metabolites Reveals the Dynamics of Mitochondrial Metabolism". *Cell*, 166 (5), 1324–1337.e11.

Cheng, Y., Grigorieff, N., Penczek, P. A., and Walz, T. (2015). "A Primer to Single-Particle Cryo-Electron Microscopy". *Cell*, 161 (3), 438–449.

Chiu, P.-L., Kelly, D. F., and Walz, T. (2011). "The use of trehalose in the preparation of specimens for molecular electron microscopy". *Micron*, 42 (8), 762–772.

Ciryam, P., Tartaglia, G. G., Morimoto, R. I., Dobson, C. M., and Vendruscolo, M. (2013). "Widespread Aggregation and Neurodegenerative Diseases Are Associated with Supersaturated Proteins". *Cell Reports*, 5 (3), 781–790.

Coudray, N., Hermann, G., Caujolle-Bert, D., Karathanou, A., Erne-Brand, F., Buessler, J. L., Daum, P., Plitzko, J. M., Chami, M., Mueller, U., Kihl, H., Urban, J. P., Engel, A., and Rémigy, H. W. (2011). "Automated screening of 2D crystallization trials using transmission electron microscopy: A high-throughput tool-chain for sample preparation and microscopic analysis". *J. Struct. Biol.*, 173 (2), 365–374.

De Carlo, S., Boisset, N., and Hoenger, A. (2008). "High-resolution single-particle 3D analysis on GroEL prepared by cryo-negative staining". *Micron*, 39 (7), 934–943.

De Carlo, S. and Harris, J. R. (2011). "Negative staining and cryo-negative staining of macromolecules and viruses for TEM". *Micron*, 42 (2), 117–131.

De Sousa E Melo, Felipe, Vermeulen, L., Fessler, E., and Medema, J. P. (2013). "Cancer heterogeneity–a multifaceted view". *EMBO Rep.*, 14 (8), 686–695.

Deegan, R. D. (2000). "Pattern formation in drying drops". *Phys Rev E Stat Phys Plasmas Fluids Relat Interdiscip Topics*, 61 (1), 475–485.

Dernick, G., Obermüller, S., Mangold, C., Magg, C., Matile, H., and Gutmann, O. (2011). "Multidimensional profiling of plasma lipoproteins by size exclusion chromatography followed by reverse-phase protein arrays." *J. Lipid Res.*, 52 (12), 2323–2331.

Diebolder, C. A., Koster, A. J., and Koning, R. I. (2012). "Pushing the resolution limits in cryo electron tomography of biological structures." *J. Microsc.*, 248, 1–5.

Dobro, M. J., Melanson, L. A., Jensen, G. J., and McDowall, A. W. (2010). "Plunge freezing for electron cryomicroscopy". *Methods Enzymol.*, 481, 63–82.

Dubochet, J., Adrian, M., Chang, J. J., Homo, J. C., Lepault, J., McDowall, A. W., and Schultz, P. (1988). "Cryo-electron microscopy of vitrified specimens". *Q. Rev. Biophys.*, 21 (2), 129–228.

Dubochet, J. and McDowall, A. W. (1981). "Vitrification of Pure Water for Electron-Microscopy". *J. Microsc.*, 124, RP3.

Eberwine, J., Lovatt, D., Buckley, P., Dueck, H., Francis, C., Kim, T. K., Lee, J., Lee, M., Miyashiro, K., Morris, J., Peritz, T., Schochet, T., Spaethling, J., Sul, J.-Y., and Kim, J. (2012). "Quantitative biology of single neurons". *J. R. Soc. Interface*, 9 (77), 3165–3183.

Einstein, A. (1906). "Eine Neue Bestimmung der Moleküldimensionen". *Ann. Phys.*, 322 (8), 549–560.

Eldar, A. and Elowitz, M. B. (2010). "Functional roles for noise in genetic circuits". *Nature*, 467 (7312), 167–173.

Elliott, C., Vijayakumar, V., Zink, W., and Hansen, R. (2007). "National Instruments LabVIEW: a programming environment for laboratory automation and measurement". *Journal of the Association for Laboratory Automation*, 12 (1), 17–24.

Engel, A. (2010). "Assessing biological samples with scanning probes. A. Gräslund, R. Rigler, J. Widengren (Eds.) in: Single Molecule Spectroscopy in Chemistry, Physics and Biology, Springer, Berlin Heidelberg", 417–431.

Engel, A. (2009). "Scanning transmission electron microscopy: biological applications. P. Hawkes (Ed.) in: Advances in Imaging and Electron Physics, Academic Press, Burlington", 357–386.

Erickson, D., Sinton, D., and Li, D. (2003). "Joule heating and heat transfer in poly(dimethylsiloxane) microfluidic systems". *Lab. Chip*, 3 (3), 141–149.

Feng, X., Fu, Z., Kaledhonkar, S., Jia, Y., Shah, B., Jin, A., Liu, Z., Sun, M., Chen, B., Grassucci, R. A., Ren, Y., Jiang, H., Frank, J., and Lin, Q. (2017). "A Fast and Effective Microfluidic Spraying-Plunging Method for High-Resolution Single-Particle Cryo-EM". *Structure*, in press.

Ferguson, R. E., Carroll, H. P., Harris, A., Maher, E. R., Selby, P. J., and Banks, R. E. (2005). "Housekeeping proteins: A preliminary study illustrating some limitations as useful references in protein expression studies". *Proteomics*, 5 (2), 566–571.

Fessenden, M. (2016). "Metabolomics: Small molecules, single cells". *Nature*, 540 (7631), 153–155.

Fiehn, O. (2001). "Combining genomics, metabolome analysis, and biochemical modelling to understand metabolic networks". *Comp. Funct. Genomics*, 2 (3), 155–168.

Flatz, L., Roychoudhuri, R., Honda, M., Filali-Mouhim, A., Goulet, J.-P., Kettaf, N., Lin, M., Roederer, M., Haddad, E. K., Sekaly, R. P., and Nabel, G. J. (2011). "Single-cell gene-expression profiling reveals qualitatively distinct CD8 T cells elicited by different gene-based vaccines". *Proceedings of the National Academy of Sciences*, 108 (14), 5724–5729.

Fox, M. B., Esveld, D. C., Valero, A., Luttge, R., Mastwijk, H. C., Bartels, P. V., Van Den Berg, A., and Boom, R. M. (2006). "Electroporation of cells in microfluidic devices: a review". *Anal. Bioanal.Chem.*, 385 (3), 474–485.

Gielen, F., Pereira, F., DeMello, A. J., and Edel, J. B. (2010). "High-resolution local imaging of temperature in dielectrophoretic platforms". *Anal. Chem.*, 82 (17), 7509–7514.

Giss, D., Kemmerling, S., Dandey, V., Stahlberg, H., and Braun, T. (2014). "Exploring the interactome: microfluidic isolation of proteins and interacting partners for quantitative analysis by electron microscopy". *Anal. Chem.*, 86, 4680–4687.

Glaeser, R. M., Han, B. G., Csencsits, R., Killilea, A., Pulk, A., and Cate, J. H. (2016). "Factors that Influence the Formation and Stability of Thin, Cryo-EM Specimens". *Biophys. J.*, 110 (4), 749–755.

Glaeser, R. M. (2016). "How good can cryo-EM become?" *Nat. Methods*, 13, 28–32.

Goldie, K. N., Abeyrathne, P., Kebbel, F., Chami, M., Ringler, P., and Stahlberg, H. (2014). *Electron Microscopy*. Ed. by J. Kuo. Vol. 1117. Methods in Molecular Biology. Totowa, NJ: Humana Press, 325–341.

Grigorieff, N. (2007). "FREALIGN: High-resolution refinement of single particle structures". *J. Struct. Biol.*, 157 (1), 117–125.

Guyon, E., Hulin, J.-P., Petit, L., and Mitescu, C. (2001). "The mechanism of the Rayleigh - Benard instability, and orders of magnitude. In: Physical Hydrodynamics, Ch. 10.2.2, Oxford University Press, Oxford".

Hale, G. M. and Querry, M. R. (1973). "Optical constants of water in the 200-nm to 200-μm wavelength region". *Appl. Opt.*, 12 (3), 555–563.

Han, F., Wang, Y., Sims, C. E., Bachman, M., Chang, R., Li, G. P., and Allbritton, N. L. (2003). "Fast electrical lysis of cells for capillary electrophoresis". *Anal. Chem.*, 75 (15), 3688–3696.

Harnett, E. M., Alderman, J., and Wood, T. (2007). "The surface energy of various biomaterials coated with adhesion molecules used in cell culture." *Colloids Surf. B Biointerfaces*, 55, 90–97.

Harris, J. R. and Carlo, S. de (2014). "Negative staining and cryo-negative staining: applications in biology and medicine". *Methods Mol. Biol.*, 1117, 215–258.

Heinemann, M. and Zenobi, R. (2011). "Single cell metabolomics". *Curr. Opin. Biotechnol.*, 22 (1), 26–31.

Henderson, G. P., Gan, L., and Jensen, G. J. (2007). "3-D ultrastructure of O. tauri: electron cryotomography of an entire eukaryotic cell". *PLoS One*, 2 (8), e749.

Henderson, R. et al. (2012). "Outcome of the first electron microscopy validation task force meeting." *Structure (London, England:1993)*, 20 (2), 205–214.

Hu, M., Vink, M., Kim, C., Derr, K., Koss, J., D'Amico, K., Cheng, A., Pulokas, J., Ubarretxena-Belandia, I., and Stokes, D. (2010). "Automated electron microscopy for evaluating two-dimensional crystallization of membrane proteins". *J. Struct. Biol.*, 171 (1), 102–110.

Hughes, A. J., Spelke, D. P., Xu, Z., Kang, C.-C., Schaffer, D. V., and Herr, A. E. (2014). "Single-cell western blotting". *Nat. Methods*, 11 (7), 749–755.

Hunter, M. S., Segelke, B., Messerschmidt, M., Williams, G. J., Zatsepin, N. a., Barty, A., Benner, W. H., Carlson, D. B., Coleman, M., Graf, A., Hau-Riege, S. P., Pardini, T., Seibert, M. M., Evans, J., Boutet, S., and Frank, M. (2014). "Fixed-target protein serial microcrystallography with an x-ray free electron laser". *Sci. Rep.*, 4, 6026.

Ibanez, A. J., Fagerer, S. R., Schmidt, A. M., Urban, P. L., Jefimovs, K., Geiger, P., Dechant, R., Heinemann, M., and Zenobi, R. (2013). "Mass spectrometry-based metabolomics of single yeast cells". *Proc. Natl. Acad. Sci. U.S.A.*, 110 (22), 8790–8794.

Jain, T., Sheehan, P., Crum, J., Carragher, B., and Potter, C. S. (2012). "Spotiton: a prototype for an integrated inkjet dispense and vitrification system for cryo-TEM." *J. Struct. Biol.*, 179, 68–75.

Janku, F. (2014). "Tumor heterogeneity in the clinic: is it a real problem?" *Therapeutic advances in medical oncology*, 6 (2), 43–51.

Jaworek, A. and Sobczyk, A. T. (2008). "Electrospraying route to nanotechnology: An overview". *J. Electrostat.*, 66 (3-4), 197–219.

Kalisky, T., Blainey, P., and Quake, S. R. (2011). "Genomic analysis at the single-cell level". *Annu. Rev. Genet.*, 45, 431–445.

Kedersha, N. L., Miquel, M. C., Bittner, D., and Rome, L. H. (1990). "Vaults. II. Ribonucleoprotein structures are highly conserved among higher and lower eukaryotes". *The Journal of Cell Biology*, 110 (4), 895–901.

Kellogg, R. A., Tian, C., Lipniacki, T., Quake, S. R., and Tay, S. (2015). "Digital signaling decouples activation probability and population heterogeneity". *eLife*, 4, e08931.

Kemmerling, S., Arnold, S. A., Bircher, B. A., Sauter, N., Escobedo, C., Dernick, G., Hierlemann, A., Stahlberg, H., and Braun, T. (2013). "Single-cell lysis for visual analysis by electron microscopy." *J. Struct. Biol.*, 183 (3), 467–73.

Kemmerling, S., Ziegler, J., Schweighauser, G., Arnold, S. A., Giss, D., Mueller, S. A., Ringler, P., Goldie, K. N., Goedecke, N., and Hierlemann, A. (2012). "Connecting microfluidics to electron microscopy". *J. Struct. Biol.*, 177 (1), 128–134.

Kim, K.-T., Lee, H. W., Lee, H.-O., Kim, S. C., Seo, Y. J., Chung, W., Eum, H. H., Nam, D.-H., Kim, J., Joo, K. M., and Park, W.-Y. (2015). "Single-cell mRNA sequencing identifies subclonal heterogeneity in anti-cancer drug responses of lung adenocarcinoma cells". *Genome Biol.*, 16, 127.

Kühlbrandt, W. (2014). "The Resolution Revolution". *Science*, 343, 1443–1444.

Lee, J., Saha, A., Pancera, S. M., Kempter, A., Rieger, J., Bose, A., and Tripathi, A. (2012). "Shear free and blotless cryo-TEM imaging: a new method for probing early evolution of nanostructures." *Langmuir*, 28 (9), 4043–4046.

Lee, M.-C. W., Lopez-Diaz, F. J., Khan, S. Y., Tariq, M. A., Dayn, Y., Vaske, C. J., Radenbaugh, A. J., Kim, H. J., Emerson, B. M., and Pourmand, N. (2014). "Single-cell analyses of transcriptional heterogeneity during drug tolerance transition in cancer cells by RNA sequencing". *Proc. Natl. Acad. Sci. U.S.A.*, 111 (44), E4726–35.

Leitner, A., Joachimiak, L. a., Bracher, A., Mönkemeyer, L., Walzthoeni, T., Chen, B., Pechmann, S., Holmes, S., Cong, Y., Ma, B., Ludtke, S., Chiu, W., Hartl, F. U., Aebersold, R., and Frydman, J. (2012). "The molecular architecture of the eukaryotic chaperonin TRiC/CCT". *Structure*, 20 (5), 814–825.

Lepault, J., Booy, F. P., and Dubochet, J. (1983). "Electron microscopy of frozen biological suspensions". *J. Microsc.*, 129 (Pt 1), 89–102.

Lepock, J. R. (2003). “Cellular effects of hyperthermia: relevance to the minimum dose for thermal damage.” *Int. J. Hyperthermia*, 19 (3), 252–266.

Li, X., Mooney, P., Zheng, S., Booth, C. R., Braunfeld, M. B., Gubbens, S., Agard, D. a., and Cheng, Y. (2013). “Electron counting and beam-induced motion correction enable near-atomic-resolution single-particle cryo-EM.” *Nat. Methods*, 10 (6), 584–90.

Liao, M., Cao, E., Julius, D., and Cheng, Y. (2013). “Structure of the TRPV1 ion channel determined by electron cryo-microscopy.” *Nature*, 504, 107–112.

Lu, Z. H., Barnard, D., Shaikh, T. R., Meng, X., Mannella, C. A., Yassin, A. S., Agrawal, R. K., Wagenknecht, T., and Lu, T. M. (2014). “Gas-assisted annular microsprayer for sample preparation for time-resolved cryo-electron microscopy”. *J. Micromech. Microeng.*, 24 (11).

Lu, Z. H., Shaikh, T. R., Barnard, D., Meng, X., Mohamed, H., Yassin, A., Mannella, C. A., Agrawal, R. K., Lu, T. M., and Wagenknecht, T. (2009). “Monolithic microfluidic mixing-spraying devices for time-resolved cryo-electron microscopy”. *J. Struct. Biol.*, 168 (3), 388–395.

Luo, W., Westcott, N. P., Pulsipher, A., and Yousaf, M. N. (2008). “Renewable and optically transparent electroactive indium tin oxide surfaces for chemoselective ligand immobilization and biospecific cell adhesion”. *Langmuir*, 24 (22), 13096–13101.

Lyumkis, D., Brilot, A. F., Theobald, D. L., and Grigorieff, N. (2013). “Likelihood-based classification of cryo-EM images using FREALIGN”. *J. Struct. Biol.*, 183 (3), 377–388.

Mader, A., Elad, N., and Medalia, O. (2010). “Cryoelectron tomography of eukaryotic cells.” *Methods Enzymol.*, 483, 245–265.

McLeod, R. A., Kowal, J., Ringler, P., and Stahlberg, H. (2017). “Robust image alignment for cryogenic transmission electron microscopy”. *J. Struct. Biol.*, 197 (3), 279–293.

McPherson, A. (2004). “Introduction to protein crystallization.” *Methods*, 34 (3), 254–65.

Medalia, O., Weber, I., Frangakis, A. S., Nicastro, D., Gerisch, G., and Baumeister, W. (2002). “Macromolecular architecture in eukaryotic cells visualized by cryoelectron tomography.” *Science*, 298, 1209–1213.

Milazzo, A.-C., Cheng, A., Moeller, A., Lyumkis, D., Jacovetty, E., Polukas, J., Ellisman, M. H., Xuong, N.-H., Carragher, B., and Potter, C. S. (2011). “Initial evaluation of a direct detection device detector for single particle cryo-electron microscopy”. *J. Struct. Biol.*, 176 (3), 404–408.

Movahed, S. and Li, D. (2011). “Microfluidics cell electroporation”. *Microfluid. Nanofluid.*, 10 (4), 703–734.

Mukhitov, N., Spear, J. M., Stagg, S. M., and Roper, M. G. (2016). “Interfacing Microfluidics with Negative Stain Transmission Electron Microscopy”. *Anal. Chem.*, 88 (1), 629–634.

Mulligan, S., Jain, T., Duggan, E., Liu, E., Speir, J. a., Cheng, A., Nolan, J., Carragher, B., and Potter, C. S. (2014). “Typhon: Multiplexed TEM Sample Preparation”. *Microsc. Microanal.*, 20 (S3), 1158–1159.

Nashimoto, Y., Takahashi, Y., Yamakawa, T., Torisawa, Y., Yasukawa, T., Ito-Sasaki, T., Yokoo, M., Abe, H., Shiku, H., and Kambara, H. (2007). “Measurement of gene expression from single adherent cells and spheroids collected using fast electrical lysis”. *Anal. Chem.*, 79 (17), 6823–6830.

Nederlof, I., Li, Y. W., Heel, M. van, and Abrahams, J. P. (2013). "Imaging protein three-dimensional nanocrystals with cryo-EM." *Acta Crystallogr. D Biol. Crystallogr.*, 69 (Pt 5), 852–9.

Nickell, S., Kofler, C., Leis, A. P., and Baumeister, W. (2006). "A visual approach to proteomics". *Nat. Rev. Mol. Cell Biol.*, 7 (3), 225–230.

Nogales, E. (2015). "The development of cryo-EM into a mainstream structural biology technique". *Nat. Methods*, 13, 24–27.

Ohi, M., Li, Y., Cheng, Y., and Walz, T. (2004). "Negative staining and image classification, powerful tools in modern electron microscopy". *Biological Procedures Online*, 6 (1), 23–34.

Ortega, J., Lee, H. S., Maurizi, M. R., and Steven, A. C. (2004). "ClpA and ClpX ATPases bind simultaneously to opposite ends of ClpP peptidase to form active hybrid complexes". *J. Struct. Biol.*, 146, 217–226.

Pan, N., Rao, W., Kothapalli, N. R., Liu, R., Burgett, A. W. G., and Yang, Z. (2014). "The single-probe: a miniaturized multifunctional device for single cell mass spectrometry analysis". *Anal. Chem.*, 86 (19), 9376–9380.

Park, J. O., Rubin, S. A., Xu, Y.-F., Amador-Noguez, D., Fan, J., Shlomi, T., and Rabinowitz, J. D. (2016). "Metabolite concentrations, fluxes and free energies imply efficient enzyme usage". *Nat. Chem. Biol.*, 12 (7), 482–489.

Patel, A. P., Tirosh, I., Trombetta, J. J., Shalek, A. K., Gillespie, S. M., Wakimoto, H., Cahill, D. P., Nahed, B. V., Curry, W. T., Martuza, R. L., Louis, D. N., Rozenblatt-Rosen, O., Suva, M. L., Regev, A., and Bernstein, B. E. (2014). "Single-cell RNA-seq highlights intratumoral heterogeneity in primary glioblastoma". *Science*, 344 (6190), 1396–1401.

Pettersen, E. F., Goddard, T. D., Huang, C. C., Couch, G. S., Greenblatt, D. M., Meng, E. C., and Ferrin, T. E. (2004). "UCSF Chimera – a visualization system for exploratory research and analysis." *J. Comput. Chem.*, 25 (13), 1605–1612.

Picotti, P., Bodenmiller, B., Mueller, L. N., Domon, B., and Aebersold, R. (2009). "Full dynamic range proteome analysis of S. cerevisiae by targeted proteomics". *Cell*, 138 (4), 795–806.

Poulin, J.-F., Tasic, B., Hjerling-Leffler, J., Trimarchi, J. M., and Awatramani, R. (2016). "Disentangling neural cell diversity using single-cell transcriptomics". *Nat. Neurosci.*, 19 (9), 1131–1141.

Prinz, M., Priller, J., Sisodia, S. S., and Ransohoff, R. M. (2011). "Heterogeneity of CNS myeloid cells and their roles in neurodegeneration". *Nat. Neurosci.*, 14 (10), 1227–1235.

Raj, A. and Oudenaarden, A. van (2008). "Nature, nurture, or chance: Stochastic gene expression and its consequences". *Cell*, 135 (2), 216–226.

Ramakrishnan, C., Bieri, A., Sauter, N., Roizard, S., Ringler, P., Müller, S. A., Goldie, K. N., Enimanev, K., Stahlberg, H., Rinn, B., and Braun, T. (2014). "openBEB: open biological experiment browser for correlative measurements." *BMC Bioinf.*, 15, 84.

Razinkov, I., Dandey, V. P., Wei, H., Zhang, Z., Melnekoff, D., Rice, W. J., Wigge, C., Potter, C. S., and Carragher, B. (2016). "A new method for vitrifying samples for cryoEM". *J. Struct. Biol.*, 195 (2), 190–198.

Rodriguez, J. A. et al. (2015). "Structure of the toxic core of α-synuclein from invisible crystals". *Nature*, 525 (7570), 486–490.

Rohou, A. and Grigorieff, N. (2015). "CTFFIND4: Fast and accurate defocus estimation from electron micrographs". *J. Struct. Biol.*, 192 (2), 216–221.

Ross, C. A. and Poirier, M. A. (2004). "Protein aggregation and neurodegenerative disease". *Nat. Med.*, 10 (7), S10–S17.

Rubakhin, S. S., Romanova, E. V., Nemes, P., and Sweedler, J. V. (2011). "Profiling metabolites and peptides in single cells". *Nat. Methods*, 8 (4s), S20–S29.

Ruskin, R. S., Yu, Z., and Grigorieff, N. (2013). "Quantitative characterization of electron detectors for transmission electron microscopy." *J. Struct. Biol.*, 184 (3), 385–393.

Russo, C. J. and Passmore, L. A. (2014). "Ultrastable gold substrates for electron cryomicroscopy". *Science*, 346 (6215), 1377–1380.

Scheres, S. H. W. (2012). "RELION: Implementation of a Bayesian approach to cryo-EM structure determination". *J. Struct. Biol.*, 180 (3), 519–530.

Scheres, S. H. W. and Chen, S. (2012). "Prevention of overfitting in cryo-EM structure determination." *Nat. Methods*, 9 (9), 853–854.

Schirmer, E. C., Glover, J. R., Singer, M. a., and Lindquist, S. (1996). "HSP100/Clp proteins: A common mechanism explains diverse functions". *Trends Biochem. Sci.*, 21 (8), 289–296.

Schmid, A., Kortmann, H., Dittrich, P. S., and Blank, L. M. (2010). "Chemical and biological single cell analysis". *Curr. Opin. Biotechnol.*, 21 (1), 12–20.

Scholz, D., Poltl, D., Genewsky, A., Weng, M., Waldmann, T., Schildknecht, S., and Leist, M. (2011). "Rapid, complete and large-scale generation of post-mitotic neurons from the human LUHMES cell line". *J. Neurochem.*, 119 (5), 957–971.

Sehorn, M. G., Sigurdsson, S., Bussen, W., Unger, V. M., and Sung, P. (2004). "Human meiotic recombinase Dmc1 promotes ATP-dependent homologous DNA strand exchange". *Nature*, 429 (6990), 433–437.

Shah, S. S., Howland, M. C., Chen, L.-J., Silangcruz, J., Verkhoturov, S. V., Schweikert, E. A., Parikh, A. N., and Revzin, A. (2009). "Micropatterning of proteins and mammalian cells on indium tin oxide". *ACS Applied Materials and Interfaces*, 1 (11), 2592–2601.

Souchelnytskyi, S. (2005). "Bridging proteomics and systems biology: What are the roads to be traveled?" *Proteomics*, 5 (16), 4123–4137.

Spurrier, B., Ramalingam, S., and Nishizuka, S. (2008). "Reverse-phase protein lysate microarrays for cell signaling analysis". *Nat. Protoc.*, 3 (11), 1796–1808.

Stewart, P. S. (2003). "Diffusion in Biofilms". *J. Bacteriol.*, 185 (5), 1485–1491.

Structural Genomics Consortium et al. (2008). "Protein production and purification". *Nat. Methods*, 5 (2), 135–146.

Subramaniam, S., Kuehlbrandt, W., and Henderson, R. (2016). "CryoEM at IUCrJ: A new era". *IUCrJ*, 3, 3–7.

Tabakman, S. M., Lau, L., Robinson, J. T., Price, J., Sherlock, S. P., Wang, H., Zhang, B., Chen, Z., Tangsombatvisit, S., Jarrell, J. A., Utz, P. J., and Dai, H. (2011). "Plasmonic substrates for multiplexed protein microarrays with femtomolar sensitivity and broad dynamic range". *Nat. Commun.*, 2, 466.

Tanaka, K., Yoshimura, T., Kumatori, A., Ichihara, A., Ikai, A., Nishigai, M., Kameyama, K., and Takagi, T. (1988). "Proteasomes (multi-protease complexes) as 20 S ring-shaped particles in a variety of eukaryotic cells." *The Journal of biological chemistry*, 263 (31), 16209–17.

Tang, G., Peng, L., Baldwin, P. R., Mann, D. S., Jiang, W., Rees, I., and Ludtke, S. J. (2007). "EMAN2: an extensible image processing suite for electron microscopy". *J. Struct. Biol.*, 157 (1), 38–46.

Tang, X. and Bruce, J. E. (2009). *Mass Spectrometry of Proteins and Peptides*. Ed. by M. S. Lipton and L. Paša-Tolic. Vol. 492. Methods In Molecular Biology. Totowa, NJ: Humana Press, 283–293.

Thompson, R. F., Walker, M., Siebert, C. A., Muench, S. P., and Ranson, N. A. (2016). "An introduction to sample preparation and imaging by cryo-electron microscopy for structural biology". *Methods*, 100, 3–15.

Tivol, W. F., Briegel, A., and Jensen, G. J. (2008). "An improved cryogen for plunge freezing." *Microscopy and microanalysis : the official journal of Microscopy Society of America, Microbeam Analysis Society, Microscopical Society of Canada*, 14, 375–379.

Tolk, M., Fenwick, O., Ahmad, S., and Cacialli, F. (2012). "The influence of the substrate thermal conductivity on scanning thermochemical lithography". *J. Appl. Phys.*, 111 (12), 1243171–1243178.

Veesler, D., Campbell, M. G., Cheng, A., Fu, C.-Y., Murez, Z., Johnson, J. E., Potter, C. S., and Carragher, B. (2013). "Maximizing the potential of electron cryomicroscopy data collected using direct detectors." *J. Struct. Biol.*, 184 (2), 193–202.

Wachter, A., Bernhardt, S., Beissbarth, T., and Korf, U. (2015). "Analysis of Reverse Phase Protein Array Data: From Experimental Design towards Targeted Biomarker Discovery". *Microarrays*, 4 (4), 520–539.

Walker, J. E. and Dickson, V. K. (2006). "The peripheral stalk of the mitochondrial ATP synthase." *Biochim. Biophys. Acta*, 1757 (5-6), 286–96.

Wang, D. and Bodovitz, S. (2010). "Single cell analysis: the new frontier in omics". *Trends Biotechnol.*, 28 (6), 281–290.

Wang, Y. and Mandelkow, E. (2016). "Tau in physiology and pathology". *Nat. Rev. Neurosci.*, 17 (1), 5–21.

Westerhoff, H. V. (2011). "Systems biology left and right". *Methods Enzymol.*, 500, 3–11.

White, H. D., Thirumurugan, K., Walker, M. L., and Trinick, J. (2003). "A second generation apparatus for time-resolved electron cryo-microscopy using stepper motors and electrospray". *J. Struct. Biol.*, 144 (1-2), 246–252.

Wilson, N. K., Kent, D. G., Buettner, F., Shehata, M., Macaulay, I. C., Calero-Nieto, F. J., Sanchez Castillo, M., Oedekoven, C. A., Diamanti, E., Schulte, R., Ponting, C. P., Voet, T., Caldas, C., Stingl, J., Green, A. R., Theis, F. J., and Gottgens, B. (2015). "Combined Single-Cell Functional and Gene Expression Analysis Resolves Heterogeneity within Stem Cell Populations". *Cell stem cell*, 16 (6), 712–724.

Yager, P., Edwards, T., Fu, E., Helton, K., Nelson, K., Tam, M. R., and Weigl, B. H. (2006). "Microfluidic diagnostic technologies for global public health". *Nature*, 442 (7101), 412–418.

Yagi, T., Tamano, K., Sato, Y., Taketoshi, N., Baba, T., and Shigesato, Y. (2005). "Analysis on thermal properties of tin doped indium oxide films by picosecond thermoreflectance measurement". *Journal of Vacuum Science & Technology A: Vacuum, Surfaces, and Films*, 23 (4), 1180–1186.

Young, M. E., Carroad, P. A., and Bell, R. L. (1980). "Estimation of diffusion coefficients of proteins". *Biotechnol. Bioeng.*, 22 (5), 947–955.

Yuk, J. M., Park, J., Ercius, P., Kim, K., Hellebusch, D. J., Crommie, M. F., Lee, J. Y., Zettl, A., and Alivisatos, A. P. (2012). "High-Resolution EM of Colloidal Nanocrystal Growth Using Graphene Liquid Cells". *Science*, 336 (6077), 61–64.

Yunker, P. J., Still, T., Lohr, M. A., and Yodh, A. G. (2011). "Suppression of the coffee-ring effect by shape-dependent capillary interactions". *Nature*, 476 (7360), 308–311.

Zhang, F., Zhang, W. B., Shi, Z., Wang, D., Jin, J., and Jiang, L. (2013). "Nanowire-haired inorganic membranes with superhydrophilicity and underwater ultralow adhesive superoleophobicity for high-efficiency oil/water separation". *Adv. Mater.*, 25 (30), 4192–4198.

Zhang, X.-M., Yin, M., and Zhang, M.-H. (2014). "Cell-based assays for Parkinson's disease using differentiated human LUHMES cells". *Acta Pharmacol. Sin.*, 35 (7), 945–956.

Zong, C., Lu, S., Chapman, A. R., and Xie, X. S. (2012). "Genome-wide detection of single-nucleotide and copy-number variations of a single human cell". *Science*, 338 (6114), 1622–1626.

Publications and meetings

Peer-reviewed articles

S. Kemmerling, S. A. Arnold, B. A. Bircher, N. Sauter, C. Escobedo, G. Dernick, A. Hierlemann, H. Stahlberg, and T. Braun, "Single-cell lysis for visual analysis by electron microscopy", Journal of Structural Biology, 183 (3), 467–473, 2013. **DOI:** 10.1016/j.jsb.2013.06.012

S. A. Arnold, S. Albiez, N. Opara, M. Chami, C. Schmidli, A. Bieri, C. Padeste, H. Stahlberg, and T. Braun, "Total sample conditioning and preparation of nanoliter volumes for electron microscopy", ACS Nano, 10 (5), 4981–4988, 2016. **DOI:** 10.1021/acsnano.6b01328

S. A. Arnold, S. Albiez, A. Bieri, A. Syntychaki, R. Adaixo, R. A. McLeod, K. N. Goldie, H. Stahlberg, and T. Braun, "Blotting-free and lossless cryo-electron microscopy grid preparation from nanoliter-sized protein samples and single-cell extracts", Journal of Structural Biology, 197 (3), 220–226, 2017. **DOI:** 10.1016/j.jsb.2016.11.002

N. Opara, S. A. Arnold, T. Braun, H. Stahlberg, M. Makita, C. David, and C. Padeste, "Direct protein crystallization on ultrathin membranes for diffraction measurements at X-ray free electron lasers", submitted, 2016.

S. A. Arnold, S. A. Müller, C. Schmidli, H. Stahlberg, and T. Braun, "Miniaturizing EM sample preparation: Challenges, opportunities and “visual proteomics””, in preparation, 2017.

Filed patents

The following patents were filed together with Unitectra AG.

S. A. Arnold, T. Braun, H. Stahlberg, "Lossless cryo-grid preparation stage for high-resolution electron microscopy", PCT/EP2015/065398, 6.7.2015

S. A. Arnold, T. Braun, H. Stahlberg, "Lossless cryo-grid preparation by controlled sample evaporation", EP16194230, 17.10.2016

Oral presentations

S. A. Arnold, "Single-Cell Analysis - New Tools to Study Mechanisms of Neurodegeneration", INASCON, Middelfart, Denmark, 2014

S. A. Arnold, "Single-cell analysis and dealing with small sample volumes", Annual SNI Meeting, Lenzerheide, Switzerland, 2014

S. A. Arnold, "The visual proteomics project. Pushing the boundaries of TEM sample preparation", Focal Area Structural Biology Biozentrum, Basel, Switzerland, 2015

S. A. Arnold, "Nanoliter sample preparation for life science applications", Nanoscience in the Snow, Zinal, Switzerland, 2016

Poster presentations

S. A. Arnold, S. Kemmerling, G. Dernick, A. Bieri, H. Stahlberg and T. Braun, "Sample conditioning and handover for single-cell analysis and nano-crystal deposition", Nanoscience in the Snow, Kandersteg, Switzerland, 2014

S. A. Arnold, S. Kemmerling, G. Dernick, A. Bieri, H. Stahlberg and T. Braun, "Single-cell lysis of adherent eukaryotic cells for protein structure and expression analysis by electron microscopy and reverse-phase arrays", Single-Cell Analysis Europe, Berlin, Germany, 2014

S. A. Arnold, S. Kemmerling, G. Dernick, A. Bieri, H. Stahlberg and T. Braun, "Single-cell lysis of adherent eukaryotic cells for protein structure and expression analysis by electron microscopy and reverse-phase arrays", Swiss Nano Convention, Brugg, Switzerland, 2014

D. Giss, S. A. Arnold, A. Bieri, S. A. Müller, A. Engel, H. Stahlberg and T. Braun, "Visual proteomics for single cell analysis", CLINAM, Basel, Switzerland, 2014

S. A. Arnold, A. Bieri, D. Giss, G. Dernick, H. Stahlberg and T. Braun, "Single-cell lysis of adherent eukaryotic cells for protein structure and expression analysis", EMBL Microfluidics, Heidelberg, Germany, 2014

S. A. Arnold, A. Bieri, M. Chami, S. Albiez, R. Sütterlin, H. Stahlberg and T. Braun, "Single-cell analysis to study the prion-like spreading of alpha-synuclein", Biozentrum Symposium, Basel, Switzerland, 2015

S. A. Arnold, A. Bieri, M. Chami, S. Albiez, R. Sütterlin, H. Stahlberg and T. Braun, "Single-cell analysis to study the prion-like spreading of alpha-synuclein", Nanoscience in the Snow, Belalp, Switzerland, 2015

S. A. Arnold, A. Bieri, M. Chami, S. Albiez, R. Sütterlin, H. Stahlberg and T. Braun, "Single-cell analysis to study the prion-like spreading of alpha-synuclein", Swiss Nano Convention, Neuchatel, Switzerland, 2015

S. A. Arnold, S. Albiez, N. Opara, C. Schmidli, A. Bieri, R. Sütterlin, H. Stahlberg and T. Braun, "Electron microscopy sample preparation from nanoliter volumes", Annual SNI Meeting, Lenzerheide, Switzerland, 2015 – Distinguished with poster award.

S. A. Arnold, A. Bieri, M. Chami, S. Albiez, R. Sütterlin, H. Stahlberg and T. Braun, "Nanoliter sample preparation for life science applications", Swiss Nano Convention, Basel, Switzerland, 2016

S. A. Arnold, A. Bieri, M. Chami, S. Albiez, R. Sütterlin, H. Stahlberg and T. Braun, "Nanoliter sample preparation for life science applications", Annual SNI Meeting, Lenzerheide, Switzerland, 2016

S. A. Arnold, S. Albiez, A. Syntychaki, N. Opara, A. Bieri, H. Stahlberg, and T. Braun, "Electron microscopy sample preparation from nanoliter volumes", Global Engage Microscopy Congress, London, United Kingdom, 2016

S. A. Arnold, C. Schmidli, S. Albiez, A. Syntychaki, A. Bieri, L. Rima, K. N. Goldie, M. Chami, R. Sütterlin, H. Stahlberg, and T. Braun, "Miniaturizing EM sample preparation: Challenges, opportunities, and visual proteomics", Biozentrum Symposium, Basel, Switzerland, 2017 – Distinguished with poster award.

S. A. Arnold, C. Schmidli, S. Albiez, A. Syntychaki, A. Bieri, L. Rima, K. N. Goldie, M. Chami, R. Sütterlin, H. Stahlberg, and T. Braun, "Miniaturizing EM sample preparation: Challenges, opportunities, and visual proteomics", Nanoscience in the Snow, Zermatt, Switzerland, 2017

Conferences organized

International Nanoscience Student Conference (INASCON), August 11–14, 2015, Basel, Switzerland